Damage Modeling, Monitoring, and Assessment of Bridge Scour and Water Borne Debris Effects for Enhanced Structural Life

Final Report
September 2024

Principal Investigator

Wei Zhang, Ph.D., P.E., Associate Professor,
School of Civil & Environmental Engineering (CEE),
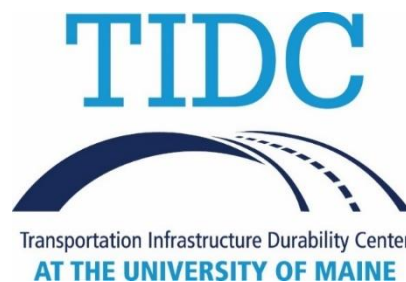University of Connecticut (UConn)

Co-PI

Ramesh B. Malla, Professor, School of CEE, UConn
Nalini Ravishanker, Professor, Department of Statistics, UConn

Authors
Alok Sharma, William Hughes, Steven Matile, Indrani Chattopadhyay
and Binit Gautam. -Graduate Assistants at School of CEE, UConn
Sreeram Anantharaman -Graduate Assistant at Department of Statistics, UConn
Wei Zhang -Associate Professor at School of CEE, UConn
Ramesh B. Malla -Professor at School of CEE, UConn
Nalini Ravishanker -Professor at Department of Statistics, UConn

Transportation Infrastructure Durability Center
AT THE UNIVERSITY OF MAINE

A report from
University of Connecticut
School of Civil & Environmental Engineering
261 Glenbrook Road, Storrs CT 06269
PI Phone: 860-486-5642
PI Email: wzhang@uconn.edu
website: www.dm2l.uconn.edu

About the Transportation Infrastructure Durability Center

The Transportation Infrastructure Durability Center (TIDC) is the 2018 US DOT Region 1 (New England) University Transportation Center (UTC) located at the University of Maine Advanced Structures and Composites Center. TIDC's research focuses on efforts to improve the durability and extend the life of transportation infrastructure in New England and beyond through an integrated collaboration of universities, state DOTs, and industry. The TIDC is comprised of six New England universities, the University of Maine (lead), the University of Connecticut, the University of Massachusetts Lowell, the University of Rhode Island, the University of Vermont, and Western New England University.

U.S. Department of Transportation (US DOT) Disclaimer

The contents of this report reflect the views of the authors, who are responsible for the facts and the accuracy of the information presented herein. This document is disseminated in the interest of information exchange. The report is funded, partially or entirely, by a grant from the U.S. Department of Transportation's University Transportation Centers Program. However, the U.S. Government assumes no liability for the contents or use thereof.

Acknowledgements

Technical Report Documentation Page

1. Report No.	2. Government Accession No.	3. Recipient Catalog No.		
4 Title and Subtitle Damage Modeling, Monitoring, and Assessment of Bridge Scour and Water Borne Debris Effects for Enhanced Structural Life		**5 Report Date** December 21, 2024		
		6 Performing Organization Code		
7. Author(s) Alok Sharma, William Hughes, Steven Matile, Indrani Chattopadhyay and Binit Gautam. -Graduate Assistants at School of CEE, UConn Sreeram Anantharaman -Graduate Assistant at Department of Statistics, UConn Wei Zhang -Associate Professor at School of CEE, UConn Ramesh B. Malla -Professor at School of CEE, UConn Nalini Ravishanker -Professor at Department of Statistics, UConn		**8 Performing Organization Report No.**		
9 Performing Organization Name and Address University of Connecticut, School of Civil & Environmental Engineering, 261 Glenbrook Road, Storrs, Connecticut 06269-3037, U.S.A.		**10 Work Unit No. (TRAIS)**		
		11 Contract or Grant No.		
12 Sponsoring Agency Name and Address Transportation Infrastructure Durability Center (TIDC) at the University of Maine, Orono, Maine, U.S.A. funded by U.S. Department of Transportation University Transportation Center (UTC) programs		**13 Type of Report and Period Covered** Final Report: 10/01/2020 to 9/30/2024		
		14 Sponsoring Agency Code		
15 Supplementary Notes				

16 Abstract

During severe storm events, bridge safety is threatened by flooding hazards, including increased hydraulic pressures and water-borne debris, such as large woody debris buildups, which could exacerbate the scour of bridge foundations. To evaluate and identify possible bridge damages and vulnerabilities during flooding events, it is necessary to assess bridge resilience on a regional level. However, existing bridge vulnerability models are typically focused on a single bridge type and cannot effectively scale to larger areas that could include various bridge types. To balance high-fidelity models with the need for simplified, scalable models, bridges need to be classified based on key characteristics. This project aims to access the flood fragility of various types of bridges in a region, and it was completed in two phases. In the first phase, a clustering-based approach is used to determine the optimal classification of bridges for vulnerability analysis to flood-related hazards. The K-prototype algorithm is utilized to consider both categorical data and numerical data. Our dataset contains all the multi-span bridges overactive waterways in Vermont. The results unveil the bridges can be optimally classified into six major clusters: short, medium, and long-span steel, concrete tee-beams and culverts, and covered wooden truss bridges. In the second phase, the most representative bridges are selected for further analysis of their vulnerability to flood. Modelling of bridges in the Python library- OpenSeesPy was done for fragility analysis.

The final outputs as probability of failure of each bridge types are presented in few easily applicable tables that is believed to serve bridge asset managers, local and state governments, and other related decision-makers to take immediate actions and strategies on the operations and maintenance of bridges during severe flood in order to mitigate the possibility of economic and human life losses.

17 Key Words Flood Fragility, Bridge Vulnerability, Scour, K-Prototype Clustering, OpenSees, wooden debris impact		18 Distribution Statement No restrictions. This document is available to the public through…		
19 Security Classification (of this report) Unclassified	**20 Security Classification (of this page)** Unclassified	**21 No. of pages** 81	**22 Price**	

Form DOT F 1700.7 (8-72)

Table of Contents

List of Figures

List of Tables

List of Key Terms

DOF: Degree of Freedom
FEM: Finite Element Modelling
HEC: Hydraulic Engineering Circular
LS: Limit State
MOI: Moment of Inertia

RCC: Reinforced Cement Concrete
SPT: Standard Penetration Test
SSI: Soil-Structure Interaction
VTrans: The Vermont Agency of Transportation.

Abstract

During severe storm events, bridge safety is threatened by flooding hazards, including increased hydraulic pressures and water-borne debris, such as large woody debris buildups, which could exacerbate the scour of bridge foundations. To evaluate and identify possible bridge damages and vulnerabilities during flooding events, it is necessary to assess bridge resilience on a regional level. However, existing bridge vulnerability models are typically focused on a single bridge type and cannot effectively scale to larger areas that could include various bridge types. To balance high-fidelity models with the need for simplified, scalable models, bridges need to be classified based on key characteristics. This project aimed to access the flood fragility of various types of bridges in a region, and it was completed in two phases. In the first phase, a clustering-based approach was used to determine the optimal classification of bridges for vulnerability analysis to flood-related hazards. The *K*-prototype algorithm was utilized to consider both categorical data and numerical data. The dataset contained all the multi-span bridges overactive waterways in Vermont. The results unveiled the bridges can be optimally classified into six major clusters: short, medium, and long-span steel, concrete tee-beams and culverts, and covered wooden truss bridges. In the second phase, the most representative bridges from each cluster were selected for further analysis of their vulnerability to flood. Modelling of bridges in the Python library- OpenSeesPy was done for fragility analysis. The final outputs as probability of failure of each bridge types are presented in few easily applicable tables that is believed to serve bridge asset managers, local and state governments, and other related decision-makers to take immediate actions and strategies on the operations and maintenance of bridges during severe flood in order to mitigate the possibility of economic and human life losses.

Chapter 1: Introduction and Background

Many critical highway and railroad bridges and facilities of the nation are across rivers or other water bodies, either along coastal lines or across inland rivers. Understanding when and how a bridge might fail is critical for maintaining bridge safety. Bridge failures can impede emergency response, commercial shipping, access to health services, and more. Among many causes of bridge failures, flood and scour are important causes. According to an investigation by (Wardhana et al., 2003), during the period between 1989 and 2000, 48.3% of the bridge collapses reported in the United States was due to hydraulic causes, as shown in Figure 1. Over the decades, climate change has been posing an increased threat to hydraulic structures. In 2011, the New England region suffered from tropical storm Irene with a rainfall recurrence interval for a 12-hour storm exceeding 500 years. More than 300 bridge damages were reported in Vermont (Anderson et al., 2017).
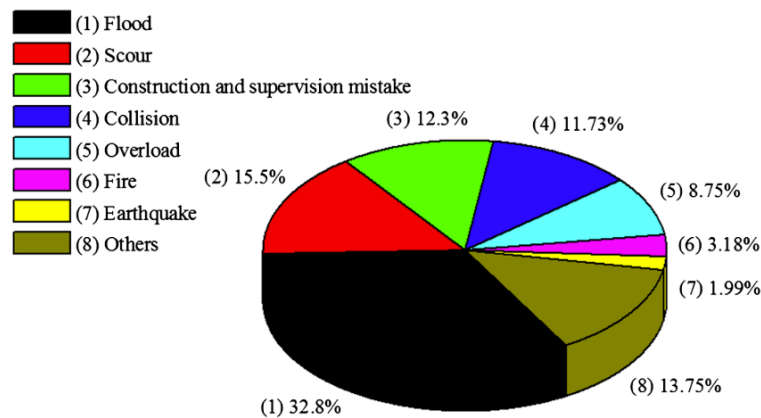
Figure 1: Distribution of causes of the reported bridge collapses in the USA from 1989-2000 (Wardhana et al., 2003)

During weather events with intense precipitation, like hurricanes, increased stream or river flows can cause greater hydraulic pressures on bridge piers, along with local scour of riverbed near pier foundations. Additionally, with strong winds and increased bank erosion and landslide potential, riparian trees can fail, falling into the river streamline and generating large woody debris (LWD) (Haehnel & Daly, 2004; Hughes et al., 2023; Kosič et al., 2023). The LWD can then flow downstream and become entrapped at bridge piers, which can increase the hydrodynamic pressure on the bridge as well as cause increased foundation scour due to constriction of the river cross-section. The combination of heightened hydraulic pressures, greater foundation scour, and potential debris impact forces may result in the collapse of bridge as shown in the Figure 2.

Figure 2: Bridge collapse due to debris buildup and pier foundation scour (HEC-09).

Forecasting the potential for bridge failures from an upcoming storm can help bridge owners better manage inspection, mobilization, and mitigation techniques during hurricanes and other significant flooding events.

1.1 Project Motivation

To this time, bridge owners and operators lack an efficient tool to inform bridge safety and assist decision making regarding bridge closures or maintenance before and during flood events. Due to the lack of such tools, properly planned and efficient mobilization of risk mitigation techniques have not been in practice. Accurate models predicting bridge vulnerability considering the combined effects of flooding, debris, and scour are needed. While several studies have investigated bridge performance under flood hazard (Kim et al., 2017; Ahamed et al., 2021; Anisha et al., 2022; Kosič et al., 2023), due to the complexities in the modeling process, the studies have generally focused on only one specific bridge or bridge type as a case study. Statistical models, scale models, and finite element models have been used to increase accuracy in predicting structural failures and scour (Ahamed et al., 2021; Kosič et al., 2023; Panici & de Almeida, 2018). While such frameworks have been developed to perform high-accuracy vulnerability analysis of specific bridges or bridge types subjected to flooding, debris impacts, or scour, their application is limited to those bridges which were used for modeling. Therefore, a fragility analysis of bridges at a regional scale is required to improve bridge safety. Such methodology should be flexible enough to extend to any other states rather than limited only to the region considered in the research.

1.2 Project Goal, Objectives, and Tasks

The goal of the project is to mitigate the risk of economic and human life loss due to bridge failures during severe flood events. During major flood events, bridges are subjected to the risk of failure due to hydrodynamic forces, accumulation of debris at piers and scouring of pier foundation. However, there are no available tools to make decisions based on quantitative studies on the flood-vulnerability of bridges. This project was hoped to assist the bridge owners with an effective tool to act upon the safety and operability of bridges under such events. It would help in the prioritization of the bridges for risk mitigation measures, based on their fragility level for a given intensity of flood.

The objectives required to be fulfilled in order to meet this goal are as follows:

i. to utilize a statistical measure to cluster bridges based on major flood parameters so that numerical modellings could be simplified.
ii. to numerically model the bridge types for each cluster using cluster mean bridges.
iii. to do the fragility analysis of each cluster for various flood and debris intensities and develop fragility curves.
iv. to generate a final output as look-up tables that are simple enough to understand by even a non-engineer personnel and could be implement easily during flood emergencies.

For efficient execution of the project, the above objectives were divided into multiple definitive tasks. The tasks were organized in two distinct phases.

Phase-I:

The first phase was mainly about statistical analysis. The tasks that were carried out in phase 1 are listed below.

  i. Literature review and data collection
  ii. Statistical Analysis
  iii. Debris dimension analysis

Phase-II:

The second phase was concerned with the numerical modelling and fragility assessment of the bridges. The following tasks fell under this phase.

  i. Data and feature extraction
  ii. Numerical modeling of bridges
  iii. Fragility analysis
  iv. Tool development

1.3 Report Overview

The report includes three chapters and several sub-chapters. The first chapter starts with the introduction of project goals, objectives, and tasks. The second chapter details the methodology used in the study. It describes a statistical clustering algorithm called 'K-prototype clustering', which has been used to classify the bridges into six clusters. The chapter also explains the methodology for debris size and scour estimations, discusses the various limit states used to derive fragility, and explores the numerical modeling of bridges and the theory of fragility analysis. In the third chapter, results and discussions are presented, including the fragility curves for various clusters at different flood and debris intensities. The result is presented in look-up table format. Next, the major limitations of this study are highlighted. Finally, the conclusion of the study is outlined, along with recommendations for its possible future extensions.

Chapter 2: Methodology

Accessing the flood fragility of bridge structures in a regional scope is a multidimensional challenge that demands statistical, structural, geotechnical and hydrological knowledge. Accurate models predicting bridge vulnerability considering the combined effects of flooding, debris, and scour have been generally focused on only one specific bridge or bridge type as a case study, and such methodology fails to include the behavior of all types of bridges in a region. Although, the most accurate way would be to model each bridge separately, detailed modelling of hundreds of bridges at an individual level is not a practical aim. The unavailability of detailed design drawings in digital form poses another hindrance for individual modelling of the bridges. For this reason, this project used statistical measures to first classify bridges into optimum n number of clusters based on major flood related parameters. Then, the numerical modelling of the n number of clusters was done. To preserve the possible variations within the clusters, Monte Carlo Simulation (MCS) method was used. The workflow is represented in the flowchart shown in Figure 3.
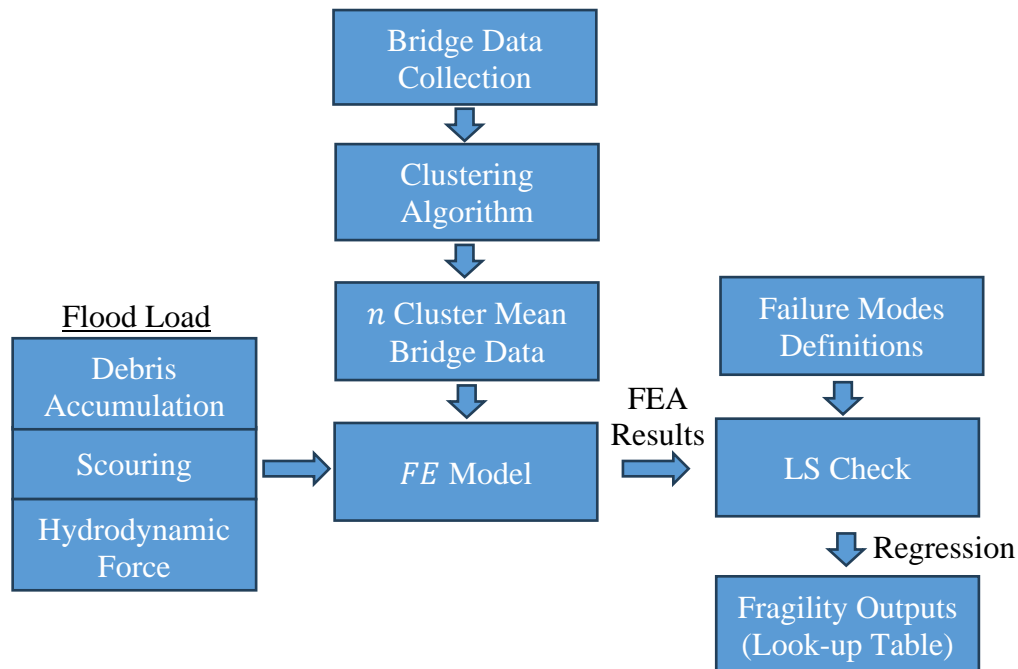
Figure 3: Flowchart of the Project's Methodology

2.1 Case Study and Data

The case study focused on bridges within the state of Vermont, a region which is highly prone to drift accumulation and scour-related damages and has been the subject of several previous studies (Anderson et al., 2017, 2020; Hughes et al., 2023). For instance, during Hurricane Irene in 2011, 300 bridges were damaged (Anderson et al., 2017). While the case study focuses on this region, the methodology can be extended to any region of interest. The bridge data were downloaded from the (National Bridge Inventory) (NBI) dataset, which offers publicly available data on bridges across the U.S., including bridge location and key characteristics related to size, material, design type, maintenance, etc. The initial dataset was comprised of 2,486 bridge structures throughout the state. To select bridges considering the objectives of evaluating/assessing their damage due to flooding, debris buildup, and foundation scour around piers, the full dataset was reduced to include

only multi-span bridges crossing active waterways (rivers, streams, brooks, etc.). As piers are a major source of debris collectors, only multi-span bridges were considered in the study. The bridges crossing lakes or bays were not considered based on the different nature of large inland lakes compared to rivers and streams. As such bridges are much less vulnerable to failure during flooding, debris buildups, and scour, they are outside the scope of the present study. After filtering based on these criteria, data related to 378 bridges remained available for vulnerability assessment and can be seen in Figure 4. Due to the large number of bridges of varying designs, creating detailed structural models is impractical due to computational and time and resource constraints. By creating representative bridge models to represent a subset of the bridges, the differences in bridge materials, designs, and sizes can be more appropriately captured while striking a balance between computational complexity and model fidelity.
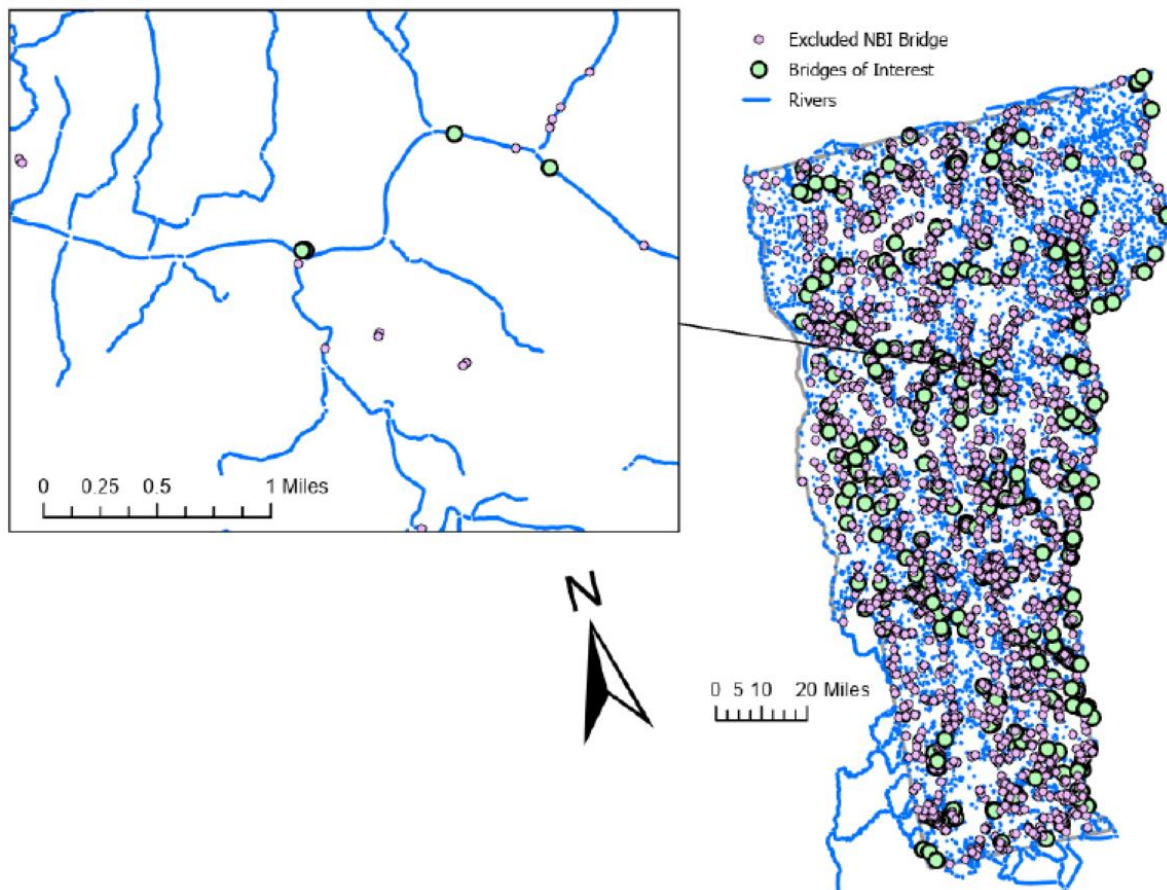
Figure 4: Bridges from the NBI joined to VTRANS spatial data

The key features for consideration in the bridge classification were selected to represent key structural parameters for modeling the bridge. While the NBI database contains over one hundred features related to the bridges, the vast majority of these parameters are not relevant to the bridge's vulnerability to flooding, debris accumulation, or scour. After removal of irrelevant or redundant features, four main parameters were identified as factors in the bridge grouping:

1. Structural material (e.g., wood, concrete, steel),

2. Design type (e.g., culvert, tee-beam, girder, truss),

3. Total structure length, and

4. Average span length.

These parameters were selected based on availability of data and engineering judgement of the key structural characteristics which could affect bridge vulnerability to flooding, debris buildup, and scour. The structural material and design type play a critical role in the structural load, response and strength, which are critical considerations in bridge vulnerability. Design type can also affect the type of failure modes of the bridges. Meanwhile, total length and average span length (derived from the number of spans and total structure length) jointly play a role to determine the extent of exposure of the bridge to flood and debris. The number of spans correlates directly with the number of bridge piers, which represent the main collector of debris, where the foundation scour can occur and lead to bridge damage. In the case of water overtopping, longer span lengths will lead to increased hydrodynamic forces. However, shorter spans could leave less room between piers for debris to flow freely, leading to higher probabilities of debris buildup.

The bridge material and design type variables represent categorical data, such that each bridge is grouped qualitatively into one material and design type category. On the other hand, the variables related to the span length and number of spans are numerical. Therefore, the four selected variables represent a mixed dataset, comprised of a combination of numerical and categorical features. While these parameters were selected in this study, in future studies, the effects of incorporation of different parameters, such as bridge width or foundation depth, can be explored. Not in consideration for clustering were the hydraulic design requirements for individual structures. As the structures were sorted to include only those with hydraulic crossings, it is the researchers' assumption that each was designed with some level of hydraulic considerations and that the level at which they were designed, or would be redesigned, is proportionate to the existing hydraulic flow. While the design level may have a direct relationship with the vulnerability of a structure, that is not within the scope of this work and could justify a standalone research topic evaluating the relationship.

2.2 Statistical Clustering

Clustering is used in a diverse range of applications, such as image processing, neuroscience, economics, and customer segmentation, among others. It serves as a fundamental step in handling novel datasets, allowing the extraction of valuable insights and comprehension of data distributions. It can also serve as both a preprocessing and intermediate step for various other algorithms, including classification, prediction, and other data mining applications. Numerous clustering algorithms have been developed, each with their unique approach and characteristics. Some notable types include:

- Hierarchical Clustering (Nielsen, 2016): This method groups data objects on the basis that objects closer to each other are more related than those farther away. It creates a hierarchical representation of clusters, either in a bottom-up (agglomerative) or top-down (divisive) manner.
- Centroid-based Clustering (MacQueen, 1967): In this approach, clusters are represented by a central vector, often referred to as the centroid. The centroid need not be an actual member of the dataset and is calculated as the average of all data points in the cluster.

- Density-based Clustering (Kriegel et al., 2011): Here the clusters are identified as sets of data objects that are grouped together based on regions of high density in the data space. It is particularly useful for irregularly shaped clusters and can handle noise effectively.

These are just a few examples of the wide range of clustering algorithms available. Each algorithm has its strengths and weaknesses, making each suitable for specific types of data and clustering scenarios. Researchers and practitioners often choose the most appropriate algorithm based on the data characteristics and the objectives of the clustering task. This study utilized centroid-based clustering. In this technique, a center is selected for each of the predetermined number of clusters K, and each data point is assigned to the cluster with the nearest center. Initially, the value of K is tentatively selected by the user, and then an optimal value for K is determined using suitable criteria. Then, a new center for each cluster is calculated based on the data points which have been assigned, and all data points are once again distributed across all K clusters. This is done to see if the new cluster center can better represent the data points within each cluster. The process continues until a point is reached where constructing new cluster centers no longer improves the representation of data within each cluster, and as a result, no data points change their assigned clusters. The K-means algorithm (MacQueen, 1967), one of the most common centroid-based methods, operates by reducing the Euclidean distance between the cluster data points and cluster centers (i.e., mean) to minimize a cost function. However, due to its use of the Euclidian distance as a measurement of data similarity, this approach is only suitable for datasets comprised of continuous variables and cannot be applied for categorical datasets. Another type of clustering, K-modes clustering (MacQueen, 1967), was introduced to accommodate data with categorical variables. In this method, the mode, rather than the mean, is used for the cluster centers. Unlike K-means, instead of reducing the Euclidean distance between cluster data points and cluster means to reduce a cost function, K-modes uses a "matching dissimilarity" measure to update cluster modes. Therefore, in the K-modes algorithm, the "distance" calculated is simply the number of disagreements between each data point and the cluster mode. As a result, K-modes can only be used for categorical data and not for continuous or mixed type datasets. To address these issues, K-prototype clustering (Huang, 1998) was employed in this analysis. K-prototype is a combination of the K-means and K-modes clustering algorithm and is suitable for mixed type datasets containing both categorical and numerical features. This algorithm combines the "means" of the numerical features and the "modes" of the categorical features to build a new hybrid cluster center "prototype". Based on the "prototype", the algorithm builds a dissimilarity coefficient formula, and the cost function is applicable to the mixed-type data. Suppose there are m features in a mixed-type dataset, of which p are numerical features and m-p are categorical features. N and C represent the numerical and categorical features. The dissimilarity coefficient D between two mixed-type variables x and q is:

$$D(x_i, q_i) = \sum_{s=1}^{p}(x_s^N - q_s^N)^2 + \gamma \sum_{s=p+1}^{m} \delta(x_s^C, q_s^C) \ \dots \ (2.2\text{-a})$$

where s represents the number of the given feature, and δ is an indicator function as defined in the equation 2:

$$\delta(x_s, q_s) = \begin{cases} 0 \ if \ x_s = q_s \\ 1 \ if \ X_s \neq q_s \end{cases} \quad \dots \ (2.2\text{-b})$$

In the equation 1, the parameter γ is introduced to control the relative influence of the categorical feature and the numerical feature on the clustering process. Higher values of γ indicate more weight is assigned to the categorical variables.

Several techniques, such as Elbow method (Thorndike, 1953), Average Silhouette Criterion (Rousseeuw, 1987), and Bayesian Information Criterion (BIC) (Zhao et al., 2008), exist to choose the optimal number of clusters. BIC was used to decide the optimal number of clusters because of its usefulness and ease of interpretation. The optimal cluster size K is that which minimizes the BIC value, calculated as:

$$BIC = \sum_{i=1}^{K}\left[\log(n_i) - n_i \log(n) - \frac{n_i d}{2}\log(2\pi) - \frac{n_i}{2}\log(\Sigma i) - \frac{n_i - K}{2}\right] - \frac{1}{2}K\log(n) \qquad \dots$$
(2.2-c)

Where,

$$\Sigma i = \frac{1}{n_i - K}\sum_{j=1}^{n_i}\|xi - C_i\|^2 \qquad \dots (2.2\text{-}d)$$

where K is the number of clusters, C_i is the cluster center of the ith cluster, n_i is the size of the ith cluster, n is the size of the data set, and d is the dimension of the dataset.

2.3 Debris Accumulation and Foundation Scour

2.3.1 Debris Shape and Size

Estimation of accumulation of debris at bridge sites is challenging, influenced by many uncertainties. As suggested by (FHWA HEC-09, 2005), size of accumulations depends mostly on the debris dimensions and delivery rate, the flow depth, and the number and proximity of gaps and piers affected.

(a)   (b)
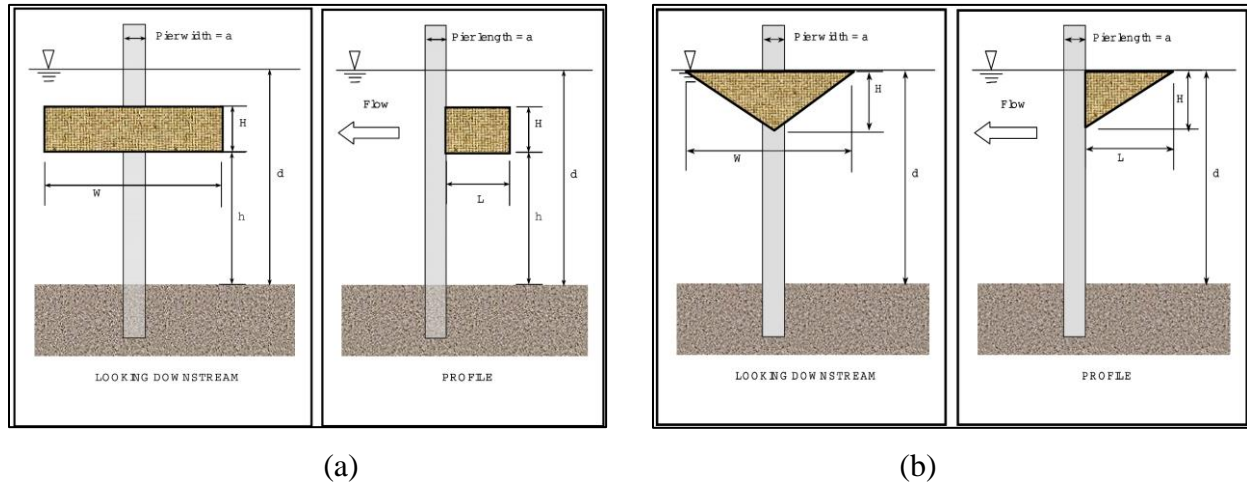
Figure 5: Idealized shapes of debris jam. (a) Rectangular shape (b) Triangular/Conical shape. (Zevenbergen et al., 2007)

Debris shape

The shape of waterborne debris accumulated at a pier is not yet fully understood (Diehl, 1997). Based on field observations, NCHRP report-653 (Lagasse, 2010) describes both triangular and rectangular debris shapes that could exist at bridge piers as shown in Figure 5. In some experimental models like (Panici & de Almeida, 2018) conical shape of debris accumulation was observed. However, the driving factors that cause the variety of debris shapes are still unknown. In comparison to the triangular or conical shape, the rectangular shape has greater projected area

for given values of height and width of debris jam, leading to a more extreme blockage of flow, higher hydrodynamic forces and greater depth of scour. Therefore, in this study, rectangular shape was adopted, thereby following a more conservative approach. However, the quantification of the sensitivity of various debris shapes to the flood fragility of bridges is suggested for the future endeavors.

Debris size

Determination of size of the debris accumulation is critical because it is associated with the hydrodynamic force imparted on the bridge. According to (Diehl, 1997), log length can be used as the width of debris jam. However, because very long trees are usually trapped along the upstream channel before reaching the bridge site, the debris width is limited to the sum of half of the span lengths on both sides of pier as recommended by New Zealand Highway Bridge Design Specification, which is also recommended by (AASHTO LRFD, 2012). Therefore, in our study, single pier accumulation is considered, in which, debris width can vary from zero (no accumulation) up to the average span length. The height of accumulation is conservatively taken as full water depth as suggested by (FHWA HEC-09, 2005).

When water is at superstructure level, debris accumulation might take place along the whole span. (FHWA HEC-09, 2005) suggests, for superstructure accumulation type, the width of debris is equal to span length and height of debris is equal to the vertical height of superstructure plus 1.2 m above and below the superstructure (Wellwood et al., 1989).

2.3.2 Scour Calculation

Scour can be defined as the erosion of riverbed due to current of water. Among three types of scours that are generally recognized (Aggradation/degradation scour, general scour and local scour), local scour occurs in the vicinity of piers, exposing the embedded foundation and thereby affecting the stability of the whole bridge. As discussed in the introduction part, scour failure of bridges is very common, and scour depth is further increased by the accumulation of debris.

Among many other methods, the commonly used guidelines to assess scour conditions for a variety of bridge foundations and hydraulic conditions is given by Federal Highway Administration (FHWA) Hydraulic Engineering Circular HEC-18 (Arneson et al., 2012). Pier scour is given by HEC-18 as:

$$\frac{y_s}{a} = 2K_1 K_2 K_3 \left(\frac{y_1}{a}\right)^{0.65} Fr_1^{0.43} \quad ... (2.3.2 - a)$$

Where:

y_s = scour depth

a = pier width

K_1 = correction factor for pier nose shape (1.0 for round nose pier)

K_2 = correction factor for angle of attack of flow = $\left(\cos\theta + \frac{L}{a}\sin\theta\right)^{0.65}$

L = length of pier

θ = angle of attack

K_3 = correction factor for bed condition (1.1 for clear-water scour)

y_1 = flow depth directly upstream of the pier

Fr_1 = Froude Number directly upstream of the pier = $V_1/(gy_1)^{1/2}$

V_1 = mean velocity of flow directly upstream of the pier

g = acceleration of gravity

The presence of debris affects the scour depth. To account the accumulation of debris on the pier, the pier width is modified based on the shape of debris as:

$$a_d^* = \frac{K_1(HW) + (y_1 - K_1 H)a}{y_1} \quad ...(2.3.2 - b)$$

Where:

a_d^* = modified pier width

K_1 = 0.79 for rectangular debris, 0.21 for triangular debris

H = height (thickness) of the debris

W = width of debris (perpendicular to the flow direction)

Although widely used, this guideline by HEC-18 has two major limitations. The first one is that the bed soil property is not considered in the equation. The second limitation is that most of the experimental validation studies have shown that the HEC-18 equation produces conservative results (Johnson et al., 2015).

2.4 Limit States for Bridges

The most essential aspect of fragility assessment of bridge structures is to determine limit state (or performance) functions. There are several possible modes a bridge might fail for a given flood hazard. Those modes of failure are either material failure or instability of the bridge. Each mode of failure is defined by a unique limit state function.

There are multiple literatures like (Anisha et al., 2022; Arora, 2023; Kim et al., 2017; Kosič et al., 2023) that did fragility assessment of bridges mainly due to flood scour and debris accumulation based on various kinds of limit state functions. Typically, the limit state functions are decided based on the failure modes observed in the past records on hydraulic failure of bridges. From the studies conducted after the floods in Queensland, Australia in 2013, (Lebbe et al., 2014) identified in their studies that the major failure criteria for bridges were deck and approach damage, pier and abutment scouring, debris build up on the structures, etc. In another study by (Lin et al., 2014), 36 cases of bridge failures pertaining to scour were analyzed based on hydraulic, structural, and geotechnical conditions. It was found that pier failure (comprising pier foundation failures) is the most common case. Three common types of failure modes are identified from that study- vertical failure, lateral failure, torsional failure and deck unseating.

As discussed in detail in (Lin et al., 2014), vertical failure could be due to buckling and inadequate soil support. For deep foundation, penetration of friction piles, undermining of pile toe and pile buckling can lead to vertical failure of a bridge. Similarly, the lateral failure consists of pushover failures of piers and structural hinging of piles. Pushover analysis is a nonlinear static analysis that is usually done for a more detailed analysis of a single bridge, which demands quite a lot of computation time and therefore it becomes difficult to do MCS of pushover analysis. Therefore,

in future, if detailed design drawings of all the bridges are available and easily incorporated in bridge modelling, pushover analysis is recommended. However, in our study, the lateral pushover limit state is indirectly realized by yielding of pier reinforcements in flexure. To add to the possible limit states for failure in lateral direction, along with the structural hinging of piles, shear failure of piles has also been incorporated in the study.

a) Deck Unseating

Failure of bridge deck during flood is mainly due to an excessive lateral hydrodynamic pressure due to water current in the case when water level exceeds the bearing elevation. Additionally, if there is debris entrapped on the deck, the area that faces the drag force increases. Buoyancy due to submergence of deck and lift force caused due to water current also act favorably for deck unseating. Simply supported spans are susceptible to flooding if the deck is not structurally attached to the piers. In elastomeric bearings, the girders simply rest over the pier head, and therefore, the connection provides no resistance (except friction) while deck tends to unseat. On the contrary, steel pin or shear key connections provide some additional resistance to sliding of deck due to the structural strength of the pins and shear strength of the shear keys. However, like in the literature (Pucci et al., 2023) in our study also, the resisting force due to bearing connection is not considered. The reason for this is mainly due to the unavailability of statistical and design data for different kinds of existing bridge bearings. Neglecting the connection strength will make our analysis more conservative. However, to accurately account the resistance of deck movement in the lateral direction, mechanisms of failure of various kinds of bridge bearings are suggested to be studied in the future.

The lateral force that tends to drive the sliding of deck is the hydrodynamic drag force due to the water current. It acts on the projected area of the obstruction, which can include debris area also. The detail about calculating stream pressure is explained in the reference (AASHTO LRFD, 2012).

$$F_x = A_p \times \frac{1}{2g} C_D \rho_w v^2 \quad \dots \quad (2.4 - a)$$

Where:

F_x = hydrodynamic force in lateral or x-direction

A_p = projected area of the obstruction

C_D = drag coefficient

ρ_w = density of water

v = velocity of fluid

To resist F_x, static friction is mobilized, which depends upon the vertical reaction. There are three vertical forces that come into picture when deck is submerged. One is the dead weight of the deck (W), another is the uplift force due to buoyancy (U), and the last one is the lift force due to hydrodynamic action (L).

The buoyant force is equal to the weight of water having volume equal to the submerged portion of the superstructure (V_{sub}).

$$U = \gamma_w V_{sub} \quad \dots (2.4 - b)$$

Where, γ_w is the unit weight of water.

Hydrodynamic lift (L) is caused because of the pressure reduction caused due to the speed of water.

$$L = \frac{1}{2}C_L \quad \dots (2.4 - c)$$

The net vertical reaction F_v is:

$$F_v = W - U - L \quad \dots (2.4 - d)$$

According to the law of static friction, maximum mobilized static friction F_f is given as:

$$F_f \; \alpha \; F_v$$

$$F_f = \mu_f F_v \quad \dots (2.4 - e)$$

Where, μ_f is the coefficient of frictional resistance between the contact area of the superstructure and substructure. μ_f depends on the material the contact surfaces are made up of.
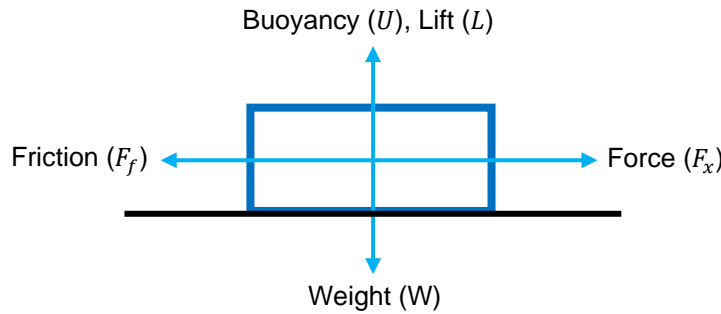
Figure 6: Free body diagram showing static friction

If the mobilized friction tends to exceed the maximum mobilized friction, then the sliding of deck occurs as shown in Figure 6. So, the limit state equation that expresses the deck displacement failure is given as:

$$\boldsymbol{F_x \geq \mu_f F_v} \quad \dots \quad (2.4 - f)$$

b) Pile Flexure Yielding

For deep foundations, the piles are subjected to mainly three kinds of forces- compressive force, shear force and flexural moment. In this section, flexural limit state is discussed. Due to lateral hydrodynamic force, the piles resist the bending moment. The magnitude of moment resisted by a pile depends upon the lateral force as well as the moment arm. If there is scour, the moment is further increased due to increased moment arm. Moreover, the entrapment of debris increases the magnitude of lateral force.

If the moment in a pile exceeds its flexural capacity, then hinging of pile occurs. Pile hinge destabilizes the pier foundation, leading to a catastrophic failure (Lin et al., 2014).
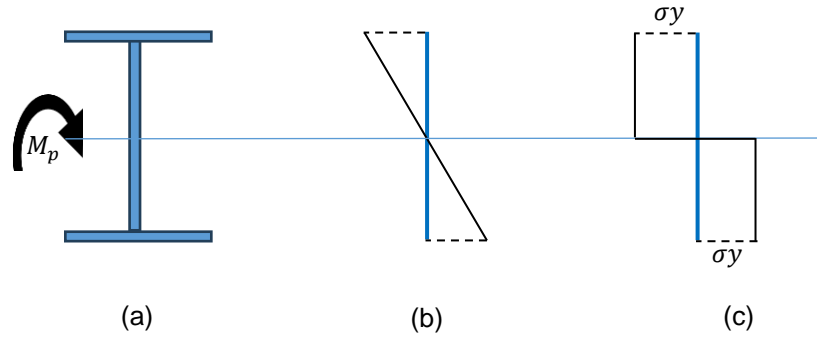
Figure 7: Fully plastic section of an I-section a) Pile section b) Strain diagram c) Stress diagram

The capacity of the piles was calculated based on the non-linear section capacity. For an I-section steel pile, the plastic moment capacity is the moment resisted by the pile when its section undergoes fully plastic.

When the section is fully plastic, a neutral axis passes through the centroid of the section as shown in Figure 7. To calculate the fully plastic section moment capacity (M_p), first, force is obtained by multiplying the yield stress (σ_y) with the area element (A_{pi}) and the moment arm (y_i) which is the distance between the neutral axis to the centroid of the area element. The numerical integration to obtain the total plastic section capacity is given as:

$$M_p = \sum_i A_{pi}\sigma_y y_i \quad \dots (2.4 - g)$$

Once the section is fully plastic, it cannot take any further moment. If a moment (M) that exceeds M_p is applied to the section, then the section will go rotation indefinitely, which indicates failure.

Therefore, the limit state equation that expresses pile flexure yielding is given as:

$$\boldsymbol{M \geq M_p} \quad \dots (2.4 - h)$$

c) Pile Buckling

Buckling of piles is another possible failure mode that destabilizes the pier foundation (Lin et al., 2014). When a long slender member is loaded with a compressive load exceeding its critical load, then it buckles. The buckling of a pile is characterized by a large lateral deformation that limits its axial load carrying capacity. For a long slender member, buckling capacity is usually less than its compressive yield capacity. Due to scouring of foundation, the non-embedded length of pile increases. This makes the piles vulnerable to buckling.

Buckling capacity can be calculated for various boundary conditions as shown in Figure 8. The equations published by Leonard Euler in 1744 are still used in design code like (AASHTO LRFD, 2012). A column may exhibit buckling in many different possible modes. The first mode of buckling shown in Figure 8-a, is the predominant mode because it is characterized by the least critical load.
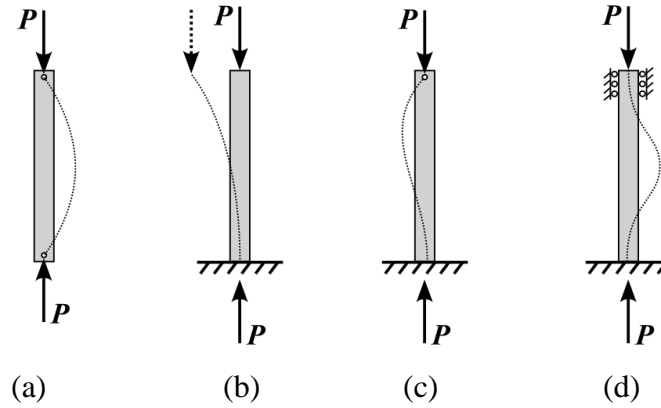
Figure 8: First buckling mode for various end conditions (a) Pinned-pinned, (b) Fixed-free, (c) Fixed-pinned, (d) Fixed-fixed

Suppose a long and slender pile with some uniform cross-section with the moment of inertia (I) about weak axis throughout its length (l). If 'E' is the material modulus of elasticity, the critical load that initiates buckling is:

$$P_{cr} = \frac{\pi^2 EI}{(Kl)^2} \quad ...(2.4-i)$$

Here, 'k' is the effective length factor in the plane of bending, which depends on the end condition. For fixed-fixed end condition, value of K is 0.5.

So, if P is the maximum actual axial force in a pile column, the limit state equation that expresses pile buckling is given as:

$$\boldsymbol{P \geq P_{cr}} \quad ...(2.4-j)$$

d) Pile Shear

If lateral load due to hydrodynamic failure is large enough, then shear force in piles can exceed their shear strength, leading to pile shear failure.

The shear capacity of a pile section can be calculated based on Chapter G of American Institute of Steel Construction (AISC). For an I-section beam, the nominal shear capacity is obtained as the 60% of the yield capacity of the web:

$$V_n = 0.6 f_y A_w \quad ...(2.4-k)$$

Where, 'f_y' is the yield stress of the steel and A_w is the area of web.

If V is the actual shear force in a pile column, the limit state equation that expresses pile shear failure is given as:

$$\boldsymbol{V \geq 0.6 f_y A_w} \quad ...(2.4-l)$$

e) Foundation Soil Bearing

Due to excessive hydrodynamic load, foundation load increases, which could lead to bearing capacity failure of the soil.

In case of deep foundation, the bearing resistance is provided by the earth in two ways- one is by skin friction, and another is by tip bearing as shown in Figure 9. The piles in which the resistance is mainly provided by the friction between the pile's circumferential area and soil around it, are called friction piles. This kind of load bearing system is used when there is no underlying firm bedrock. On the other hand, if the load is transmitted mainly through the tip area of the piles, then it they called tip (or end) bearing piles. This kind of system is used when there is a firm underlying rock where pile tips could rest on. A mixed type of pile load resisting mechanism uses both the skin friction as well as end bearing resistance to support the vertical load.
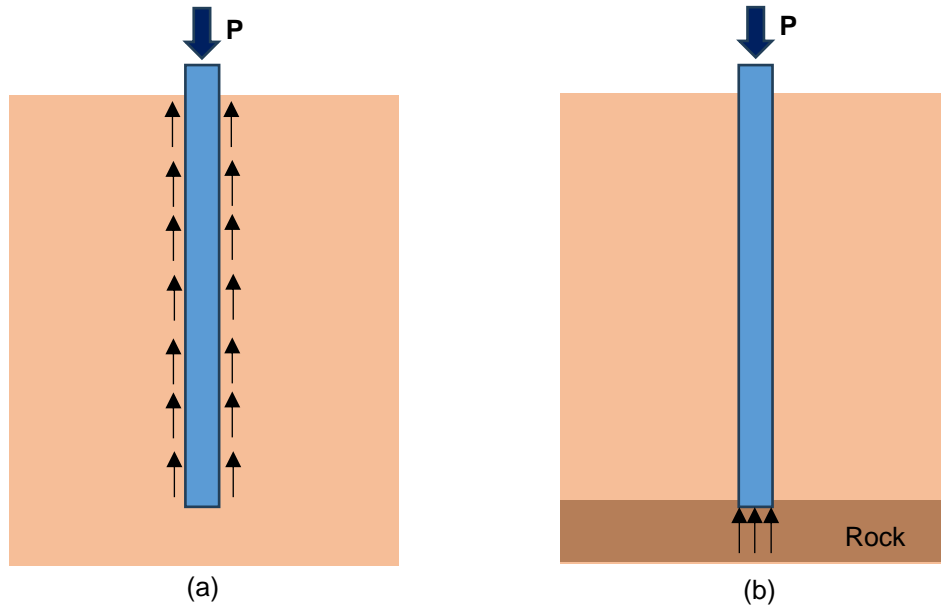
Figure 9: Load resisting mechanisms of piles. (a) Friction pile, (b) End-bearing pile

To determine the soil support strength, various dynamics and statics methods as described in (AASHTO LRFD, 2012). If we have SPT value of cohesionless soil, Mayerhof, 1976 method can be used to obtain the tip and friction strength of the soil.

If a pile with diameter 'd' ft is embedded to a depth 'D'ft, then the nominal unit tip resistance 'q_p' is obtained as:

$$q_p(ksf) = \frac{0.8(N1_{60})D}{d} \leq q_l \quad \dots (2.4 - m)$$

Where, $N1_{60}$ (blows/ft) = is the SPT value near the pile tip corrected for overburden pressure.

q_l is the limiting top resistance. For sands, $q_l = 8 \times N1_{60}$, and for silt, $q_l = 6 \times N1_{60}$. For non-circular pile, D is calculated using effective area. For a steel H-pile, during penetration, the soil between the flanges moves as a bulk. So, the effective area of H-pile is a rectangular area:

$$A_{eff} = l_{flange} \times l_{web}$$

So, diameter $D = \frac{A_{eff}}{\pi/4}$

Similarly, the side resistance for non-displacement piles (e.g., steel H-piles) is obtained by the following formula:

$$q_s(ksf) = \frac{\widehat{N}l_{60}}{50} \quad ...(2.4-n)$$

Where, $\widehat{N}l_{60}$ (blows/ft) = average corrected SPT-blow count along the pile side.

In case the $N1_{60}$ value is not directly available from the SPT, but soil friction angle is known, the correlation modified after (Bowles, 1997) can be used as mentioned in (AASHTO LRFD, 2012), which is shown in Table 1.

Table 1: Correlation between SPT N160 values and soil friction angle

$N1_{60}$	ϕ_f
<4	25-30
4	27-32
10	30-35
30	35-40
50	38-43

When there is excessive axial load in a pile, the skin friction and tip bearing resistance is fully mobilized. This will cause penetration of piles into the earth, thereby causing large vertical displacement and instability of the foundation. If $'P'$ is the total axial load in the pile with embedded circumferential area 'A_s' and tip circular area 'A_p', the total strength of soil support in the axial direction of a pile is:

$$P_u = q_s \times A_s + q_p \times A_p \quad ...(2.4-o)$$

For a H-section piles, A_p is calculated by using equivalent diameter 'D' and A_s is calculated using effective rectangular area.

The limit state equation that expresses the failure of soil bearing capacity is:

$$\boldsymbol{P \geq q_s \times A_s + q_p \times A_p} \quad ...(2.4-p)$$

For deflection of soil mass in lateral direction, p-y curves are important. However effective depth of embedment can be used to avoid complex modelling that uses soil springs. The more about equivalent depth of embedment will be expounded later in modelling section. Similarly, group failure of piles is also mentioned in (AASHTO LRFD, 2012) for design purpose, where the capacity of one pile is multiplied by the number of piles (when spacing > 2.5D) to obtain the group strength. However, the lateral hydrodynamic load does not affect the total vertical loads in piles. During flood, the moment due to hydrodynamic load causes piles at extreme ends to bear higher axial load than in normal condition. Therefore, piles are expected to fail individually rather than group failure, and therefore, strength at individual level is dealt in our analysis.

f) Pile Undermining

(Lin et al., 2014) mentions undermining of pile tip to be another possible mode of failure of a deep foundation. The foundation may fail if there is deep scour (D_s) that exceeds the foundation depth (D_f). Hence, the limit state equation is:

$$D_s > D_f \quad ... (2.4 - q)$$

This limit state is more important for pile foundation if the piles are end-bearing type. In the case of piles with skin friction as dominant load resistant mechanism, the piles will fail in bearing capacity way before scour reaches to the pile tip. However, this limit state was included in the fragility analysis so that failures in case where the tip bearing is dominant, would not be missed.

g) Pier Flexure

Excessive hydrodynamic load in a bridge added by debris loads can lead to large bending moments at the base of tall piers. If the bending moment exceeds the flexural capacity of the pier section, then the pier may fail. Calculation of section capacity is therefore important to assess the vulnerability of a pier member.

For a reinforced cement concrete section, section capacity is usually accessed by doing moment-curvature analysis, as discussed in the reference, LRFD Seismic Analysis and Design of Bridges Reference Manual, (FHWA, 2014). After the moment curvature analysis, the damage state is calibrated using ductility ratio, (μ_Δ) which is defined as the ratio of displacement of the bridge pier to the yield displacement at the same location. Displacement ductility is more related to structure limit state. But (Priestley et al., 1996) suggests that the term limit state can be applied to member response as well.

A member limit state can be defined for various stages of member failure. In the reference (Priestley et al., 1996), four different limit states are discussed for a reinforced concrete member – cracking, first-yield, spalling and ultimate limit state, as shown in the Figure 10.
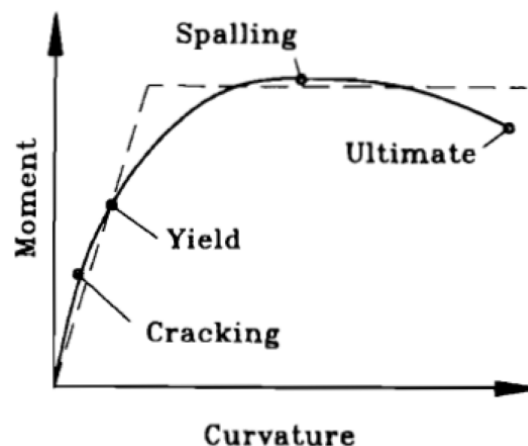

Figure 10: Concrete member limit states

First-yield limit state is defined as a point at which a significant change in stiffness occurs due to onset of yield in the extreme tension reinforcement. In Figure 10, it can be seen that the moment required for yielding of reinforcement steel is much less than the moment required for ultimate

capacity. In our analysis, as will be later seen in the results, the moment is not enough even to make the yielding of reinforcement as predominant failure mode among the other fragility modes discussed before. Therefore, yielding of reinforcement bars can be safely taken as the limit state of pier flexure failure. The calculation for this limit state does not involve developing a full moment-curvature plot, which makes the analysis relatively easier.

The calculation procedure for axial-moment strength interaction relationship (or the limit state moment at which yielding of steel occurs), is similar to the process of calculating the moment-curvature curve as outlined in (FHWA, 2014). The algorithm that can be used to calculate the yield moment is given below:

Steps:

i. Model section with geometric and stress-strain relations for concrete, confined concrete, and steel.
ii. Set extreme steel yield strain, ϵ_{sy}.
iii. Guess the neutral axis depth, c.
iv. Calculate strains at various depths of section, ϵ_x.
v. Calculate the stress in bars and in slices of concrete based on constitutive models, f_{sx} and f_{cx}.
vi. Sum the forces and compare to applied axial load, $P = P_{applied}$.
vii. If the total force matches the applied axial load, go to step () otherwise go back to (iii) and guess a new depth.
viii. Sum moments about the center of gravity of section to get M.

In this iterative process, bisection method can be used while guessing the neutral axis depth for the new iterations.

The constitutive models of both steel and concrete are non-linear stress-strain relationships. For steel, bilinear elastic - perfectly plastic model has been used. Since the limit state is characterized by the first attainment of yield stress, modelling of strain-hardening is not required in our case. For the concrete, Modified Hognestad Model (Hognestad, 1951) has been used, in which the stress-strain relationship is described by the combination of quadratic and linear curves as shown in Figure 11.
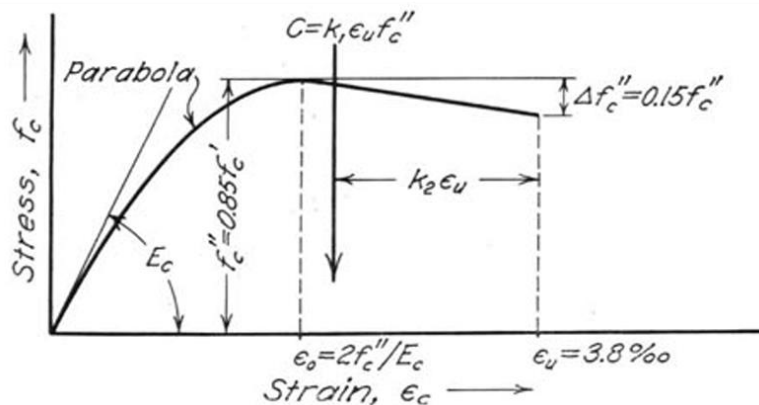

Figure 11: Hognestad Model for concrete, snippet from (Hognestad, 1951)

The parabolic part of the curve is defined by the following relationship:

$$f = f_c'' \left[2\frac{\epsilon}{\epsilon_0} - \left(\frac{\epsilon}{\epsilon_0} \right)^2 \right] \quad \dots (2.4 - r)$$

For linear part,

$$f = f_c'' - \Delta f_c'' \times \frac{\epsilon - \epsilon_0}{\epsilon_u - \epsilon_0} \quad \dots (2.4 - s)$$

Where,

f_c'' = maximum stress in flexure of concrete; nominal capacity (obtained from cube or cylinder tests).

$\epsilon_0 = \frac{2f_c''}{E_c}$

$E_c = 4700\sqrt{f_c''}$ is the initial tangent modulus of the concrete.

ϵ_u = ultimate strength of concrete

The concrete in tension has insignificant strength. Therefore, for the tensile strain, the concrete stress is set to zero.

If $M_{applied}$ and $P_{applied}$ are the moment and axial force applied at the base of the pier column, and moment M_y is the moment capacity of the pier section at which the first yielding of reinforcement bars occurs (calculated as prescribed above), then the limit state equation that expresses the flexure capacity of pier is:

$$\boldsymbol{M_{applied} \geq M_y} \quad \dots (2.4 - t)$$

2.5 Limit States for Culverts

There has not been much research on flood fragility analysis of highway culverts. Typically, the failure modes of culverts are different from bridge failure modes Hydraulic Design of Highway Culverts (Schall et al., 2012). (Rodwell et al., 2023) used empirical survey data collected in the aftermath of 2015 Illapel tsunami that occurred in Chile to fit fragility curves based on water depth. But such methodology is limited to particular case studies only. Moreover, the objective of the project was to develop fragility curves based on easily assessable parameters, and measuring absolute depth of water during severe floods is not an easy task.

In the design manual, (Schall et al., 2012) points out that the failure of a culvert can be identified as the exceedance of its allowable headwater. Here, the definition of allowable headwater hinges on economic considerations, regulatory constraints, AOP considerations and agency constraints. As our project is mainly concerned about human safety and operability that requires emergency actions, only economic considerations are studied. However, in future, for the study of long-term vulnerabilities, other criteria are also recommended to be incorporated.

In the economic consideration, during flood, the failure modes described in the design manual are embankment piping, severe outlet scour due to high outlet velocities and roadway overtopping. The primary cause of all these failures is the increase in water levels beyond allowable limits. Study about embankment piping requires detailed site-specific geotechnical data. On the other hand, scour prediction equations available in (Arneson et al., 2012) are for piers only, which can't be applied to closed bottom culverts (like box culverts). Method to determine the fragility of box

culverts due to scour is not simple. It requires rather complex hydraulics, geotechnical and structural modelling. Factors like channel bed, bank material, velocity and depth of flow at outlet and channel, amount of sediments, etc. might all affect the scour potential and therefore scour prediction is rather subjective topic as per (Schall et al., 2012). Usually for the estimated high outlet velocities, the scour protection measures at the outlet sites are considered in the designs, which puts further uncertainty in its fragility analysis. The results of the study used for site specific cases can't be used to generalize the fragility in a regional scale, and to perform numerous site-specific studies, the unavailability of detail data for each culvert and the demand of huge computational power checks the motivation. For all these reasons, the roadway overtopping was chosen as the limit state for culvert failure.

If 'H_{ih}' is the depth of water (hydrostatic head) at inlet of the culvert and H_{RW} is the height of roadway top measured from the riverbed (or barrel invert), the limit state equation that expresses the culvert failure is:

$$H_{ih} \geq H_{RW} \quad ...(2.5-a)$$

Although the limit state function does not tell, the roadway overtopping also signifies the risk of piping and outlet because of the high head at the inlet. More importantly, the increase in water level beyond a certain limit poses the risk of flood damage to the buildings and properties in the vicinity of the upstream reach. Taking the economic loss due to flood inundation might be challenging as it requires detailed site-specific data and therefore results can't be generalized for a whole region. For this reason, roadway elevation was used as the limit state level for the culvert failure.

2.6 Numerical Modelling

Individual numerical modelling of all the bridges was not practical. As the first step, statistical clustering method was used to categorize all of the bridges into n number of clusters based on four important flood related parameters. That reduced the problem to numerically modeling each cluster separately. Then, only n basic bridge models, that in general, represented all the bridges in their respective clusters, were needed to be developed. For this purpose, the mean bridges of the clusters were used. The detailed design drawings of the n mean bridges were obtained from VTrans. The mean bridges were modeled in OpenSees, which will be discussed in detail later in the report. Modeling of one representative bridge and generalizing the results for the whole cluster couldn't be an accurate approach because the design of each one of the bridges within a cluster is also different. Therefore, the model had to be dynamic in nature where various parameters were not deterministic. Uncertainty of various modelling parameters was therefore considered in the numerical modelling process. The design drawings of the mean bridges allowed to have the sense of how the bridge geometry parameters are proportioned for the cluster, and Monte Carlo Simulation (MCS) method was used to take care of uncertainty within the clusters.

2.6.1 Parameters Uncertainties

As discussed before, although the detailed design data of a cluster representative bridge were considered, the uncertainties of various parameters that may exist within a cluster were also needed to be accounted in the model. It was assumed that all the bridges within a cluster were designed based on the same basic design principles that the cluster representative bridge was designed on. This assumption is reasonable because bridges are designed following the same fundamental

design code like- (AASHTO LRFD, 2012), although over the course of decades, some minute details of the code might have been updated.

Data were collected from National Bridge Inventory (NBI) and Vermont Agency of Transportation (VAOT) Bridge Inventory System (BIS). Using MCS for uncertain parameters had to be wisely utilized, considering the practicality of the randomly generated bridge geometry. As for an example, a randomly generated bridge span could be very long, meanwhile, the randomly generated concrete pier section area for the same bridge could be too small to withstand even the deadload of the superstructure. Therefore, using MCS for all of the parameters without due consideration to the correlation among the parameters and practicality of the parameters' values could not ensure reliable results. Another challenge that was needed to be dealt with was the unavailability of data. For MCS, we need some range of possible values with some distribution type for each of the uncertain parameters. NBI did not have substructure (pier geometry and foundation type) and geotechnical data of the bridges. Neither other resources could provide some common range for those parameters because design parameters' values of bridges are always unique based on the local condition of bridge site, designer choices, indeterministic factor of safety used in the design, etc. So, these two challenges had to be overcome.

To solve the first challenge, for MCS, random bridges from within a cluster were chosen rather than varying parameters independently. This made sure that the randomly generated bridge would always be a realistic one. In the table 2, i^{th} bridge means a randomly selected bridge among all the bridges within a cluster. Most of the bridge geometry parameters were picked from i^{th} bridge. However, the bridge substructure data was not available. This second challenge was overcome by using the geometry proportional factors. The authors utilized the mean bridge to get different representative proportional constants for girders, pier section and foundation.

Girders

The number of longitudinal girders affects the deadload and stiffness of the deck. Data for the number of girders was not available for all the bridges. Therefore, using the mean bridge, the number of girders in the ith bridge was determined. A number of factors like superstructure type, material, slab thickness, span length, etc. come into play in the design of girders. However, since the chosen cluster parameters are such that the above-mentioned parameters do not quite vary among the bridges of the same cluster. Therefore, it was assumed that the number of girders is affected only by the slab width. With this assumption, the number of girders is proportionate with respect to the width of the slab in a linear fashion. The proportionality constant was obtained from the mean bridge. If w_{s0} and n_{g0} are the width of slab and number of girders of the mean bridge, the proportionality factor $\boldsymbol{k_g}$ can be defined as the number of girders per unit width of the slab.

$$\boldsymbol{k_g} = \frac{n_{g0}}{w_{s0}} \quad ...(2.6.1-a)$$

If w_s is the slab width of the ith bridge, the number of longitudinal girders in it is obtained as:

$$n_g = w_s \times \boldsymbol{k_g} \quad ...(2.6.1-b)$$

The minimum value for n_g is set to be 2.

Pier Section

The pier section area determines the projected area, lateral capacity as well as dead load on the pier base and foundation. For the piers, it has been assumed that the dead load at the base of the pier determines the size of the pier section. If W_{p0} and W_{d0} are the weight of pier and deck of the mean bridge respectively, then the dead load at the base of the pier (W_0) is:

$$W_0 = W_{p0} + W_{d0} \quad ... (2.6.1 - c)$$

If A_{p0} is the pier area of the mean bridge, the proportionality factor, k_p can be defined as the area per unit dead load.

$$k_p = \frac{A_{p0}}{W_0} \quad ... (2.6.1 - d)$$

Based on k, pier area of a random i^{th} bridge (A_p) can be obtained using its superstructure weight and pier height. If H_p, W_d and ρ are the height of pier, weight of deck and density of RCC of the ith bridge respectively, then the dead load at the base of pier (W) is:

$$W = W_d + \rho H_p A_p \quad ... (2.6.1 - e)$$

Using the proportionality factor,

$$A_p = W \times k_p$$

$$A_p = (W_d + \rho H_p A_p) \times k_p$$

$$A_p = \frac{k_p W_d}{1 - \rho k_p H_p} \quad ... (2.6.1 - f)$$

Pier width (w_p) can be calculated as:

$$w_p = \frac{A_p}{l_p} \quad ... (2.6.1 - g)$$

Where, the length of pier l_p can be assumed to be equal to the slab width. This assumption was derived from the mean bridge geometry. The minimum horizontal dimension of pier is 2 feet (New York City Laws). If pier width in the calculation above came out to be less than 2 feet, then the width was set to the minimum value (2 feet) and the length of l_p was calculated by conserving the area A_p. Also, the height to width ratio of pier was set to the maximum of 12 (New York City Laws). Therefore, for higher ratio, w_p was calculated as:

$$w_p = \frac{H_p}{12} \quad ... (2.6.1 - h)$$

And the pier length was calculated by conserving the area A_p.

Foundation

A similar method described above was be adopted to calculate the pile geometry in the pier foundation using the mean bridge as the reference. The number of piles in the foundation was proportioned based on the dead load on it. If N_{p0} is the number of piles in the foundation of the

mean bridge, the number of piles in the ith bridge can be calculated by using a new proportionality factor k_f, which can be defined as the number of piles per unit dead load at the base of the pier:

$$k_f = \frac{N_{p0}}{W_0} \quad \dots (2.6.1 - i)$$

Now,

$$N_p = W \times k_f$$

$$N_p = \left(W_d + \rho A_p H_p\right) \times k_f \quad \dots (2.6.1 - j)$$

Uniform arrangement of piles was adopted. If w_c, l_c, n_r and n_c are the pile cap width, pile cap length, number of pile rows and number of pile columns of the ith bridge,

$$N_p = n_r \times n_c$$

$$\frac{n_r}{n_c} = \frac{w_c}{l_c}$$

Solving the above two equations, we get:

$$n_r = \sqrt{\frac{w_c}{l_c} \times N_p}$$

And,

$$n_c = \frac{N_p}{n_r} \quad \dots (2.6.1 - k)$$

Next came the total length of the piles. Length of piles becomes an important parameter when there is excessive scour. A sufficiently long pile system may ensure safety in bearing capacity failure, but the piles may still fail in flexure and buckling if they are exposed to a sufficient length, where the cross section of the pile becomes a more important parameter. As mentioned before, the foundation data of all the bridges were not available, and therefore the data of the reference bridges were used to derive the parameters' values for the other bridges.

Design value of pile length is basically guided by the bearing capacity of the soil (AASHTO LRFD, 2012). The total length of pile was proportioned based on the skin friction of the soil. If q_{s0} and l_{p0} are the frictional resistance and total length of the piles in the mean bridge, and q_s is the frictional resistance of the piles in the ith bridge in the cluster, then the total length of the piles in the ith bridge 'l_p' was obtained by using proportionality factor k_l:

$$k_l = \frac{q_{s0}}{q_s} \quad \dots (2.6.1 - l)$$

Now,

$$l_p = l_{p0} \times k_l \quad \dots (2.6.1 - m)$$

For the sake of simplicity, only the side resistance was considered. If more detailed estimation is to be made, the tip resistance can also be used (which in turn depends on the pile length, and this

will make the problem non-linear). However, for future guidance, to get more accurate pile lengths, it is advised to use survey data from as many design drawings as possible. The authors, with the use of limited data due to time constraints, believed it to be an optimum way of analytically deriving the pile lengths of all the bridges within a cluster.

The following tables (Table 2 and Table 3) summarize all the uncertain parameters used in the model. Table 2 lists the correlated parameters. By correlation, it means that the parameter is somehow related to either the randomly chosen bridge index (i^{th} bridge) or to the value of the mean bridge of the cluster. Table 3 contains the uncorrelated parameters. The value of these parameters is not related to the bridge index. They are uncertain even in the mean bridge.

Parameters	Values/Relations	Remarks And/or References
Bridge length	i^{th} bridge	
Skew	i^{th} bridge	
Span length	i^{th} bridge	
Slab width	i^{th} bridge	
Number of girders	α (slab width)	basis- mean bridge, minimum 2
Slab thickness	10 "	mean bridge
Railing height	1 m	mean bridge
Channel side slope	2:1	mean bridge
Debris shape	Rectangular	HEC-9
Debris width	Random tree height	Upper 90% size (Ref bridge), HEC-9
Debris height	Water depth	HEC-9
Pier shape	Round nose	mean bridge
Pier section area	α (dead load)	basis- mean bridge
Pile cap height	Same as reference bridge	mean bridge
Pile cap width	Pier width + 6 feet	mean bridge
Pile cap length	Equal to pier length	mean bridge
Foundation	I-section piles	mean bridge
Number of piles	α (dead load)	basis- mean bridge
Sub-soil type	'sand'	mean bridge

As mentioned before, the clustering parameters segregated bridges based on common superstructure features that are related to flood, debris accumulation and scour. Therefore, mean bridge value for slab thickness, railing height, channel side slope, etc. were used. For unknown substructure parameters like pier shape, pile cap dimensions, pile section, pile arrangement and sub-soil type, the values of the mean bridges were used. They should be varied stochastically based on all possible ranges of their values. However, two reasonings prevented the authores from doing so. First is that the data of valid ranges for all of these parameters were not available, and even if available, they would be region specific. One of the objectives of this project was to be able to deliver the methodology which could be applied in any region, rather than only localized for Vermont State. The second reason is that, even if the ranges are available for some parameters (for example, in (HEC-18, 2012), some common pier shapes are tabulated), the statistical distribution of the bridges that have those piers shape is not available. So, there always exists a possibility of

making the results biased, unless all bridge geometry information of sufficient number of bridges is readily available. If that is possible, the concept of mean bridge would also not be necessary. However, it should also be noted that there is one advantage of adopting the deterministic values from the mean bridge especially for the foundation and sub-soil. The benefit is that keeping the same values of those parameters for all the bridges in a cluster provides the same ground for comparing the effect of debris size and flood level on the different superstructure types. In other words, this makes fragility comparison more focused on the superstructure types, debris sizes, and flood level, rather than the foundation and soil types. This was good here especially because the clustering parameters themselves were mainly superstructure based, and not substructure based.

In Table 3, uncorrelated uncertain parameters are listed along with the distribution they follow. These parameters are independent of the cluster type and follow some standard statistical distribution.

Table 3: Uncertain independent parameters used in the modelling

Parameters	Probability Distributions	References
Concrete compressive strength (f_c)	$Normal(\mu = 25\ MPa, COV = 0.2)$	(Kosič et al., 2023)
Steel yield strength (f_y)	$Log\text{-}normal(\tilde{m} = 250\ \text{MPa}, COV = 0.07)$	(Kosič et al., 2023)
Steel elastic modulus (E_s)	$Log\text{-}normal(\tilde{m} = 2 \times 10^5\ GPa, COV = 0.03)$	(Kosič et al., 2023)
Water drag coefficient (CD)	$Normal(\mu = 0.7, COV = 0.1)$	(AASHTO LRFD, 2012; Kim et al., 2017)
Soil angle of friction (ϕ_f)	$Uniform(25, 35)$	(Clarke, 2018a)
Water angle of attack (θ_w)	$Normal(\mu = 0^0, \sigma = 5^0)$	Assumed

Concrete and steel mean strengths were taken as 25 MPa and 250 MPa respectively. Various possible mean strengths were statistically varied to make the modelling more comprehensive. However, most of the bridges in the clusters were decades old, and therefore characteristics of the same materials had to be used that were used in the construction of those bridges. In this study, these two mean strength values were used for all the bridges because of multiple reasons. First was the unavailability of the data to quantify the exact distribution of the mean strengths among the bridges. The second reason was that the mean bridges in the cluster have these strengths, which in a way signifies that these material strengths were commonly used in bridge construction. The third reason was that the use of same material type would provide a same ground to make comparison of bridge vulnerabilities based on flood related clustering parameters and debris size, which are easily assessable parameters in comparison to the material strength.

Soil friction angle is a very important geotechnical parameter that is used to calculate the bearing capacity of the foundation as discussed previously. It is also used to determine the depth of fixity of the elastic foundation. However, finding out the subsoil nature at each bridge site was not feasible. Due to such unavailability of the data, the authors tried to make use of some common range of all possible soil friction angles in the state of Vermont. Upon review of literature, the topsoil and subsoils were predicted. Subsoil is a more stable soil type and is usually based on the

parent material. In Vermont state, in general, Tunbridge soils (characterized by well-drained, loamy, acidic nature) are found between 20 to 40 inches below the soil surface and glacial till is one of the most common parent materials in the northeastern United States, the depth of which varies from very shallow (just a few inches thick) to well over 20 to 30 feet thick (Thomas Villars, 2021). The parent material composition is sandy and gravelly glaciofluvial deposits as evident in the Windsor County (USDA, 2015). For the sake of comprehensive study, as a rough estimation of engineering property of the subsoil in Vermont state, typical range of soil friction angles found for glaciofluvial deposits is used. Based on the study (Clarke, 2018b), the friction angle varying within the range 25^0 to 35^0 was used in this project. Although this approximation may result in unrealistic prediction of soil type at a randomly sampled bridge sample, use of all possible range of soil friction angle is hoped to give a general trend of subsurface properties. This study has also ignored the variability of soil type with respect to soil depth at any particular bridge site. However, this uncertainty was not independent because the analysis required an average value of soil friction angle along the depth. Obviously, a more detailed subsoil geo-survey and discretization of Vermont's geo-map based on sub-soil type is strongly recommended at this point for refining the input data in order to get more accurate results.

Another variable parameter was angle of attack of water current. It can be defined as the angle that exists between the water current vector and the pier transverse length vector. As suggested by the mean bridge drawings, the piers are usually built in such a way that the angle of attack is minimized to zero degrees. However, during a heavy flood, due to turbulence and the possibility that the bank erosions on the upstream, the angle of attack might be little deviated from zero degrees. Until now, the authors have not found any literature that quantifies the uncertainty in the angle of attack. However, for the sake of completeness, small variability of 5^0 standard deviations in the mean value of 0^0 was arbitrarily assumed. As for the future work, sensitivity analysis of the angle of attack is recommended in order to in what degree the angle of attack affects the results.

2.6.2 Modelling of Bridges in OpenSees

To access the vulnerability of bridges, calculation of exceedance of limit states becomes a vital step. Limit state functions require both the capacity as well as demand calculations. Capacity calculation does not require detailed bridge modelling. However, calculation of member forces (demand) for a given flood load requires mechanistic modelling of the bridge. If the whole bridge is a deterministic structure, the member forces can be easily calculated by using simple structural statics formulae. However, the presence of multiple piles embedded in the ground and also due to the fact that some of the bridges are continuous span, solving the indeterminate structure became necessary in this project. Finite Element Modelling (FEM) has been extensively used by researchers to model indeterminate bridge structures. The authors have used OpenSeesPy, a finite element library in Python to do the Finite Element Analysis (FEA) of the bridges.

OpenSees Modelling Platform

OpenSees was developed for the simulation of structural and geotechnical system response to earthquake loading, and it has been used extensively for earthquake engineering simulations of bridge structures (Aygün et al., 2010; Seo & Linzell, 2013; Liang et al., 2016). In hydraulic engineering aspect, (Zhu et al., 2018) used particle finite-element method of modelling in OpenSees to verify the tsunami induced hydrodynamic load on bridges. The objective of the project is not about detailed modelling of a single bridge, but to statistically model hundreds of bridges over a region, accounting for different uncertainties. For this reason, a simplified bridge

model using beam-column elements was developed as also done in the previous literature- (Kosič et al., 2023).

A fully parameterized 3D model of bridge was made in OpenSeesPy. Some of the important aspects of modelling are explained below.

Elastic beam-column elements: Elastic beam-column elements as shown in Figure 12 were used to model the decks, piers and piles. As recommended in seismic design of bridges (FHWA, 2014), demand in a member can be calculated using elastic methods of analysis of the bridge, and explicit nonlinear techniques are applied to assess the capacity of the bridge to resist these demands. Therefore, elastic beam-column elements could be used to determine the demand forces in various bridge components. Examples of beam-column modellings can be found in Caltrans' technical report reference- (Almutairi et al., 2016).
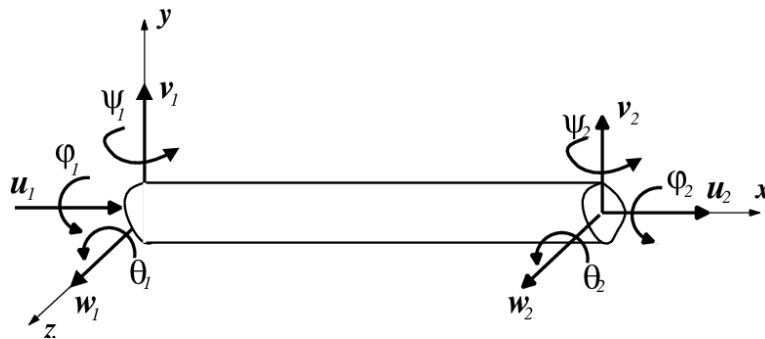
Figure 12: Beam column element with six DOFs

Span supports: Two spans connect at the top of a pier. The connection may be simply supported, where only rotational DOF of the connecting nodes is released; or the joint can be continuous, where none of the DOFs of the connecting nodes are released as shown in Figure 13. The pier of the continuous span bridges tends to displace comparatively less in the lateral direction due to higher lateral stiffness.

To simulate these two kinds of support conditions in OpenSees, equalDOF() command was used.
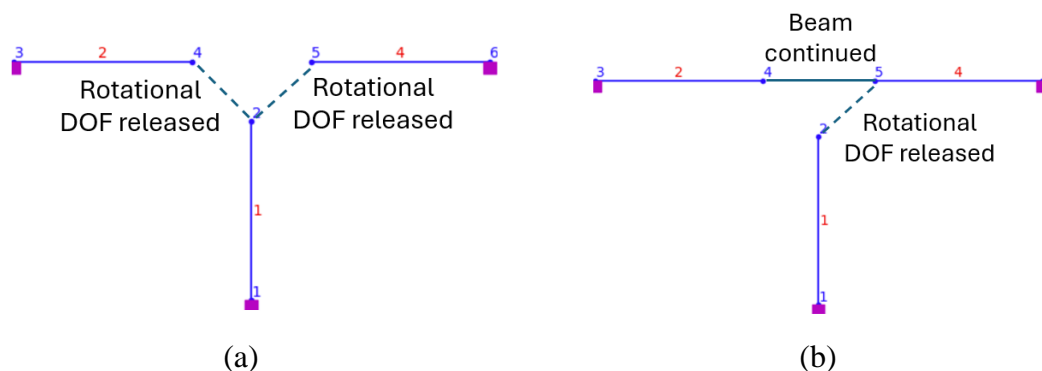
Figure 13: Support conditions: a) simple support condition. b) continuous support condition

In Figure 13, one end of each span (nodes 3 and 6) was fixed in all DOFs except rotation about global x (river flow direction) and z (pier axis direction). Rotation about global y (bridge axis direction) was not released, because the support bearing was present in multiple locations on the

pier that the bridge is effectively rigid in rotation about its axis. In such a way hinge support is simulated at the two ends.

When water level exceeds the pier height, hydrodynamic force on the deck has to be transmitted to the pier. This needed appropriate modelling of the bearing support on the pier. The two spans (3-4 and 5-6) are supported at node #2 of the pier. In figure 13(a), nodes 4 and 2 are constrained in such a way that they have equal DOFs in global x and z directions. They can have relative movement along the global y directions. This essentially simulates roller support. Hence, figure 13(a) represents simply support spans.

Figure 13(b) is the model for a continuous span superstructure. A new elastic beam-column element connected between nodes 4 and 5 has the same property as the two spans. This makes the spans continuous. The continuous span rests on node #2 of the pier. The support is simulated by using the similar function used for the simply support spans support. The only difference is that, instead of two, only one connection is required.

Rigid pile cap: Pile cap was assumed to be a rigid plate. Beam type Rigid links (rigid beams) were used to connect the pier bottom with the top of all piles, thus simulating a rigid plate condition. As per (AASHTO LRFD, 2012), pile caps were designed as flexure members. However, no distinct flood-damage limit state of the pile caps was found in the literature. Therefore, in this study, pile caps were viewed as an ideal rigid member that was used to transfer the dead load and flood load to the piles below it. The conventional approach for pile loads approximation is plate-on-elastic-foundation as mentioned in (AASHTO LRFD, 2012). For a vertical load 'P' that is eccentric 'e' from the foundation CG, the load 'R' shared by a pile at distance 'x' from CG,

$$R = \frac{P}{n} + Pe.\frac{x}{\sum x_i^2} \quad ...(2.6.2 - a)$$

Where, x_i is the distance of ith pile from the CG.

This simplified analysis fails to calculate bending moments that may occur in the piles. In order to study the pile flexure limit state, piles bending moments had to be calculated. So, in this study, foundation was modeled as an indeterminate structure where pile cap was assumed to be a rigid plate. It should however be noted that research like (Chaimahawan et al., 2021; El Hammouli et al., 2021) has shown that pile cap stiffness can affect load distribution among the piles and this effect becomes negligible if the pile cap is thick enough. For the sake of simplicity of the analysis and reduce computation time, the authors have assumed that the pile cap is thick enough as well as bridge piers rest over a significant area of pile cap to make the pile cap behave essentially like a rigid plate. At this point, nevertheless, for a more accurate and detailed analysis in the future (with much efficient computational resources), it is recommended to model pile caps with flexible shell elements.
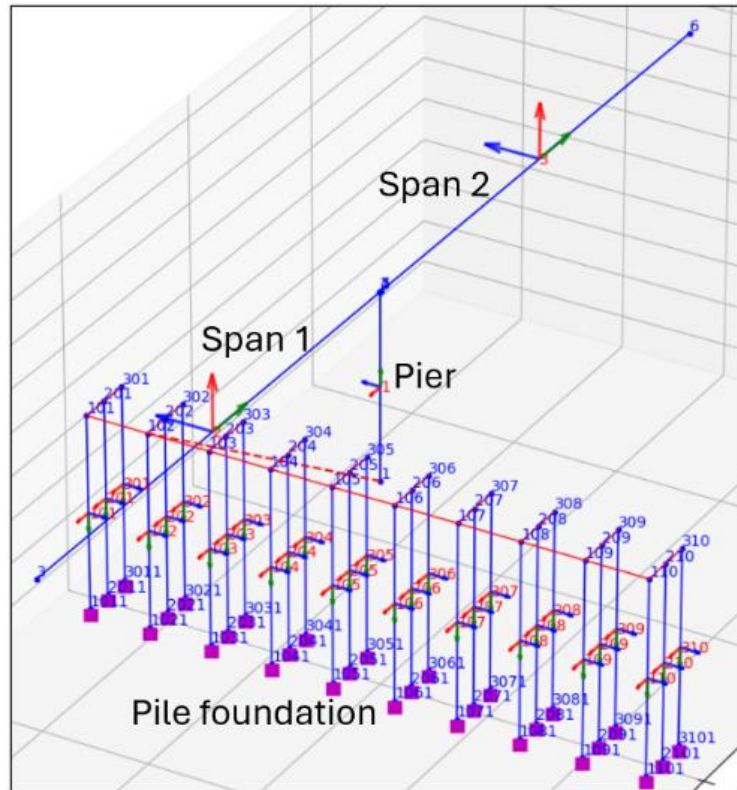
Figure 14: Bridge model in OpenSees showing rigid pile cap

As shown in Figure 14, Beam type rigid links (red color continuous line) continuously tie the top nodes of each pile. Then, the base of the pier is connected to a node in the rigid beam frame (red color dashed line). This effectively creates a rigid connection between the base of the pier and the top of the piles. In other words, rigid pile cap was simulated. OpenSees offers two kinds of rigid links- bar and beam. In 'rigidLink bar', only the translational DOFs will be constrained to be the same between two connected nodes. This might create rotational problem in our case because all pile tops may not have the same rotation because of the relative vertical displacements they go when loaded. However, in 'rigidLink beam', both translation and rotational DOFs are constrained. Therefore, beam type rigid link can accurately simulate the rigid pier-pile cap-pile connection.

Soil Structure Interaction (SSI)

To access the pile load and determine the nominal lateral resistance of pile foundation, (AASHTO LRFD, 2012) suggests soil-structure-interaction (SSI) modelling. Such modelling can take into account the elastoplastic nature of the soil. P-y curves particular to the existing soil and pile dimensions are necessary for SSI modelling. Most literatures so far like (Kim et al., 2017; Ahamed et al., 2021; Kosič et al., 2023) use soil springs to simulate the SSI.

Although the accuracy of displacement-based pushover analysis is improved with detailed SSI modelling, the analysis demands significantly high processing time. However, the objective is to run MCS with thousands of simulations of the bridge models, and to realize the lateral pushover limit state with pier and pile flexure limit states rather than displacement-based calculations. Therefore, to account for the SSI, an alternative approach mentioned in (AASHTO LRFD, 2012) has been adopted in this project, which is explained as following.

For preliminary assessment, (AASHTO LRFD, 2012) recommends the work of (M.T. Davisson & K.E. Robinson, 1965) where pile bottoms are treated to be fix supported. The depth to fixity below the ground 'd_f', in ft, may be taken as:

$$d_f = 1.4 \left[E_p l_w / E_s \right]^{0.25} \text{ ... } (2.6.2 - b) \text{ (for clays)}$$

$$d_f = 1.8 \left[E_p l_w / n_h \right]^{0.25} \text{ ... } (2.6.2 - c) \text{ (for sands)}$$

Where,

E_p = modulus of elasticity of pile (ksi)

I_w = weak axis MOI for pile (ft^4)

E_s = soil modulus for clays = 0.465 S_u (ksi)

S_u = undrained shear strength of clays (ksf)

n_h = rate of increase of soil modulus with depth for sands as specified in Table C10.4.6.3-2 of (AASHTO LRFD, 2012)

These equations are recommended mainly for axial loads on the piles. Quantifying the error in the bending moment estimations obtained by these formulae and the bending moment distribution along the length of the piles supported by elastic soil around it becomes a separate topic for research. However, increase in the unsupported pile length by d_f, certainly makes the analysis more accurate and conservative than simply taking zero depth of fixity.

2.7 Fragility Analysis for Bridges

Fragility curves can be used to understand the flood vulnerability of bridges. A fragility curve can be computed as the conditional probability of exceeding a certain limit state when a specific hazard magnitude occurs. In earthquake engineering, peak ground acceleration (PGA) is commonly used as the hazard magnitude (also called an intensity measure or in short 'IM'). In the case of flood hazard, the IM can be either water velocity or discharge level or water depth or sometimes scour depth (Ahamed et al., 2021; Argyroudis & Mitoulis, 2021; Kosič et al., 2023). Most of the literature use velocity as a single IM for their fragility analysis, for example- (Kim et al., 2017; Anisha et al., 2022). However, in some cases, complex hydraulic conditions exist due to variable backwater effect of the tributary rivers located downstream from the bridge site. This makes the velocity-water depth relationship not unique, and hence both the velocity and water level have to be used as IMs to develop fragility curves. For example, (Kosič et al., 2023) developed a three-dimensional fragility surface for this reason. In this study, the authors aimed to develop fragility curves with respect to velocity only, but such curves would be developed for multiple water levels. In this way, the non-unique relationship between water depth and velocity was included in the fragility analysis.

Fragility Function

So far, the fragility functions can be modeled with two different mathematical formulations. The first one is the lognormal cumulative distribution function (CDF), and the second one is logistic regression. These two methods are explained as follows.

In earthquake engineering, the lognormal cumulative distribution function (CDF) has been commonly adopted as the fragility function. Flood fragility assessment of bridges is a comparatively recent research field, and until now, many researchers like (Arora, 2023; Pucci et al., 2023) have used a similar lognormal CDF as the flood fragility function. In this method, the cumulative distribution function (CDF) for damage state 'D' exceeding a predefined limit state value 'd' for a given value of intensity measure 'x' can be expressed as:

$$F(x) = P[D \geq d \mid X = x] = \Phi\left(\frac{\ln(x/c)}{\zeta}\right) \quad \dots (2.6.2 - d)$$

where, the two fragility parameters (median, c, and log-standard deviation ζ) are estimated using the maximum likelihood method. The likelihood function is expressed as:

$$L = \prod_{i=1}^{n} [F(x)]^{k_i} [1 - F(x)]^{1-k_i} \quad \dots (2.6.2 - e)$$

where 'k_i' represents realizations of the Bernoulli random variable K_i and $k_i = 1$ or 0 depending on whether or not the structure sustains the state of damage under intensity x.

Although this methodology of developing a fragility curve is widely used in earthquake engineering, it is not quite suitable for our case. This study, as will be discussed later, required the multiplication of the fragility function with the normalized velocity density function to obtain a single numerical value that could represent the probability of failure. To achieve this, fragility function had to be a probability density function (PDF) instead of a CDF. Also, as mentioned by (Porter, 2021), the lognormal CDF, although widely used, is not a universal function for fragility assessment. To suit authors' particular need, they have chosen logistic regression to fit the fail/safe outcomes, as previously used by (Lee et al., 2007) to derive seismic fragility curves. It should be mentioned here that some researchers like (Anisha et al., 2022; Kosič et al., 2023) have used a direct probability method (using the ratio of the number of trials where the bridges failed to the total number of trials) to derive the fragility curves. However, the use of this third method was optional to the authors as the preliminary study showed that, with sufficient number of simulations, the logistic regression curve approximated the curve obtained by using direct probability method.

Logistic regression (or logit regression) is used for binary variables that take values of either 1 or 0, and the output is the probability bounded between 0 and 1. A logistic model (or logit model) is a statistical model that assumes the log-odds of an event as a linear combination of one or more independent variables. Logistic regression estimates the parameters of a logistic model.

If 'p' is the probability of a certain event occurring, the logit (log-odds) function is obtained by taking the natural logarithm of the odds of occurring the event.

$$Logit(p) = \log(odds(p)) = \log\left(\frac{p}{1-p}\right)$$

This can be transformed as:

$$p = \frac{1}{1 + e^{-logit(p)}} \quad \dots (2.6.2 - f)$$

The general form of the multivariable logistic regression model is the following linear combination:

$$Logit(p) = \beta_0 + \beta_1 X_1 + \beta_2 X_2 + \cdots + \beta_n X_n$$

Therefore,

$$p = \frac{1}{1 + e^{-(\beta_0 + \beta_1 X_1 + \beta_2 X_2 + \cdots + \beta_n X_n)}} \quad \ldots (2.6.2-g)$$

where,

$\beta_0, \beta_1, \beta_2, \ldots \beta_n$ are the regression coefficients.

$X_1, X_2, \ldots X_n$ are the independent variables.

The regression coefficients are determined using the maximum likelihood method, as discussed before with the lognormal CDF method.
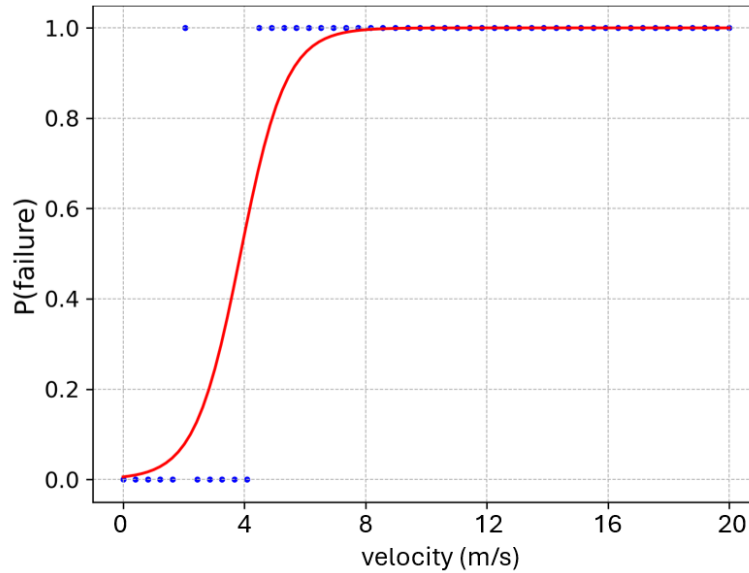

Figure 15: Example of logistic regression

In this study, for each Monte Carlo Simulation (MCS) realization, a random bridge was selected from the cluster. Then a set of values for the required parameters was selected, with uncertain parameters randomly selected from their respective distribution. For a given water velocity, the structural and geotechnical analysis resulted in one Bernoulli outcome- the bridge either fails or remains safe. In probabilistic terms, failure was assigned a value of 1 (certainty of failure) and the safe case was assigned a value of 0 (certainty of safe). Such analysis was performed for 'N' number of equally spaced velocities ranging from 0 m/s to 20 m/s. This range of velocity, as will be discussed later, represented all possible velocities that may occur at any of the bridge sites in the dataset. The accuracy of the curve fitting depends on the number of simulations (N). A higher N would ensure consistent results. The 1's and 0's thus obtained from a sufficiently large number of simulations could be fitted using the logistic regression method. Figure 15 shows an example fragility curve for a particular mode of failure. A series of binary outcomes from the analysis (blue dots) was fitted with a smooth Sigmoid curve.

It should be noted that authors have used only velocity as the IM, which is the single independent variable in the regression model. As mentioned before, in previous literature also, velocity has been commonly used as the independent variable to obtain the fragility curves. Water depth and

debris size were other possible independent variables that could be used together with the velocity in the model. For ease of interpretation of the results, however, the authors have developed multiple independent fragility curves for different water levels and debris sizes. Thus, only velocity was used as the independent variable in the logistic model.

Fragility function can be expressed as follows:

$$F_f = P\big(g(v) \leq 0 \mid (h = h_i)\&(s = s_i)\big) = \frac{1}{1 + e^{-(\beta_0 + \beta_1 v)}} \quad \dots (2.6.2 - g)$$

Where,

$g(v)$ = (capacity- demand) is the limit state function.

h = depth of water expressed as percentage of the pier height.

s = size of debris expressed as percentage of the span length.

This function computes the probability of exceeding the limit state at any velocity (v) for a given water level and debris size.

Logistic models make it easy to describe fragility in terms of the probability of failure. These monotonically increasing curves are easy to interpret and approximate the 'S' shape with comparatively less datapoints (although consistency of the fragility function increases with the datapoints). But like other models, logistic model also has limitations. One major limitation of the logistic model is that it assumes a linear relationship between the log-odds and the independent variables, which may not always hold true. If, in reality, the failure probability is not a smooth S-shaped function (i.e., if there is any unusual behavior at particular values of IMs), then the predictions made using logistic curves might be misleading.

Velocity Distribution

Fragility curves alone do not allow us to draw definitive conclusions, because in reality, for a given water depth, the mean stream velocity can take any value. Therefore, it becomes important to determine at what velocity the probability of failure should be assessed. All possible stream velocities had to be considered in order to infer the extent of vulnerability based on fragility curves. The discussion so far leads us to derive some kind of statistical distribution of velocities that can occur for a particular cluster (or bridge type) at a given water level. Within one cluster, there are several bridges that have various channel widths, pier heights, bed slopes and bed roughness. These variations result in different possible velocities for a given water depth (expressed as a percentage of pier height). The procedure that was adopted to obtain the velocity distribution is explained as follows.

Manning (1889) developed a formula to determine the flow velocity for open channels.

$$v = \frac{1}{n} A R^{2/3} S^{1/2} \quad \dots (2.6.2 - h)$$

Where,

n = Manning's bed roughness coefficient, which depends on the bed material Table 4.

A = wet perimeter of the channel.

R = hydraulic radius, which is expressed as the ratio of wetted area (A) and wetted perimeter (P) of the channel.

S = slope of the channel.

For various bed material types, the Manning's roughness coefficient was obtained using the USGS guidelines (Arcement & Schneider, 1989) as shown in .

Table 4: Manning's roughness coefficient for various soil types.

Bed material	Base n value	
	Straight uniform channel	Smooth channel
Concrete	$0.012 - 0.018$	0.011
Rock cut	$-$	0.025
Firm soil	$0.025 - 0.032$	0.020
Coarse sand	$0.026 - 0.035$	$-$
Fine gravel	$-$	0.024
Gravel	$0.028 - 0.035$	$-$
Coarse gravel	$-$	0.026
Cobble	$0.030 - 0.050$	$-$
Boulder	$0.040 - 0.070$	$-$

To generate the velocity distribution of the bridges in a particular cluster at particular depth of water, parameters A, P, R and S could be determined in a deterministic manner for all the bridges. However, Manning's roughness coefficient 'n', as shown in Table 4, is not deterministic. Therefore, MCS was used to account for the uncertainty in Manning's n. The available bridge data contains bed material type, and from the Table 4, a range of base n values was determined for an idealized straight uniform channel.

For each MCS realization, a random bridge was picked from the cluster, and the velocity was calculated using Manning's equation. The n value was chosen randomly from assumed uniform distribution based on the lower and upper limits found in Table 4. A sufficient number of trials would generate a stable distribution of velocities. Different velocity distributions were obtained for different water levels in each cluster. As an example, fragility function (P_f) and normalized histogram of velocity distribution (V_d) for a cluster at a specific water level is shown in Figure 16.
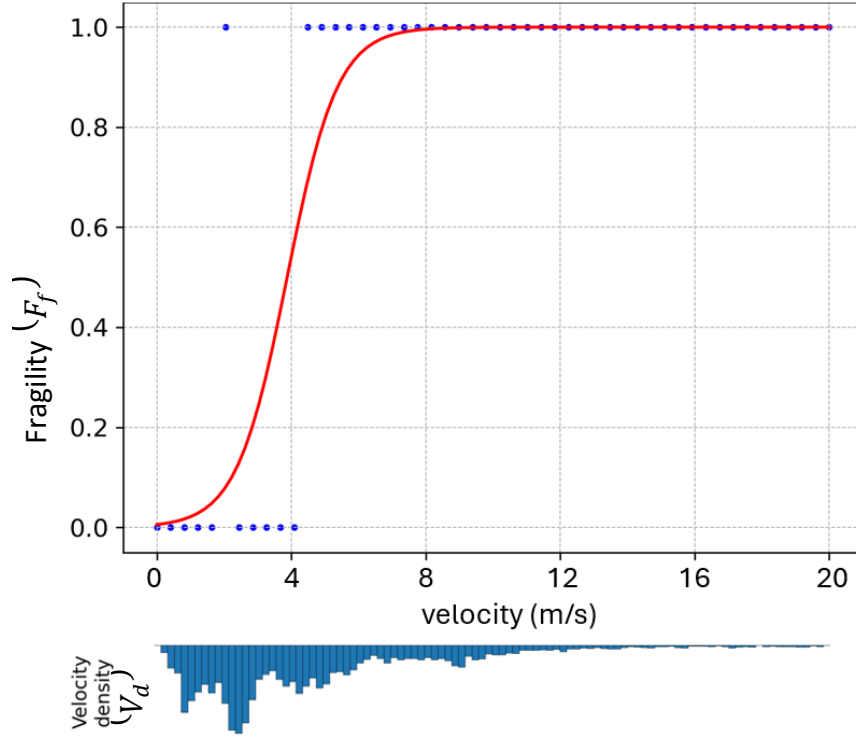
Figure 16: Fragility curve and velocity distribution in a single plot

Since the velocity distribution histogram is normalized, the areas of the histogram bars sum to unity. In other words, the velocity density function V_d represents the probability distribution of velocities in the cluster at a particular water level. Thus, the probability of occurrence of any velocity (area bounded by velocity density function) as well as the probability of failure of bridge at that velocity (fragility function) was determined. The numerical integration of the product of these two functions- V_d and F_f with respect to velocity, results into a single value of probability P_f.

$$P_f = \sum_{v_0}^{v_n} (V_d \times \Delta v) \times F_f \quad \dots (2.6.2 - i)$$

Where,

v_0 and v_n = 0 m/s and 20 m/s respectively in this study.

Δv = velocity step.

This numerical value P_f could be obtained for different failure modes (limit states). The maximum P_f indicates the dominant failure mode. The same process could be repeated to get P_f for different water levels and debris sizes.

2.8 Fragility Analysis for Culverts

Fragility analysis for culverts differs from bridges, especially because of the different kinds of limit state functions that we use for them, and also because of the way authors want to shape the output tables. As mentioned in the objective of this project, look-up tables are targeted as the final output, using which safety and operability of the bridges could be ensured during the emergency time of extreme floods events. In the case of bridges, look-up table would provide a value P_f, which is the probability of failure (roadway overtopping) for a given size of debris and water level. By reading the debris size and water level, one can decide whether it is important to close the bridge operation, remove debris as soon as possible, take any immediate actions to divert the flood water at bridge site, etc. in order to mitigate the flood damage to the bridges. However, when it comes to culverts, the water level itself is the mark of failure. If a certain size of debris clogs the culvert barrel, the water level at inlet increases gradually, and if the increased head is not able to discharge out the incoming water, it will not take much time to overflow the roadway. Thus, there won't be time available to react once a certain debris size and discharge level exists at culvert site. Therefore, authors couldn't use debris size and discharge level as the fragility-reading parameters as was done in the case of bridges. Instead, some technique could be developed to tell the probability of failure of a culvert based on the return period of flood. Discharge uniquely corresponds to a return period, and hence, flood discharge could be used as the intensity measure.

Previous research like (Ahamed et al., 2021; Pucci et al., 2023) have used discharge as intensity measure. The probability of failure of culvert for a certain discharge 'Q' (corresponding to return period 'T') can be obtained by using the basic probability concept as previously used by (Anisha et al., 2022; Kosič et al., 2023) in their work.

$$F_f = P(y \geq h \mid T = T_i) = \frac{N_{y \geq h}}{N} \quad \dots (2.6.2 - j)$$

where,

y = depth of water in the upstream side (m)

h = height of roadway measured from the invert of culvert (m)

T = return period (years)

$N_{y \geq h}$ = number of trials at which limit state exceeds

N = total number of trials

For each trial, a culvert was picked from the dataset following the principle of MCS. The data of height of roadway 'h' was not available for the culverts in the dataset. Using the h of one representative culvert may not be an accurate choice as 'h' could vary among culverts based on local topography. Therefore, h was needed to be estimated based on design guidelines from Hydraulic Manual, VTrans (Wark et al., 2015). 'h' could be expressed as the sum of two parameters- culvert rise or barrel/culvert height h_b and earthen fill height h_f.

To estimate the barrel height h_b, design return period of 50 years was used to first calculate the allowable head h_a. As per the hydraulic criteria for allowable headwater at culverts mentioned in the manual,

$$h_b \geq \frac{h_a}{1.2} \quad \dots (2.6.2 - k)$$

It was assumed that $h_b > 36\ inches$, which is a more conservative case. The fill height could be found by simply deducting the barrel height from the channel depth h_0.

$$h_f = h_0 - h_b \quad ...(2.6.2 - l)$$

However, most of the channel depths in the dataset were unknown. For those cases, fill heights could be estimated using the guideline in the manual, which states that the closed bottom structures were to be embedded to 30% of the height of the opening.

$$h_f = 0.3 \times h_b \quad ...(2.6.2 - m)$$

The assumptions made here may not accurately represent the real scenario. However, the manual is believed to provide good approximation on how culvert elevations are proportioned in design practices. Nevertheless, for future works, it is highly recommended to use real barrel height and channel depth data obtained by actual survey of the culvert sites. Moreover, in our assumption, we have neglected the variation of channel side slopes with the channel depth. Inundation can occur well before road overflow if roadway elevation is higher than flood plain elevation. Therefore, in the future, these design-based data results are expected to be backed up by real survey-based data results.

Effect of Debris

In hydraulic design of culverts, certain return period (typically 100-yrs (Schall et al., 2012)) was considered. The reason culvert could fail in roadway overtopping well before a design discharge is due to the presence of debris. Debris accumulation at the inlet or inside the barrel reduces the barrel cross-section. According to the continuity equation, the velocity in the barrel must increase in order to balance the inflow and outflow of flood water. Further, to increase the velocity, the driving hydrostatic head must be higher. In such way, presence of debris could lead to the roadway overtopping failure of culverts.

Since increase in the upstream water level is related to the debris blockage, prediction of prediction of debris size becomes a crucial step in the fragility assessment. The following discussion is two-fold. First, the extent of culvert blockage that usually occurs during floods is discussed. And then, the upstream depth is related with the blockage.

The degree of blockage was be measured as the ratio of area blocked by the debris to the total cross-sectional area of the culvert barrel. 0% blockage referred as an unblocked culvert, while 100% referred as a fully blocked culvert. Until now, the author has not found any established relationship between the discharge and degree of blockage. In the study by (Rigby et al., 2004), the debris impact on 63 culverts in 1998 flood in Wollongong, Australia was surveyed. The results give insights into the degree of blockage among the surveyed culverts. Table 5 is obtained from that study.

Degree of Blockage %	Percent of structures
$0 - 10$	44
$11 - 40$	17
$41 - 60$	5
$61 - 90$	6
$91 - 100$	28

Accumulation of debris at culvert inlet depends on multiple uncertain factors including upstream vegetation fragilities, discharge level, water velocity and turbulence, entrapment probability, etc. With no established wholistic research on this direction, the accumulation of debris was assumed to be a stochastic process, independent of discharge return period. A probability distribution based on such observed after-flood debris status was adopted.

Once the degree of cross-section blockage was obtained, the next job was to predict the level of water increased due to the reduced inlet area. In this regard, energy balance equation recommended by FHWA (Schall et al., 2012) for culvert designs could be used. Figure 17 shows the head losses during flow in the culvert barrel. During full barrel flow, if H_i and H_o are the energy heads at inlet and outlet respectively, H_{Loss} is the head loss, the energy equation can be written as:

$$H_i = H_o + H_{Loss} \quad ... (2.6.2 - n)$$

Inlet and outlet heads can be expressed as the sum of hydrostatic, velocity and elevation heads.

$$(H_{ih} + H_{iv} + H_{ie}) = (H_{oh} + H_{ov} + H_{oe}) + H_{Loss} \quad ... (2.6.2 - o)$$

Here, the difference between H_{iv} and H_{ov} can be assumed to be negligible because of the fact that upstream water level is limited to the roadway elevation, and hence the channel flow cross section will not be significantly large. Elevation difference $(H_{ie} - H_{oe})$ was calculated using slope of channel 'S' and length of barrel 'L'.

$$\boldsymbol{H_{ih} = H_{oh} + H_{Loss} - L \times S} \quad ... (2.6.2 - p)$$

We can calculate H_o using Manning's equation. Head loss was obtained from the following formula.

$$H_{Loss} = \left[1 + K_e + K_u \frac{n^2 L}{R^{1.33}} \right] \frac{v^2}{2g} \quad ... (2.6.2 - q)$$

where,

K_e = entrance loss coefficient

K_u = a constant for unit conversion (19.63 for SI unit)

n = manning's roughness coefficient (0.11 for smooth concrete USGS guideline (Arcement & Schneider, 1989))

R = hydraulic radius (ratio of wetted area to wetted perimeter)
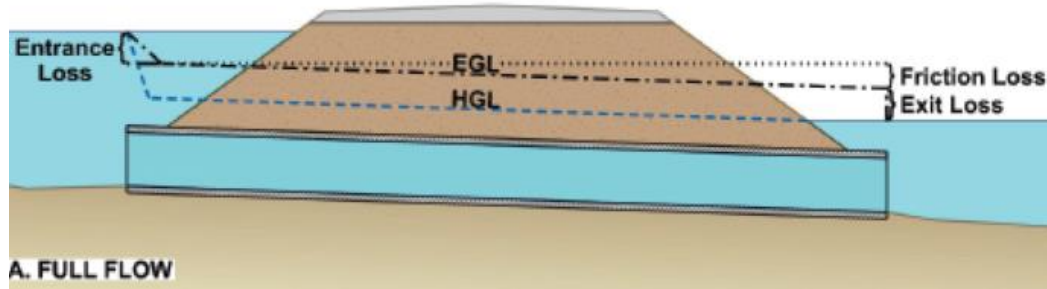
Figure 17: Head losses in pipe flow (Schall et al., 2012)

Once discharge for a certain return period 'T' was obtained, in order to calculate the upstream depth, the only unknown parameter was the entrance loss coefficient 'K_e'. This constant should depend upon the blockage degree. The author did not find any literature that provides K_e particular for culverts when riparian debris blockage was considered. So, in order to fill this gap, the empirical results were used. (Sellevold et al., 2024) performed an experiment to determine the entrance loss coefficient for various blockage percentages. Among various blockage shapes used in the experiment, the square edge best represents the floating debris. As seen in the Figure 18 below, the relation between the entrance loss coefficient (related to the barrel velocity) and the blockage degree (ratio) was approximately linear which can be expressed as:

$$K_e = 1.405 \times (A_b/A) + 0.5$$
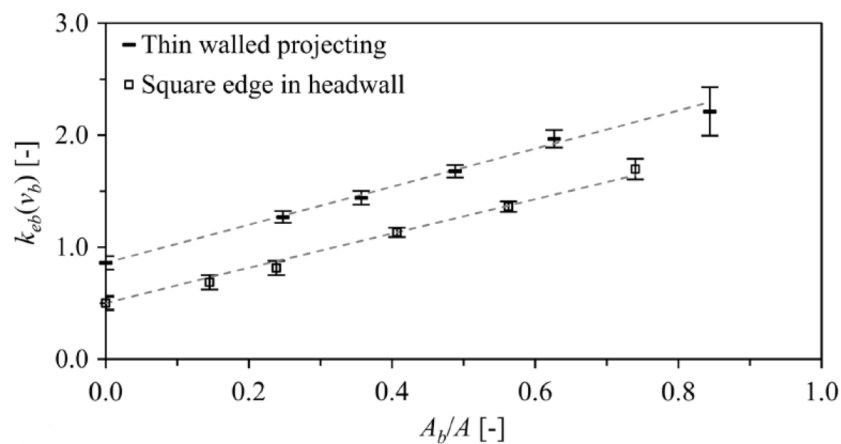
Figure 18: Relationship between entrance loss coefficient and blockage ratio (Sellevold et al., 2024).

During floods, if the water level doesn't exceed the barrel height, there is low risk of debris accumulation to the size which would cause the backwater to overtop the road. (Rigby et al., 2004; Schall et al., 2012). Mostly, the overtopping is caused when the flood discharge is higher than the design discharge for which culvert is designed to safely pass the flood water through it. As mentioned in the (Rigby et al., 2004) that among the surveyed structures, most culverts and bridges diverted flood water from their normal stream channels to residential and commercial areas because of the high volume of flood water at the culvert and bridge sites. For these reasons, in this

study, it is assumed that if the flood water was low enough that it didn't even submerge the barrel, then debris blockage is insignificant and road overtopping was not expected.

There are two major limitations of using the K_e values from the above discussed experiment reference. That experiment was done on circular culverts of relatively small size. However, authors assumed that it is equally applicable for rectangular box culverts. In addition to that, 'bottom-up' nature of blockage has been used in this experiment. Although (Rigby et al., 2004) observed mostly 'top-down' nature of blockages caused floating vegetation, there is no established entrance loss study for top-down blockage. Bottom-up blockage usually happens due to progressive buildup of sediment scoured from upstream bed and banks. Although the blockage degree remains the same, the difference in the value of K_e for the two cases (bottom-up and top-down blockages) can result out of the different nature of turbulence caused by them at inlet. Therefore, for future works, it is recommended to do further research on debris top-down blockage on box culverts for a more accurate prediction of K_e. Furthermore, rather than standard blockage shapes, study of stochastic nature of debris shapes that could occur at culvert inlet is also encouraged.

In this study, the dataset is limited only to the multi-span structure mainly because of our analysis focused on debris accumulation and scour at the piers. However, since culverts limit state is only about the roadway overtopping, it is informed here that the single span culverts could also be equally included in this analysis without any further modification in this methodology.

Chapter 3: Results and Discussion

The results are organized into different sections. First, the clustering results are obtained where bridges are optimally divided into six clusters. Next, velocity distribution and simulation sensitivity are discussed. Then, fragility curves for each of the clusters for different water levels are presented. And finally, the output is summarized in look-up tables along with some major limitations of this study.

3.1 Clustering Results

To select the best representative bridge classes and corresponding characteristics, the *K*-prototypes clustering technique was applied to group these bridges based on key features while considering the correlations between these parameters. As the structure material and design type were categorical in nature, while total length and average span length were numerical variables, the *K*-prototypes method was utilized.

The clustering analysis was carried out in Python using the *KPrototypes* function in the *Kmodes* package (Nelis J. de Vos.). To test the optimal cluster size, the bridges were clustered with cluster size K ranging from 2 to 10, with the optimal cluster size investigated using BIC. In addition to the number of clusters K, the weight parameter γ was also adjusted with the goal of creating intuitive clusters which can be easily interpreted and correlate with typical bridge classifications. For example, it should be expected that short-span concrete culverts and long-span steel girder bridges should be clustered separately, and that of the mentioned features, the material and design type should have more weight in determining the grouping than the span length. By varying γ, the categorical and numerical features were given different weightings, and based on the results, the appropriateness of the clusters was checked. Finally, the most appropriate clusters were obtained using γ = 5 and K = 6 based on the smallest BIC value. By adding more weights, the K-prototype algorithm can cluster the bridges in a more intuitive way, while other methods which cannot apply differential parameter weighting may not be able to differentiate the bridge types as effectively.

The six optimal clusters, along with the characteristics of each cluster's centroid, are presented in Table 6, while the pie chart in Figure 19 shows the percentage of data in each cluster. Based on the predominant characteristics, each cluster was assigned a representative name. Three clusters were found to be comprised almost entirely of steel, indicating a large variability in the steel bridge designs and lengths, which was expected considering about 69% of the studied bridges are steel. These bridges were further subdivided based on their span length into short, medium, and long bridges, with the most representative total span lengths, i.e., the centroid of each cluster, as about 50, 100, and 250 m, respectively. By applying the clustering, these subsets of bridges are unveiled, along with their predominant characteristics, and the different bridges can be accordingly grouped. Similarly, concrete bridges were grouped into two major categories, differentiated primarily based on the design type, as concrete culverts and concrete tee beams, with tee beams typically longer than culverts. The strengths of the clustering algorithm are again highlighted in the ability to break down the concrete bridges into two distinct subclasses. Finally, a sixth cluster, corresponding to wood truss bridges, was unveiled. These bridges are distinctly separate from the other bridge types both in terms of material and design type, and although these are rare, comprising only 2% of all bridges, the clustering algorithm was still able to detect this category due to the heightened weighting on the categorical variables. This is a critical model benefit as such bridges may have distinctly different failure modes and forces. For instance, such historic wooden covered bridges

may be more vulnerable to wind and could therefore require a more robust wind analysis than a steel girder overpass bridge.

Table 6: Bridge clusters centroids

Cluster ID	Material	Structure Type	Average Span Length (m)	Total Structure Length (m)
Short-Span Steel	Steel	Stringer/multi-beam or Girder	20.33	51.76
Medium-Span Steel	Steel	Stringer/multi-beam or Girder	38.28	104.88
Long-Span Steel	Steel	Stringer/multi-beam or Girder	54.00	246.48
Concrete Culverts	Concrete	Culvert	5.64	12.24
Concrete Tee Beam	Concrete	Tee Beam	14.82	34.08
Wood Truss	Wood	Truss	36.60	76.13
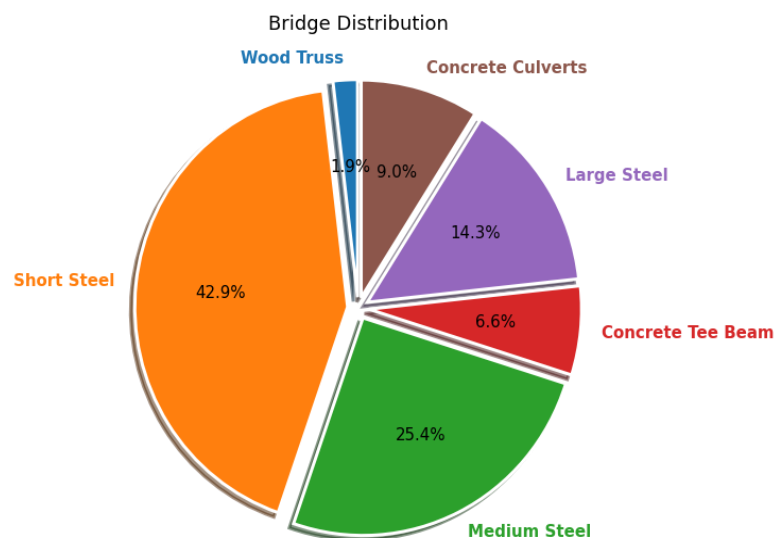
Figure 19: Breakdown of different bridge types in optimal clusters

Based on the defined clusters, the most representative bridge of each category, as defined in Table 7, can be selected to represent the geometry model for larger population of bridges in the clusters. In this case, the most representative bridges were chosen based on their distance from the centroid as defined within the K-7 prototypes algorithm. Figure 20 shows the breakdown of the bridge types throughout the state and highlights the location of the most representative of each of the six selected bridge types. Some photos of the representative bridge types are shown in Figure 21 for demonstration purpose. The differences between the different bridge types are clearly highlighted,

emphasizing the need for appropriate classification to properly model the bridges. For instance, the concrete culvert could experience different failure modes and vulnerabilities than a steel girder bridge.

Table 7: Most representative bridges within database selected for modelling references

Bridge ID	Cluster ID	Material	Structure Type	Average Span (m)	Total Structure Length (m)
200211001404082	Short-Span Steel	Steel	Stringer/Multi-beam or Girder	17.57	52.7
200016006614182	Medium-Span Steel	Steel	Stringer/Multi-beam or Girder	35.37	106.1
200089017N14172	Long-Span Steel	Steel	Stringer/Multi-beam or Girder	63.55	254.2
207000012703112	Concrete Culvert	Concrete	Culvert (includes frame culverts)	6.4	12.8
200120004L02052	Concrete Tee Beam	Concrete	Tee Beam	16.45	32.9
100514B01705141	Wood Truss	Wood	Truss	40.55	81.1
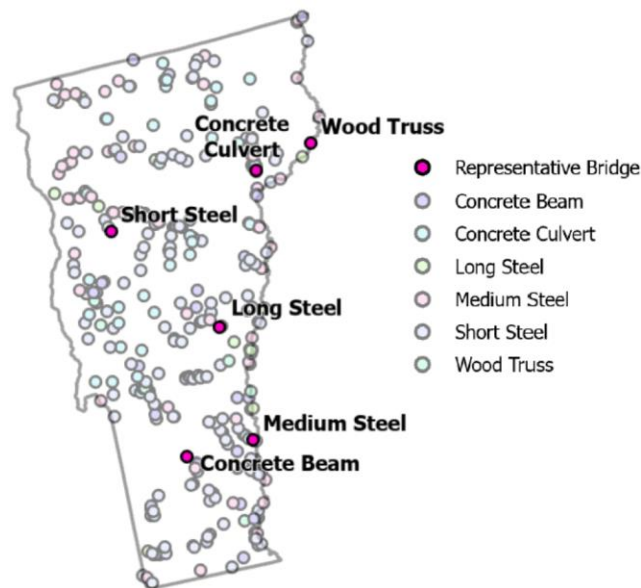
Figure 20: Spatial distribution of bridges in Vermont and the most representative of each type

Figure 21: Examples of selected optimal representative bridges of concrete tee-beam (left), concrete culvert (middle), and short-span steel (right) bridges

3.2 Velocity Distribution

Using MCS, the distribution of flood water velocity that may exist at different water levels is presented for separate clusters in Figure 22. As a preliminary study, the number of MCS 'N' were gradually increased to see the sensitivity of N on the velocity distribution. It was concluded that 500 simulations are needed to obtain a consistent distribution. All the histograms are normalized.

1(a)

1(b)

1(c)

2(a)

2(b)

2(c)

3(a)

3(b)

3(c)

4(a)

Velocity Density
(cluster 4, 1.0_depth)

4(b)

Velocity Density
(cluster 4, 1.0_submerged_depth)

4(c)

Velocity Density
(cluster 5, 0.75_depth)

5(a)

Velocity Density
(cluster 5, 1.0_depth)

5(b)

Velocity Density
(cluster 5, 1.0_submerged_depth)

5(c)

Velocity Density
(cluster 6, 0.75_depth)

6(a)

6(b)   6(c)
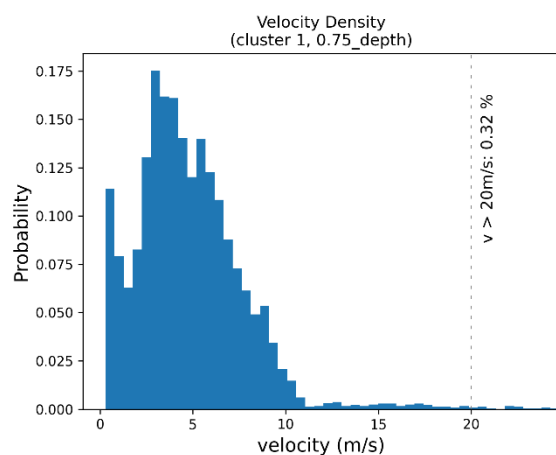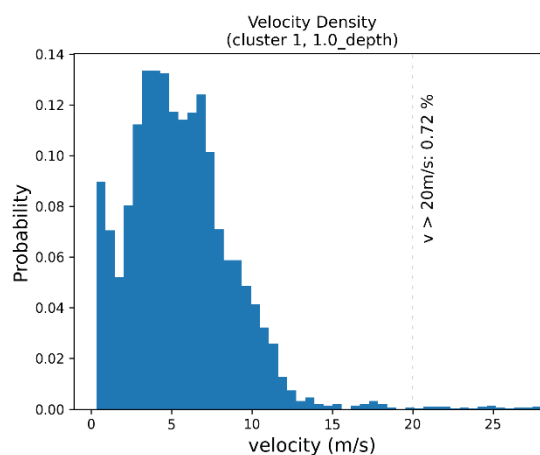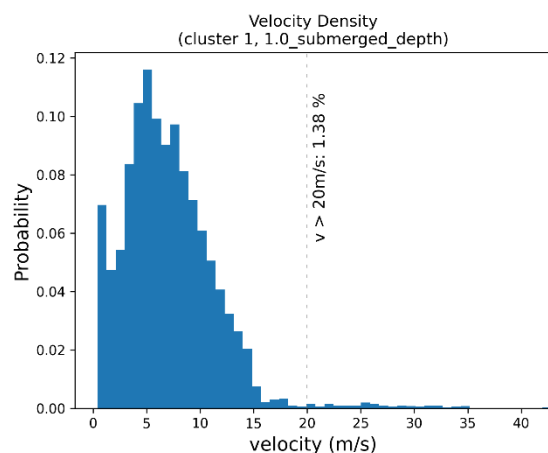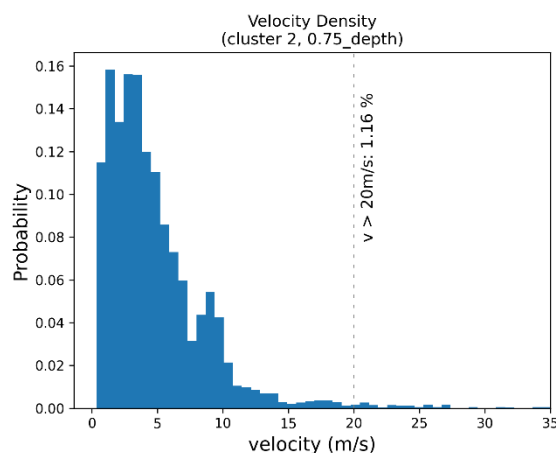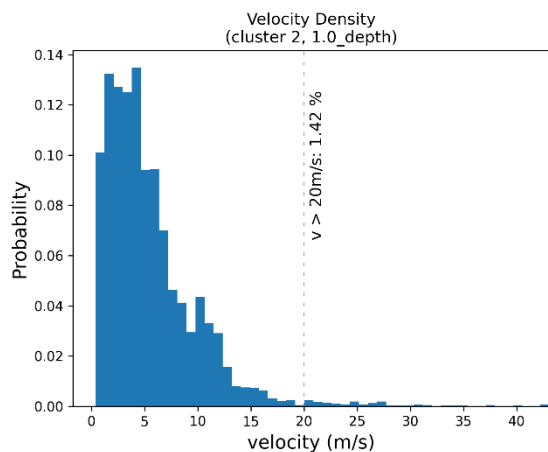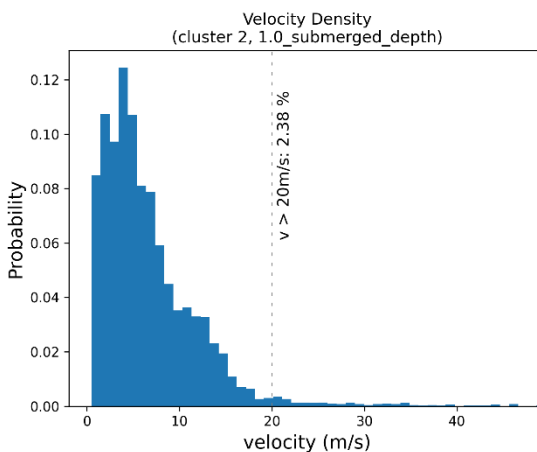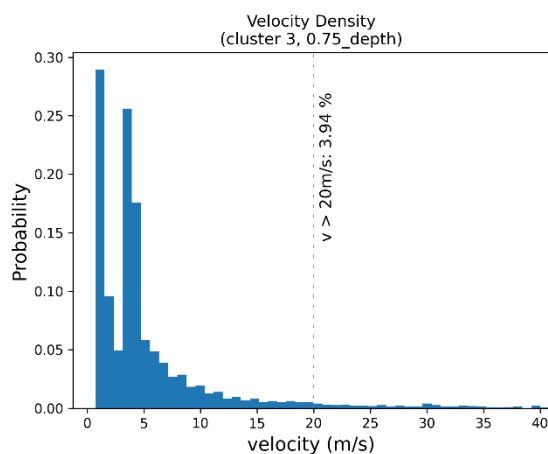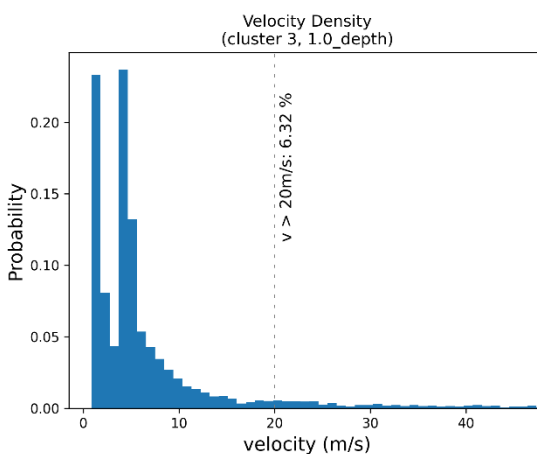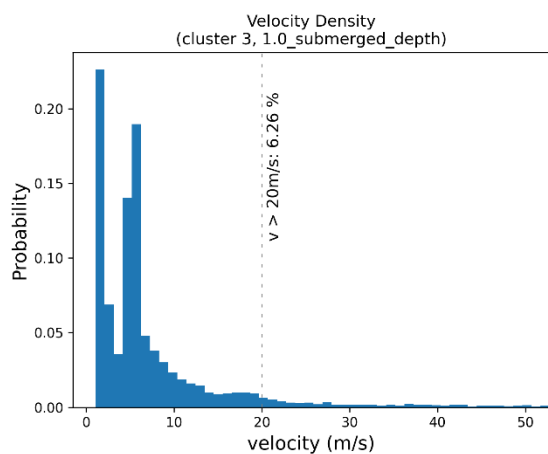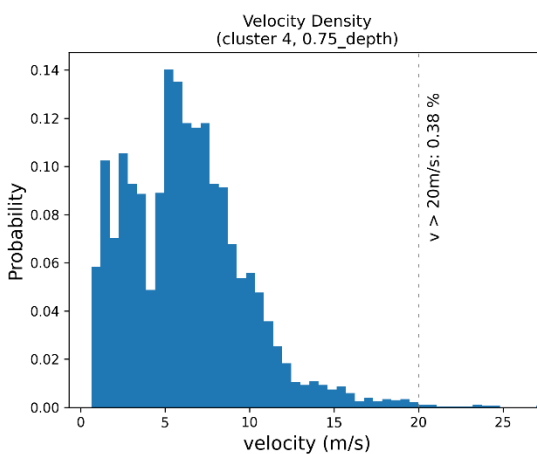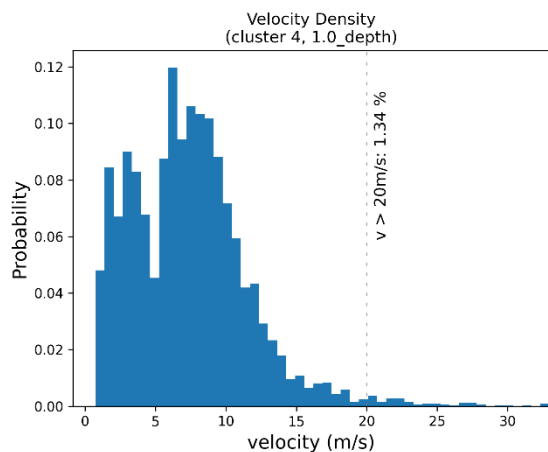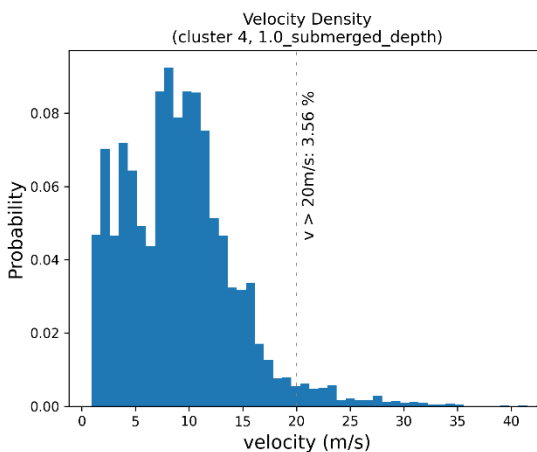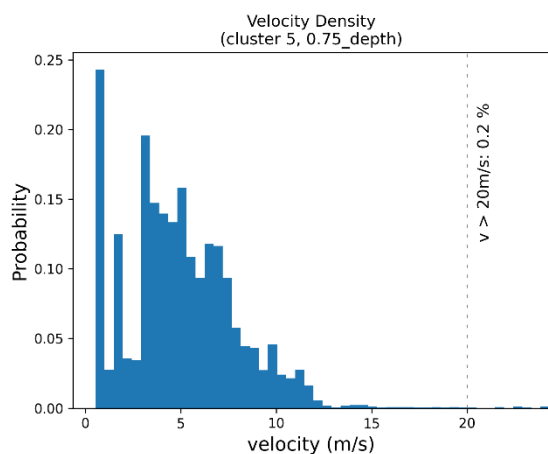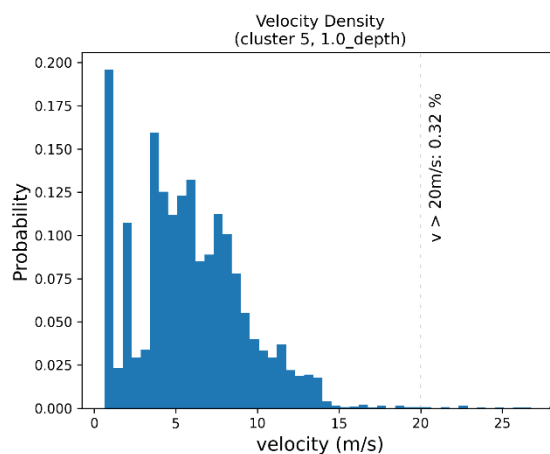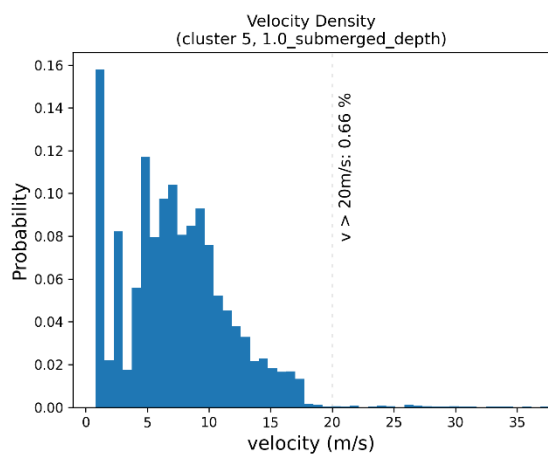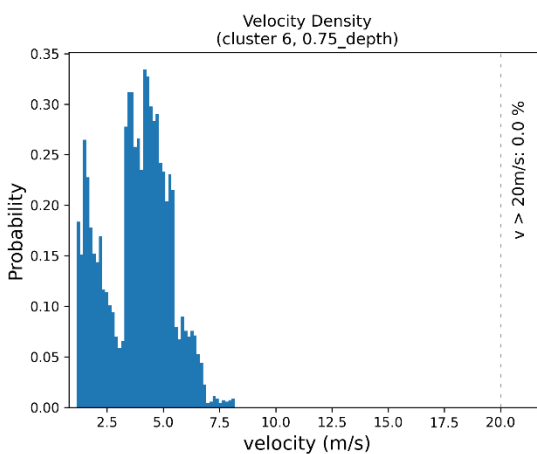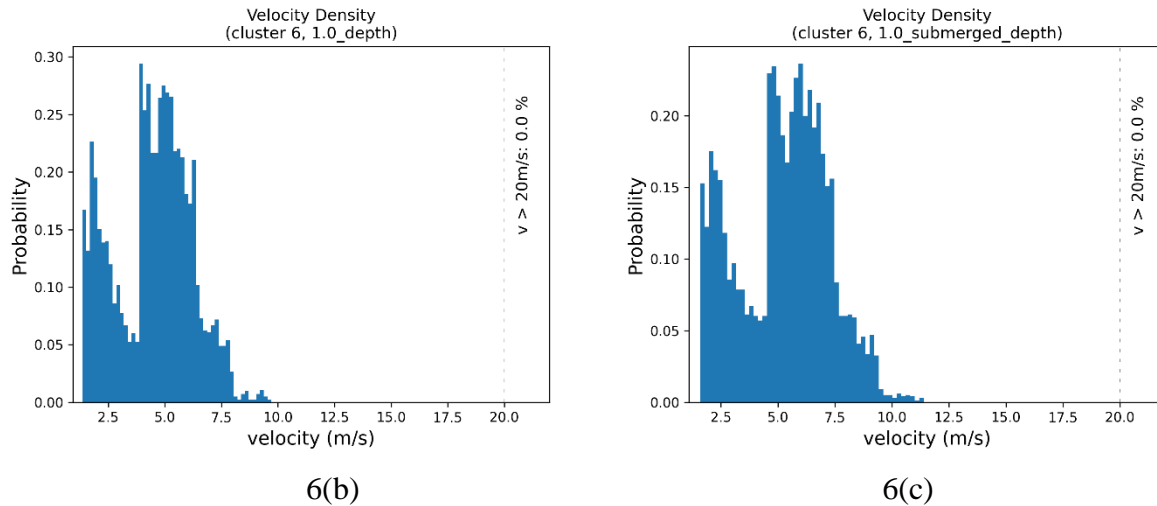
Figure 22: Velocity density for different water levels for each cluster. Clusters- 1,2,3…6. Water levels- (a) 75% pier height, (b) 100% pier height, (c) deck submergence.

In each plot, the probability of exceeding the velocity by 20 m/s is written adjacent to the dashed vertical line. It can be seen from the plots that in all the cases the chance that velocity exceeds 20 m/s is very low. Neglecting this high range of velocity in the fragility analysis can be justifiable. This low percentage of the data won't affect the numerical integration results (P_f) significantly. If we look at the plots above, a little higher percentage of such rare velocity can be found to be in the long span steel bridges at high water level. Usually in the long span bridges, as the detail drawings of the representative bridge suggest, the piers are usually very tall, and the area under the bridge is large, and therefore the free board is high. In such a case, the extreme water level like deck submergence is a highly unlikely event. However, for the future motivation, this reasoning can be more detailly investigated by calculating the discharge based on practically high return period at the bridge sites. In case the high velocity (>20m/s) exists, the output table can be readily updated adding the percentage of the high velocity to P_f because we can conservatively approximate the 'S' shaped fragility function to be close to 1 at very high velocity.

3.3 Simulation Sensitivity

The sensitivity of the fragility curves with respect to the number of simulations is important. The accuracy of the regression curves was improved by increasing the number of simulations, but it is well understood that the simulation time is directly proportional to the number of simulations. Therefore, to decide the optimum number of simulations, we ran a few trial simulations to study the sensitivity of simulations on the shape of the fragility curves. Cluster number 2 with water level exceeding the pier height was chosen so that sensitivity in all of the limit states could be visualized.
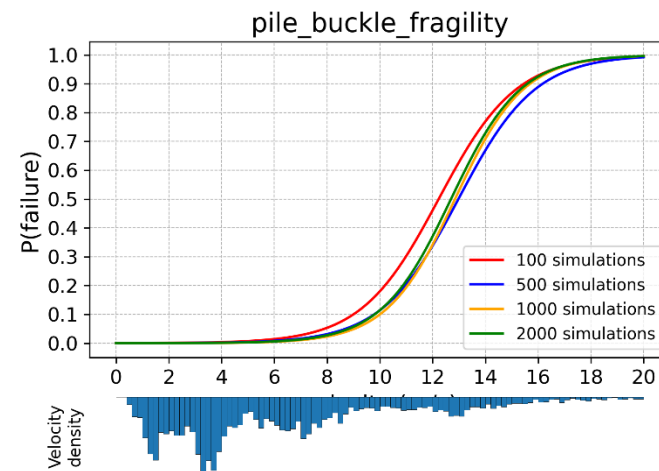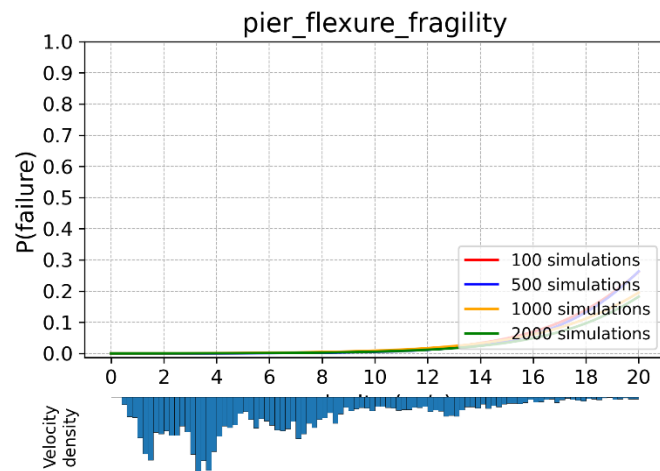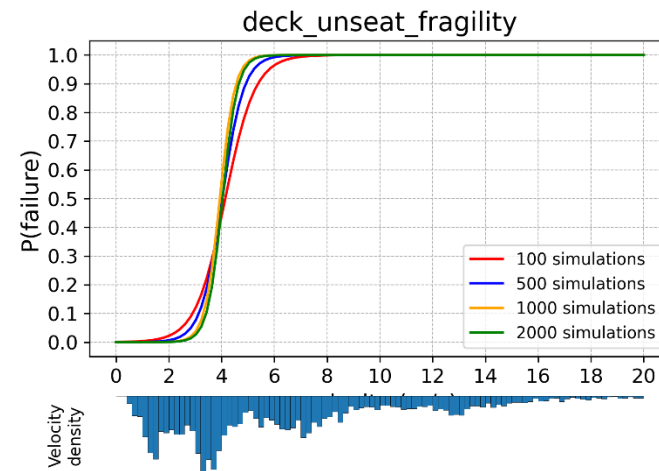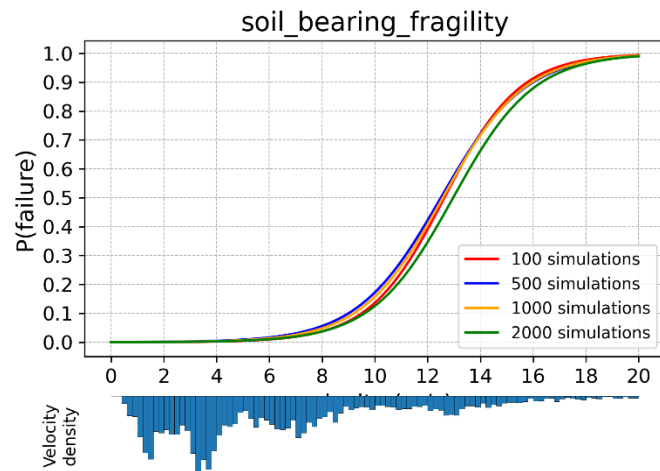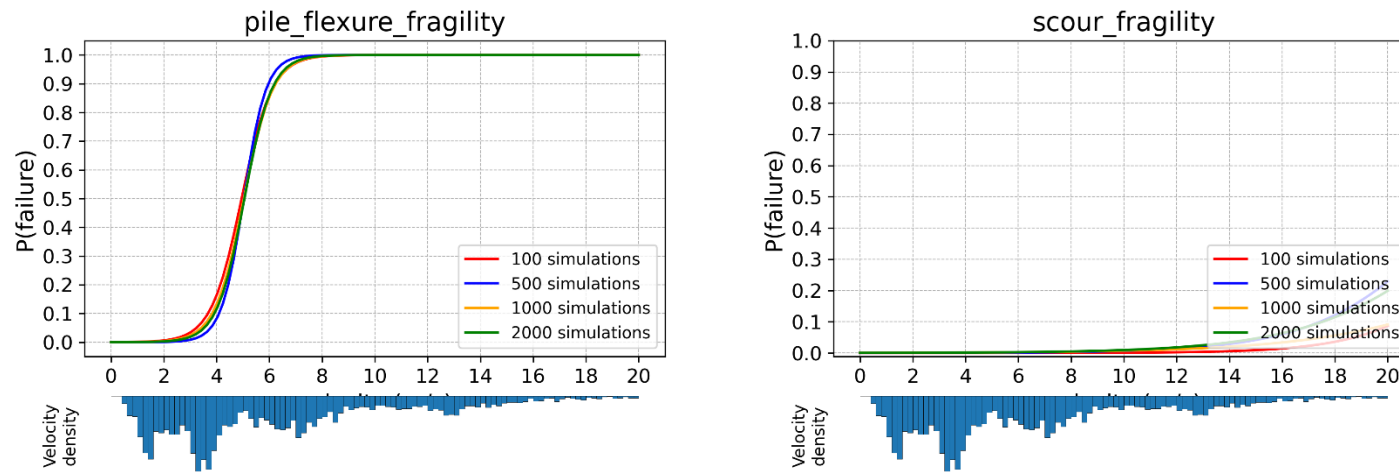
Figure 23: Sensitivity of fragility curves to the number of simulations (N)

As we see in Figure 23, as the number of simulations increases, the discrepancy between the curves minimizes. 100 number of simulations is not acceptable as it tended to deviate significantly. 500 simulations curves is good approximation but in case of deck unseating and pile buckling fragility, it is little off. If we compare 1000 and 2000 number of simulations, there is not much improvement. That's why, 1000 was chosen as the optimum number for the MCS.

3.4 Cluster-1 (short-span steel) Fragility Curves

The first cluster represents short-span steel bridges. Fragility curves for various water levels and debris size for cluster-1 bridges were obtained. The curves for all the discussed limit states are presented below in Figure 24.
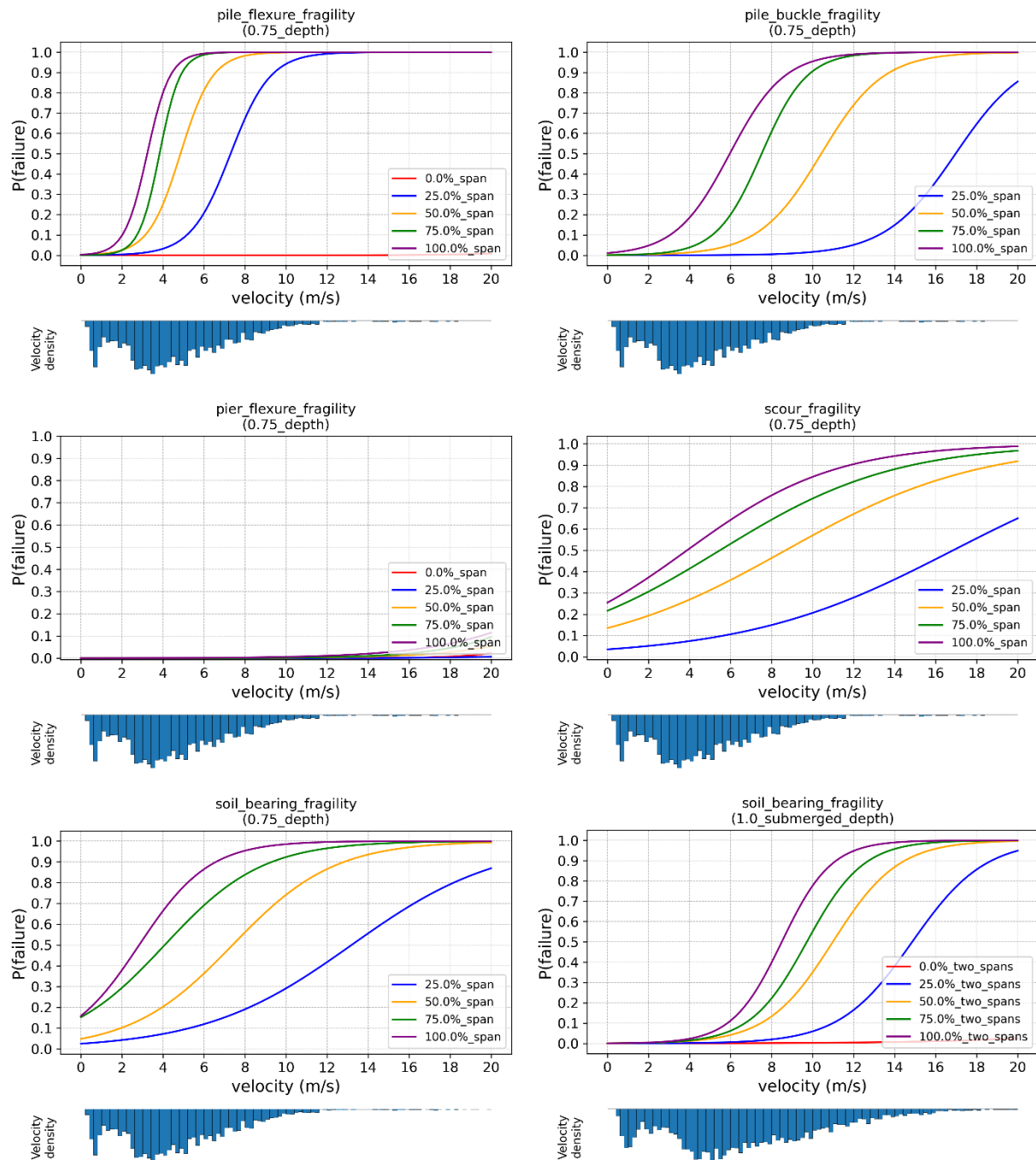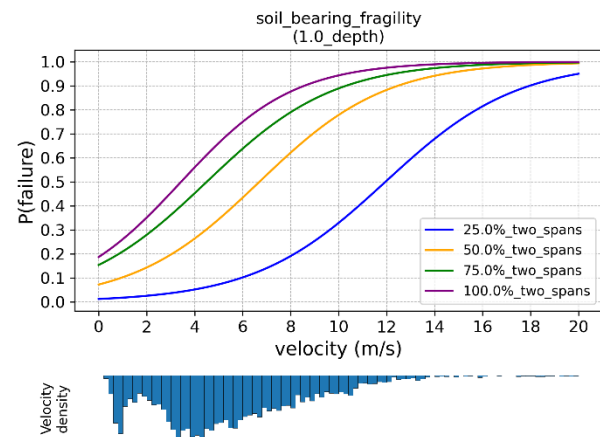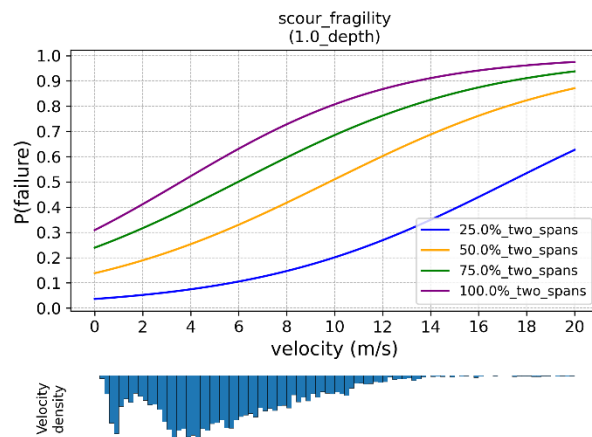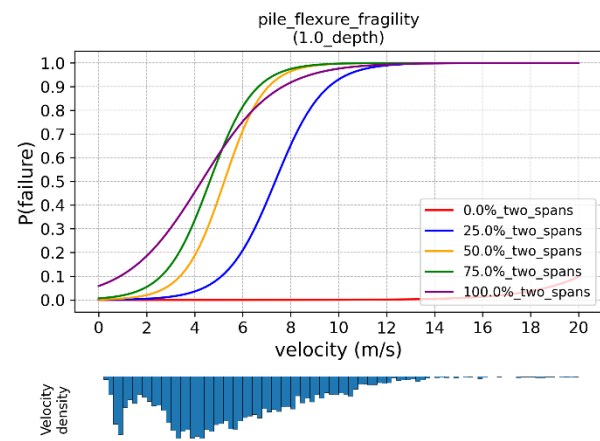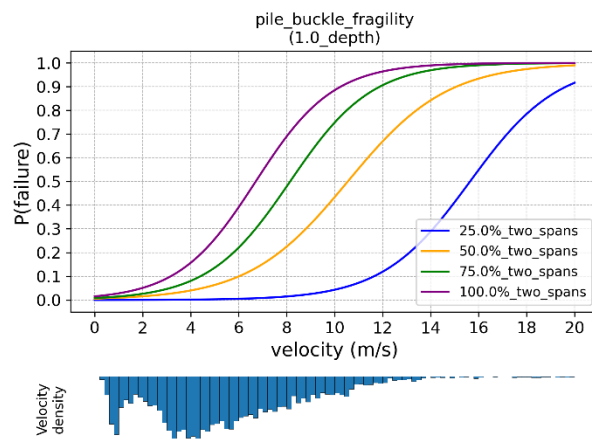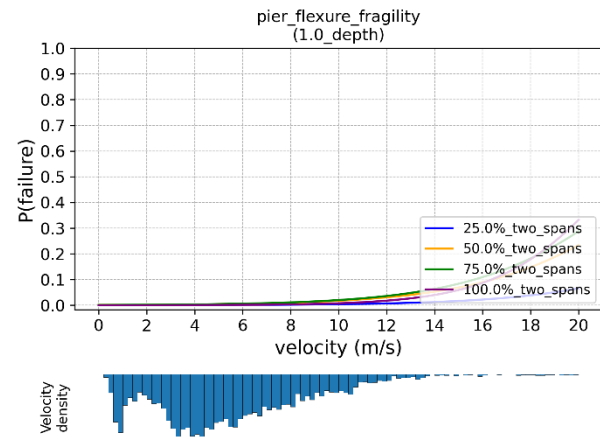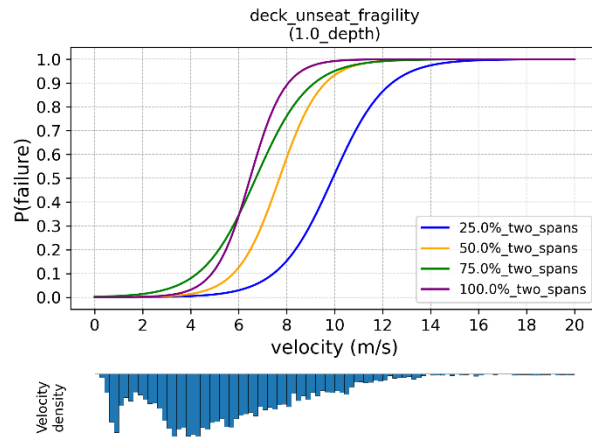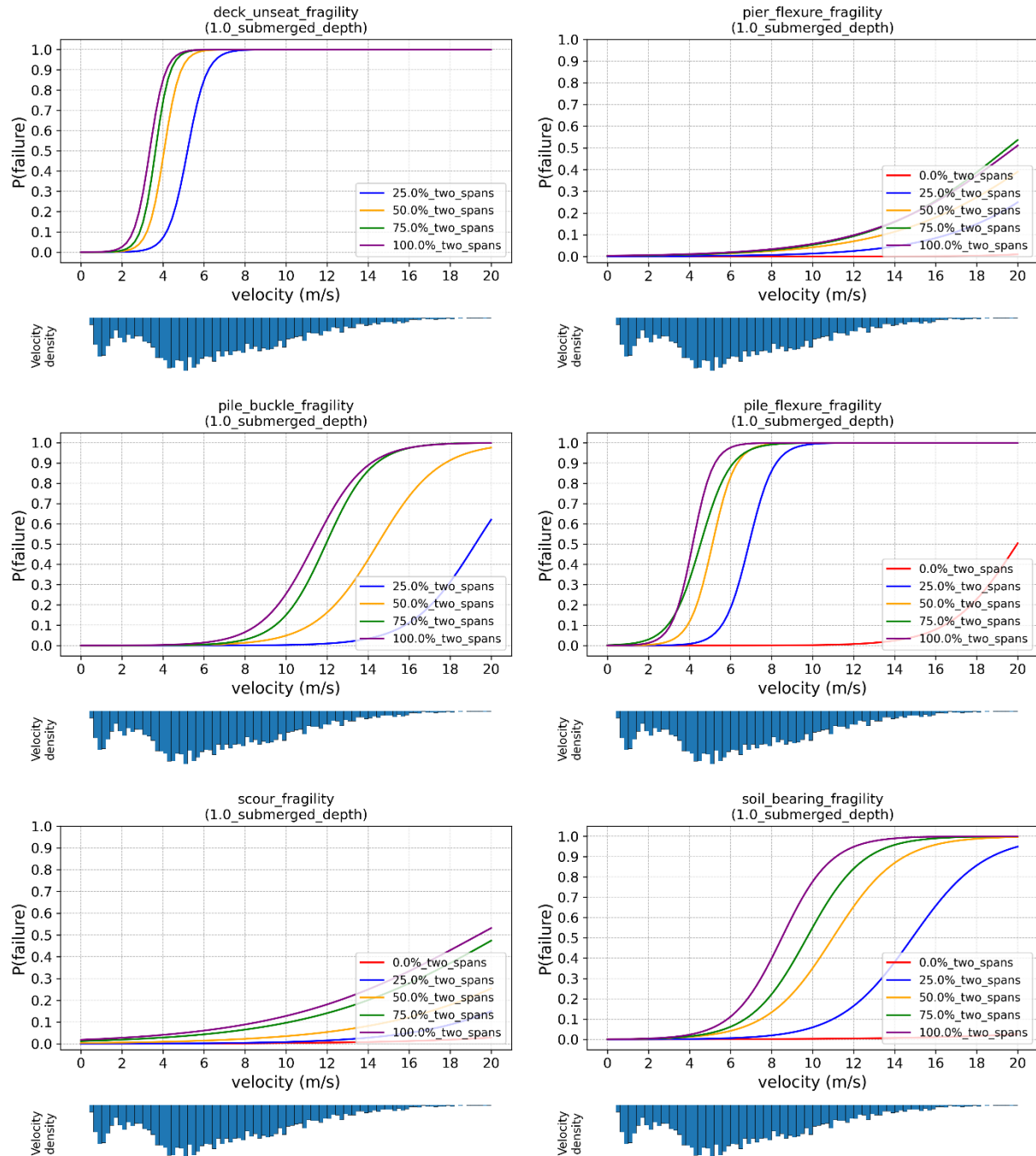
Figure 24: Cluster 1 (short-span steel) Fragility curves

Table 8: Cluster-1 P(failure) when depth = 75% of pier height

Debris (% span)	Deck unseating	Pile flexure	Pile buckle	Pile shear	scour	Soil bearing	Pier flexure
0%	0	**0**	0	0	0	0	0
25%	0	**0.1929**	0.0063	0	0.0933	0.1048	0.0001
50%	0	**0.4341**	0.0704	0	0.3077	0.2825	0.0006
75%	0	**0.5706**	0.1847	0	0.4518	0.536	0.0007
100%	0	0.661	0.3336	0	0.5424	**0.6647**	0.002

Table 9: Cluster-1 P(failure) when just submergence of pier

Debris (% span)	Deck unseating	Pile flexure	Pile buckle	Pile shear	scour	Soil bearing	Pier flexure
0%	0	**0.0005**	0	0	0	0	0
25%	0.1129	**0.2722**	0.0177	0	0.1073	0.1232	0.0018
50%	0.2374	**0.48**	0.1373	0	0.3158	0.3936	0.0077
75%	0.3337	**0.5529**	0.2487	0	0.4709	0.5557	0.0087
100%	0.34	0.5875	0.3563	0	0.5862	**0.6431**	0.0037

Table 10: Cluster-1 P(failure) for deck submergence

Debris (% span)	Deck unseating	Pile flexure	Pile buckle	Pile shear	scour	Soil bearing	Pier flexure
0%	0	**0.0044**	0	0	0.0026	0.0021	0.0001
25%	**0.6156**	0.4385	0.0061	0	0.0063	0.0527	0.0099
50%	**0.7446**	0.6246	0.0523	0	0.0241	0.1755	0.0286
75%	**0.7875**	0.685	0.1122	0	0.0648	0.2373	0.0363
100%	**0.8103**	0.7306	0.1427	0	0.086	0.3167	0.0391

The probability values are written in Table 8-10 for various limit states. The most likely failure mode of a bridge will be the one with highest value of P(failure). Therefore, a new table will be shown later based on the maximum values of P(failure) among various failure modes for each of the debris size in each of these water levels. The result will be the look-up table. Such tables for each of the clusters will be presented at the end.

It can be easily seen in the plots that when water level increases, the sigmoid curves for various failure modes shift towards lower velocity, indicating increased vulnerability. As can be observed in the Tables 8-10, when the water depth is 75% and 100% of the pier height, mostly, the pile flexure fragility has the highest probability of failure (P_f) indicating the foundation failure to be

the dominant mode of failure. However, when the water level increases beyond pier height, the unseating of deck becomes the most important mode of failure. In all the cases, the probability of pier flexure failure is insignificant. This can be attributed to the high second moment of area of the pier section about the bridge axis. Also, pile shear fragility is the least significant one among all.

The presence of debris is quite significant. As the debris size increases, the projected area of obstruction to the water current increases and therefore the hydrodynamic force on the bridge increases. This eventually increases the risk of bridge failure. As debris size increases from 0% to 100% of the span length, the fragility in all the failure modes increases quite rapidly.

It should be noted here as the limitation of the logistic regression that especially in the cases of excessive scour depth failure and soil bearing capacity failure, there is non-zero probability of failure near the zero velocity. Practically, this does not make any sense because a bridge can't fail in the above discussed failure modes when the water is still. This can be attributed to excessive randomness in the distribution of the data points (binary- 1's and 0's). And therefore, there is underfitting of such dataset with the sigmoid curve. In most of the other cases, there exists a narrow cutoff velocity range, which is greater than 0 m/s, from where there is tentative transition from safe mode (0's) towards failure mode (1's).

A more distilled and readable table is presented in the 'Look-up Table' section.

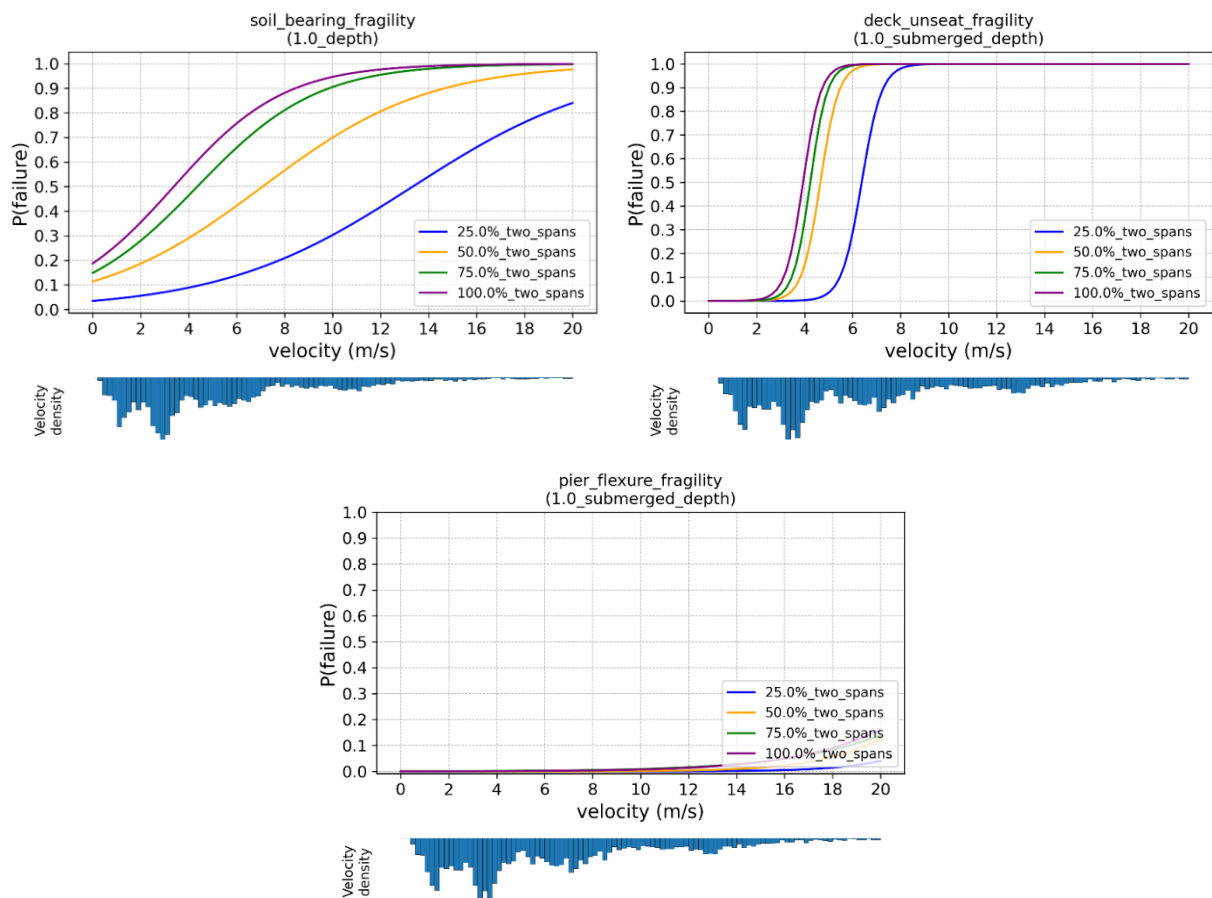## 3.5 Cluster-2 (medium-span steel) Fragility Curves
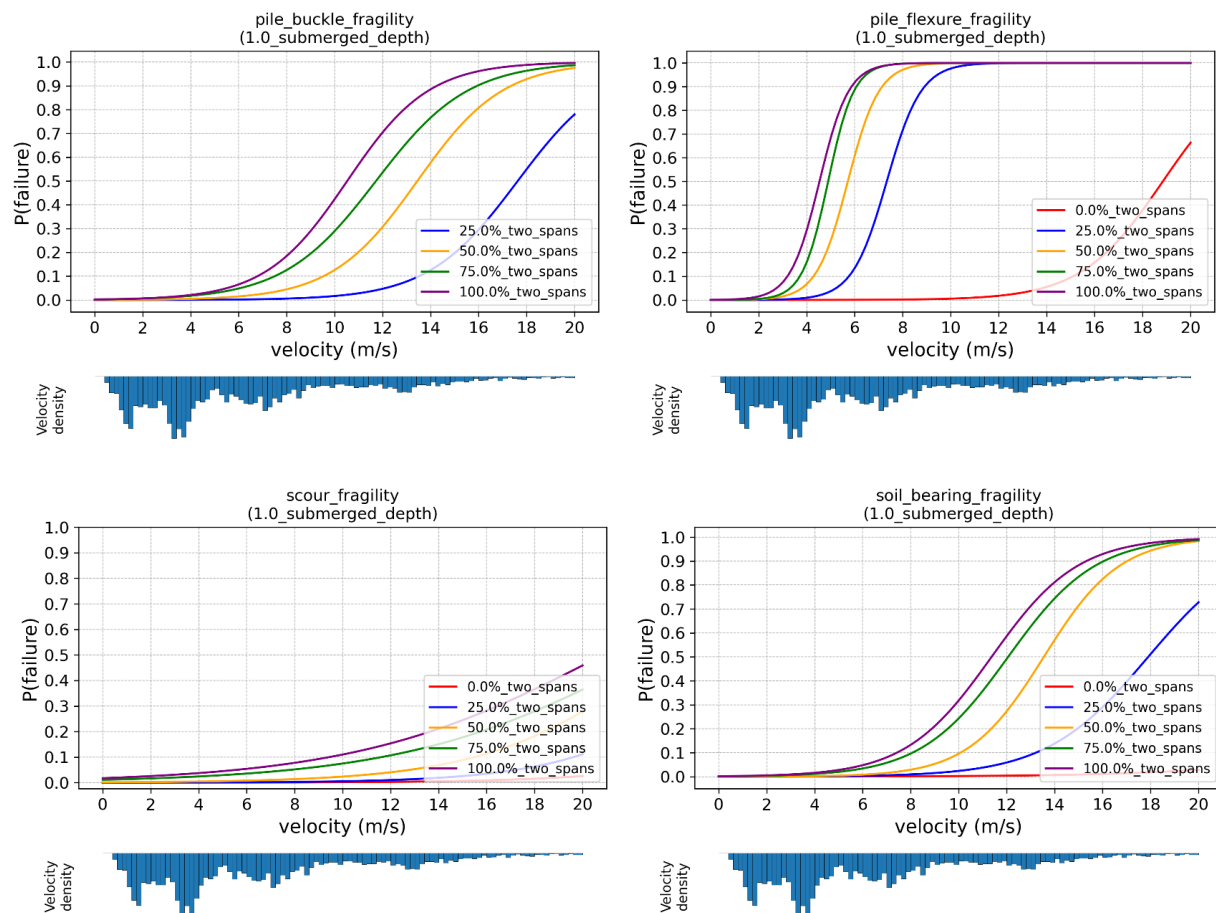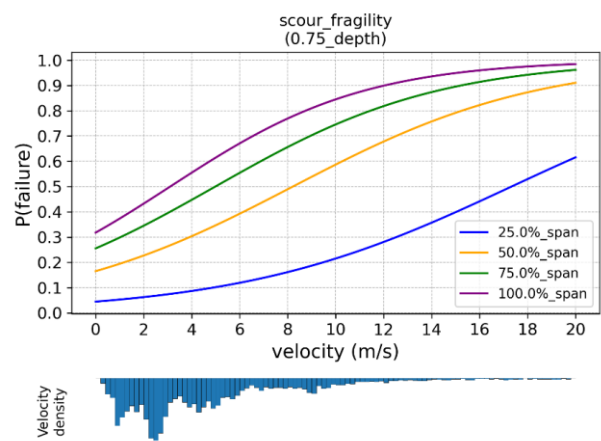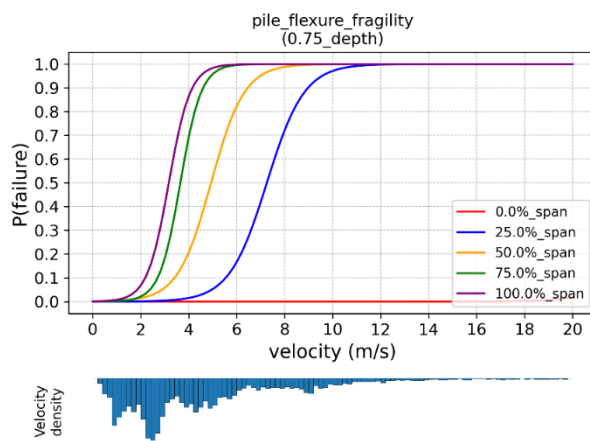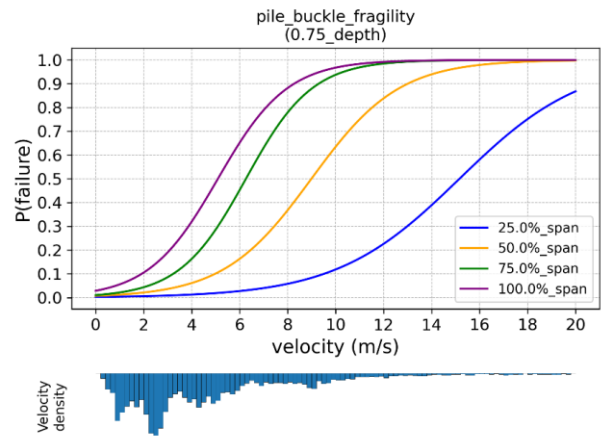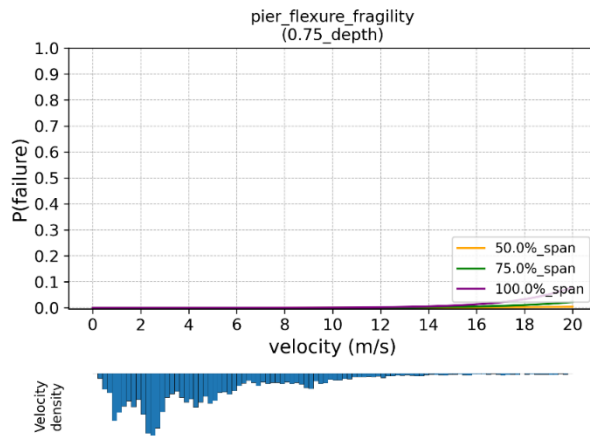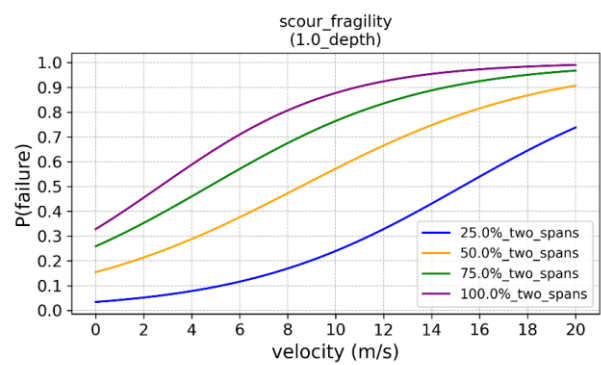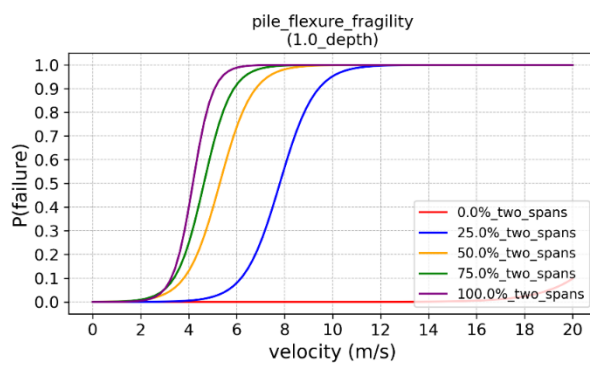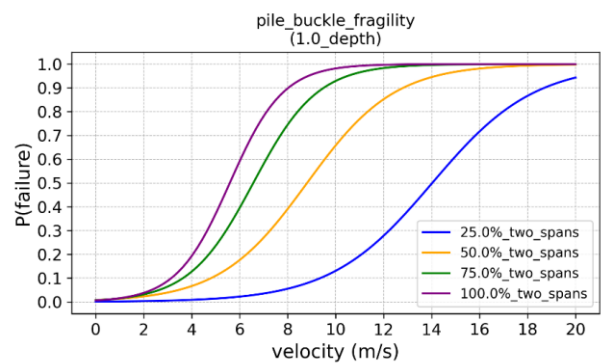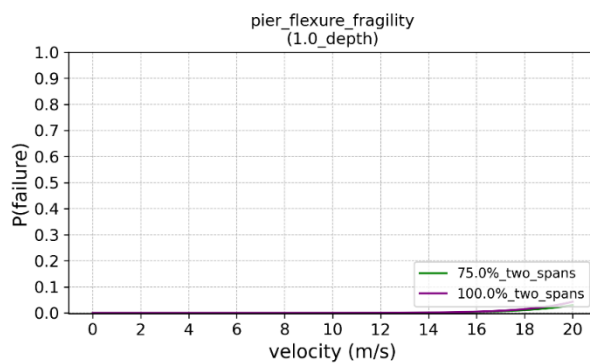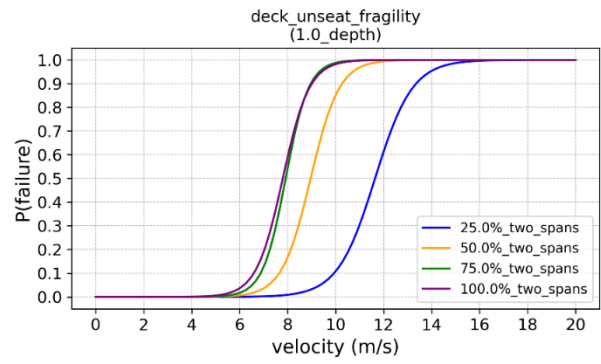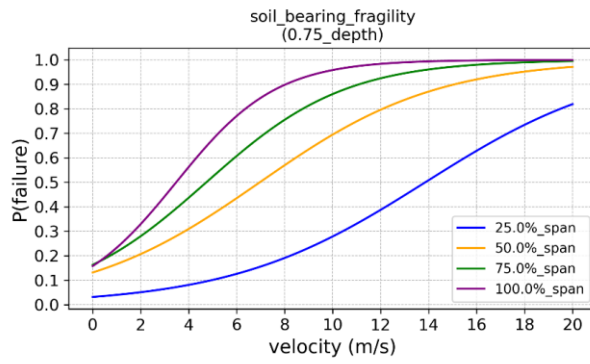
Figure 25: Cluster 2 (medium-span steel) Fragility curves

Table 11: Cluster-2 P(failure) when depth = 75% of pier height

Debris (% span)	Deck unseating	Pile flexure	Pile buckle	Pile shear	scour	Soil bearing	Pier flexure
0%	0	0.0001	0	0	0	0	0
25%	0	0.2057	0.0443	0	0.1098	0.1191	0
50%	0	0.3654	0.1665	0	0.3375	0.3546	0.0003
75%	0	0.4981	0.2953	0	0.4721	0.4673	0.0003
100%	0	0.5607	0.3928	0	0.568	0.5563	0.0008

Table 12: Cluster-2 P(failure) when just submergence of pier

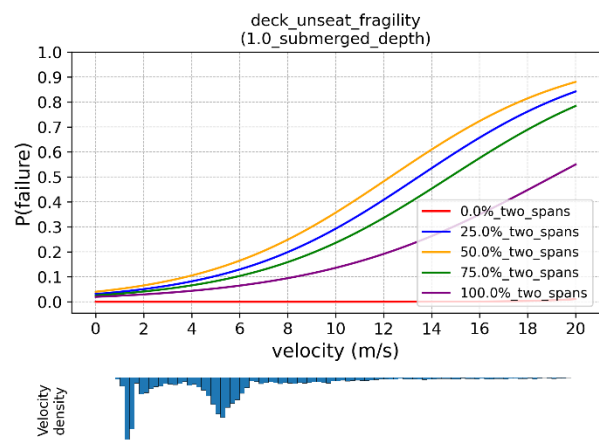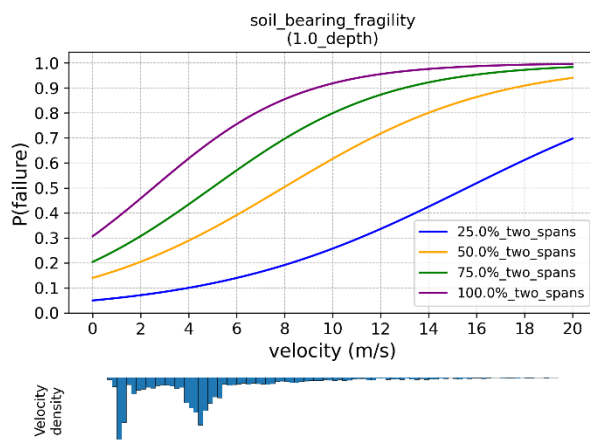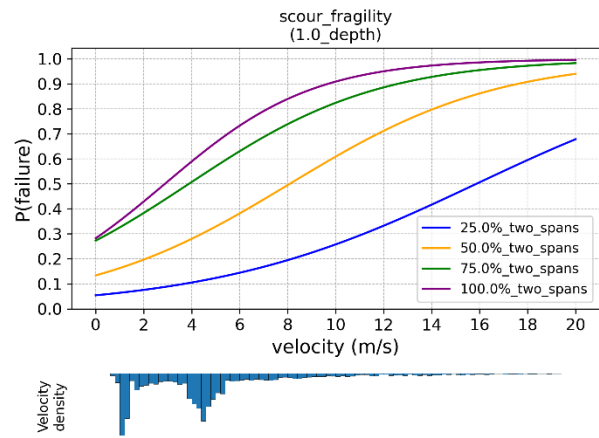| Debris (% span)	Deck unseating	Pile flexure	Pile buckle	Pile shear	scour	Soil bearing	Pier flexure
0%	0	0.0005	0	0	0	0	0
25%	0.085	0.2276	0.0649	0	0.1262	0.1513	0
50%	0.1792	0.3999	0.2205	0	0.3514	0.3787	0
75%	0.2161	0.4607	0.3275	0	0.5149	0.5327	0.0003
100%	0.2224	0.5034	0.3923	0	0.6276	0.6073	0.0004

Table 13: Cluster-2 P(failure) for deck submergence

Debris (% span)	Deck unseating	Pile flexure	Pile buckle	Pile shear	scour	Soil bearing	Pier flexure
0%	0	0.0161	0	0	0.0016	0.002	0
25%	0.4087	0.3392	0.0298	0	0.0052	0.032	0.0006
50%	0.533	0.4588	0.1074	0	0.019	0.0997	0.0028
75%	0.5692	0.5199	0.1664	0	0.0523	0.1514	0.0077
100%	0.6037	0.554	0.206	0	0.0758	0.1755	0.0071

The discussion for cluster 2 is similar to that of the cluster 1 discussion.

3.6 Cluster-3 (long-span steel) Fragility Curves
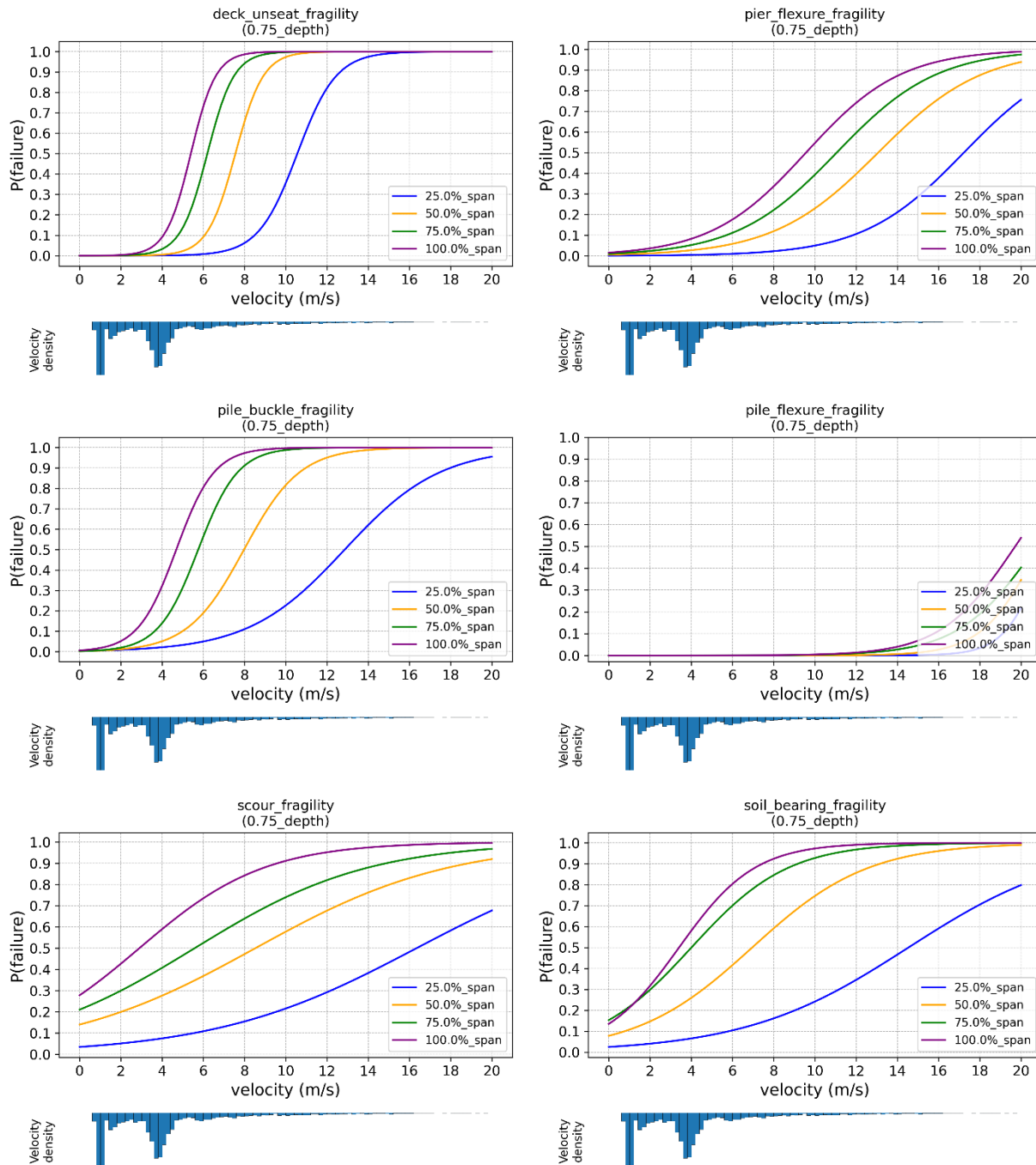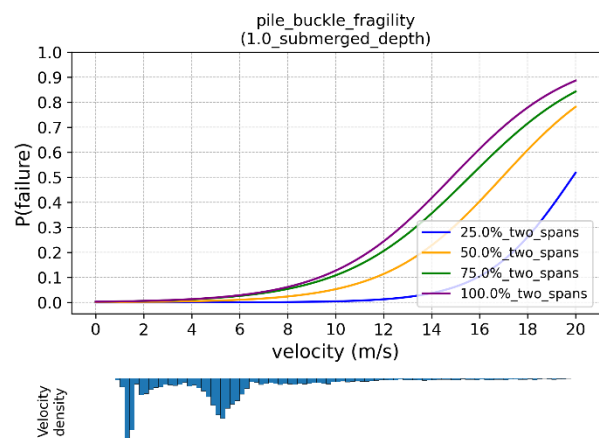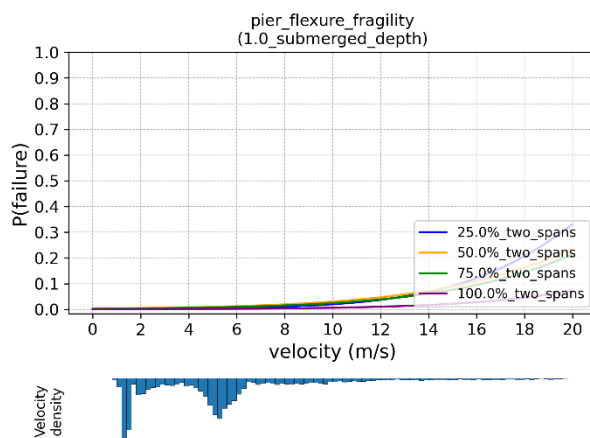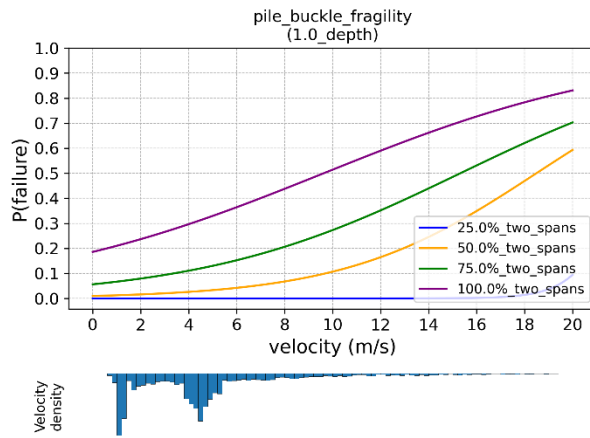
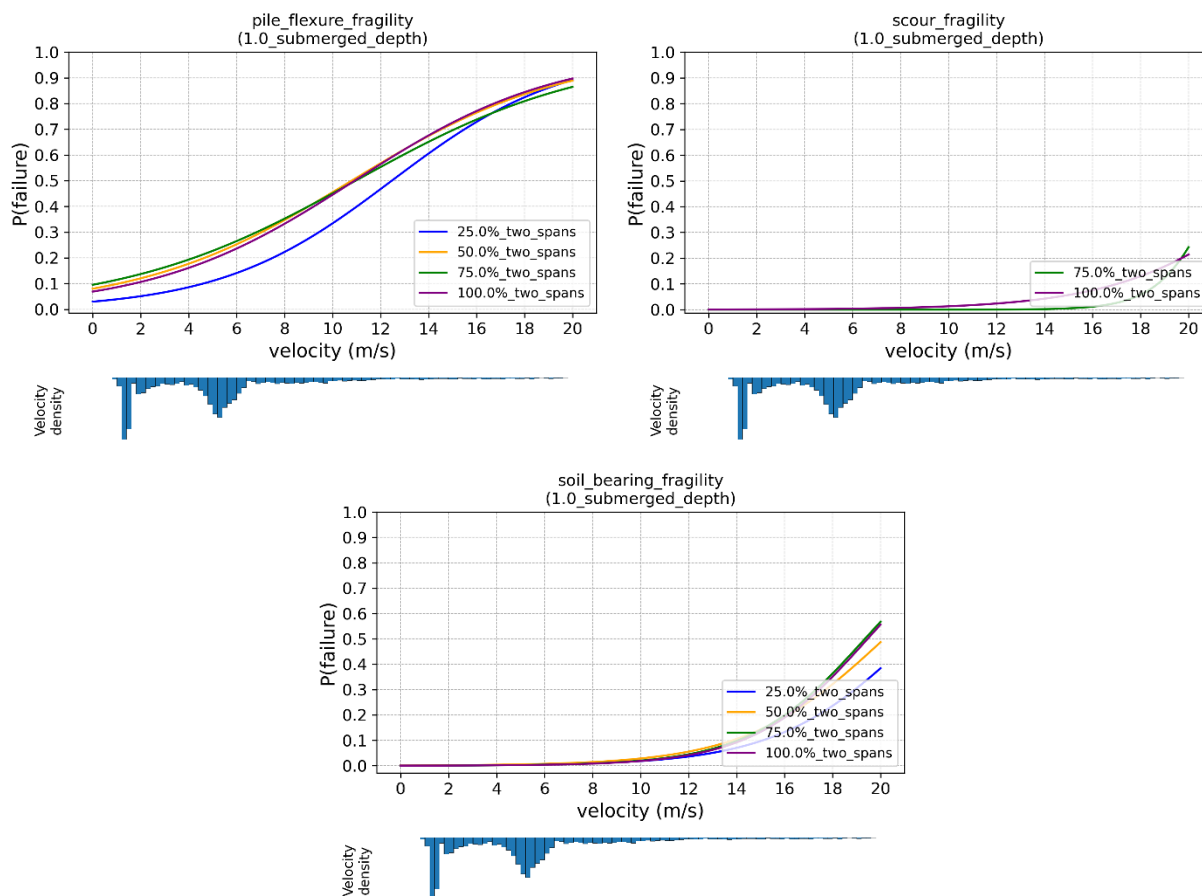*Figure 26: Cluster 3 (long-span steel) Fragility curves*

Table 14: Cluster-3 P(failure) when depth = 75% of pier height

Debris (% span)	Deck unseating	Pile flexure	Pile buckle	Pile shear	scour	Soil bearing	Pier flexure
0%	0	0	0	0	0	0	0
25%	0.0583	0.0002	0.0554	0	0.0897	0.0863	0.0158
50%	0.1266	0.0008	0.1418	0	0.2905	0.2863	0.0591
75%	0.1881	0.0021	0.2427	0	0.4112	0.4774	0.0965
100%	0.2413	0.0029	0.3444	0	0.5646	0.5264	0.1348

Table 15: Cluster-3 P(failure) when just submergence of pier

Debris (% span)	Deck unseating	Pile flexure	Pile buckle	Pile shear	scour	Soil bearing	Pier flexure
0%	0	0	0	0	0	0	0
25%	0	0	0.0002	0	0.1339	0.1301	0
50%	0	0	0.0466	0	0.3275	0.3357	0
75%	0	0	0.1411	0	0.5364	0.4736	0
100%	0	0	0.3276	0	0.6067	0.6308	0

Table 16: Cluster-3 P(failure) for deck submergence

Debris (% span)	Deck unseating	Pile flexure	Pile buckle	Pile shear	scour	Soil bearing	Pier flexure
0%	0.0001	0	0	0	0	0	0
25%	0.1475	0.1613	0.0088	0	0	0.0133	0.0133
50%	0.1794	0.252	0.036	0	0	0.0194	0.0176
75%	0.1215	0.2619	0.0581	0	0.0017	0.0174	0.0144
100%	0.076	0.2386	0.0656	0	0.0087	0.0165	0.0038

The discussion for cluster 3 is similar to that of the cluster 1 discussion.

3.7 Cluster-4 (concrete culvert) Fragility Curves

The limit state for the culverts is totally different than that for bridges. Also, as discussed in the methodology, due to the additional fact that the parameters for look-up table for culverts need to be different than that for bridges, the intensity measure for the culverts was chosen to be discharge corresponding to return period 'T'. Based on that, the following fragility curve was generated for up to 500 years of flood intensities.
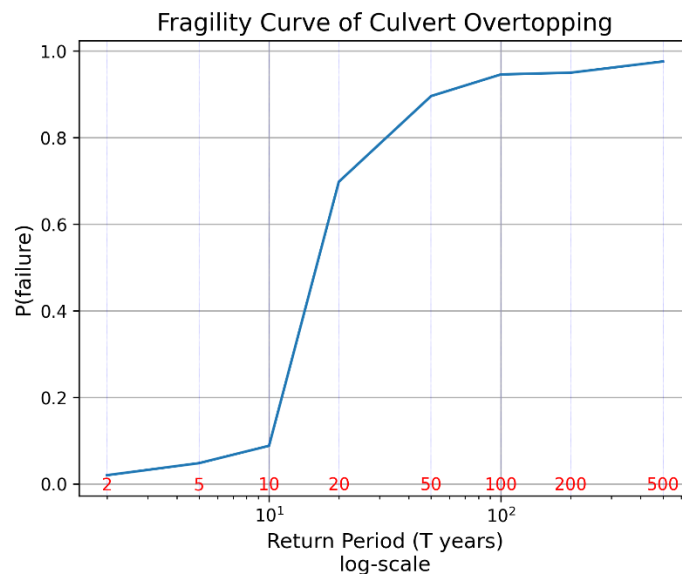

Figure 27: Cluster 4 (culverts) fragility curves

500 number of MCS were used at each return period, as beyond that, the curve did not noticeably change. The probability of failure P_f can be noted directly at each T, without the need for numerical integration method that we used for the bridges. The results are tabulated as below in Table 17:

Return Period (years)	Probability of failure (P_f)
2	0.020
5	0.048
10	0.088
20	0.698
50	0.896
100	0.946
200	0.950
500	0.976

The parameters based on which the fragility tables were developed were different for the culverts and the bridges. However, the meaning of P_f was same for both, and the values of P_f of culverts could be directly compared with that of the bridges for the prioritization purpose.

3.8 Cluster-5 (concrete t-beam) Fragility Curves
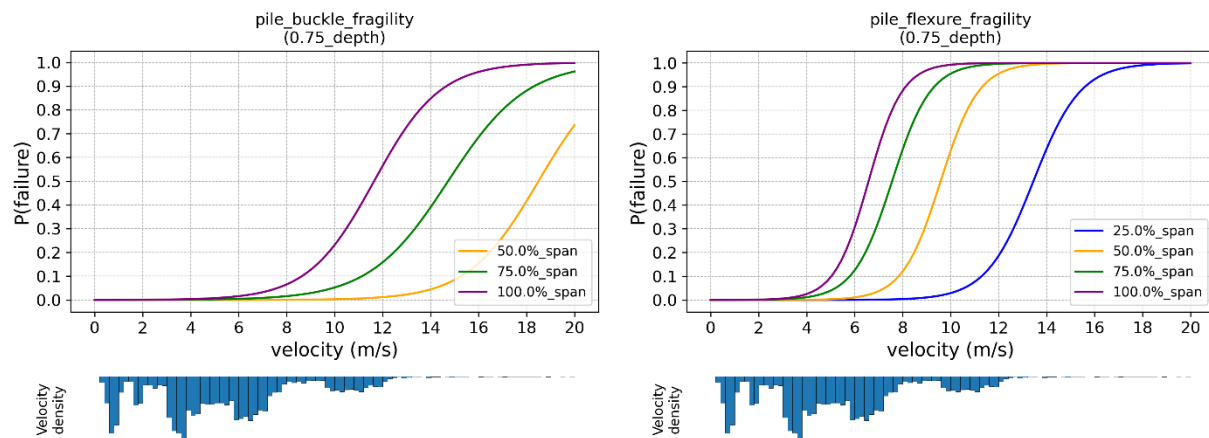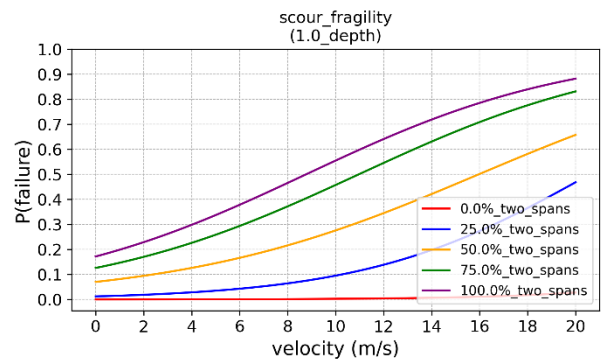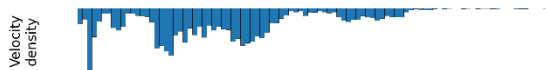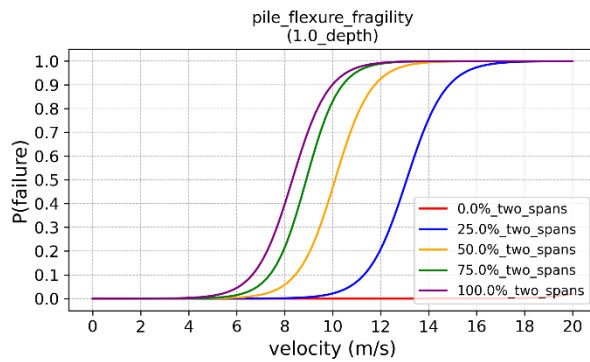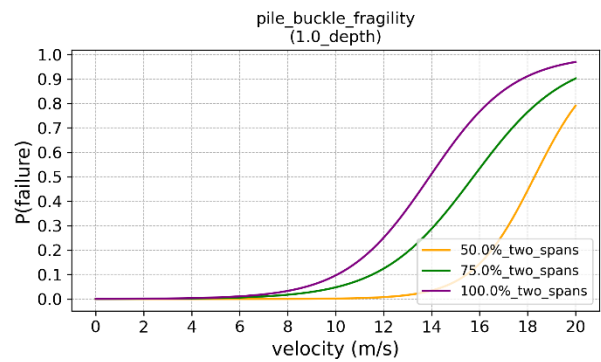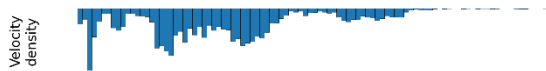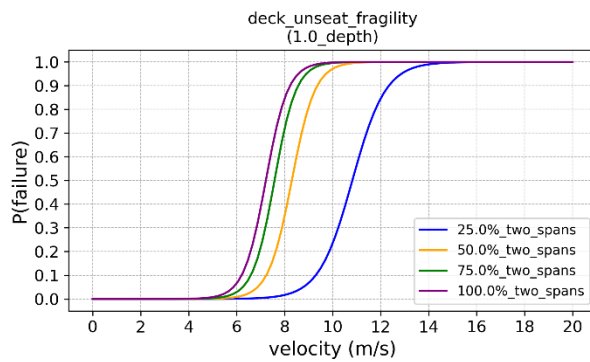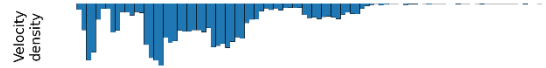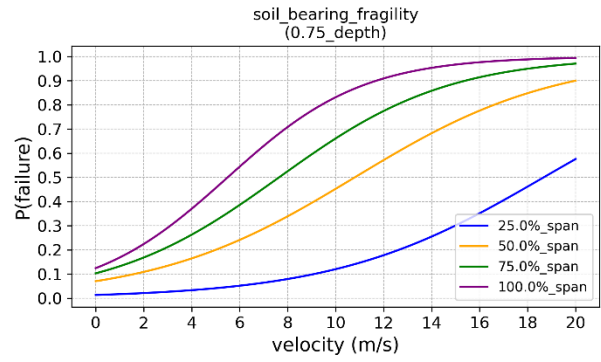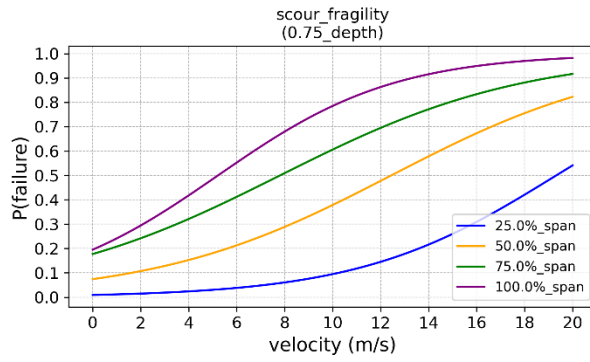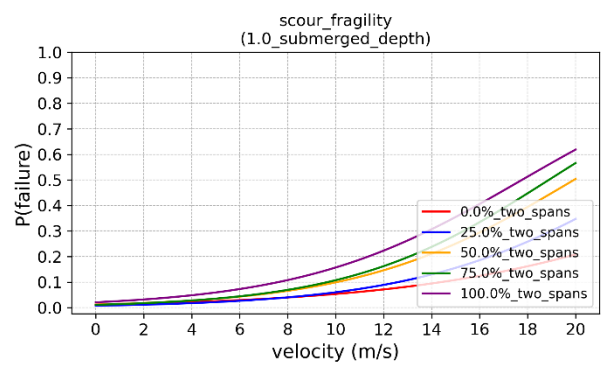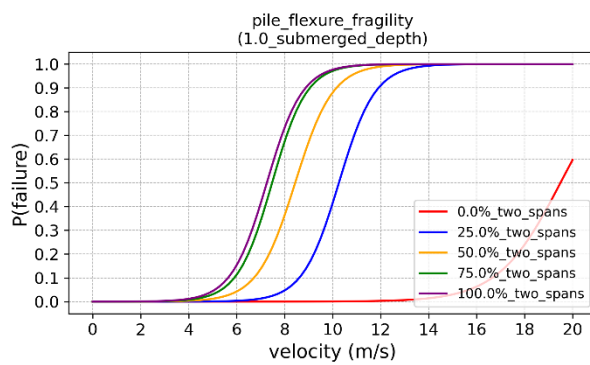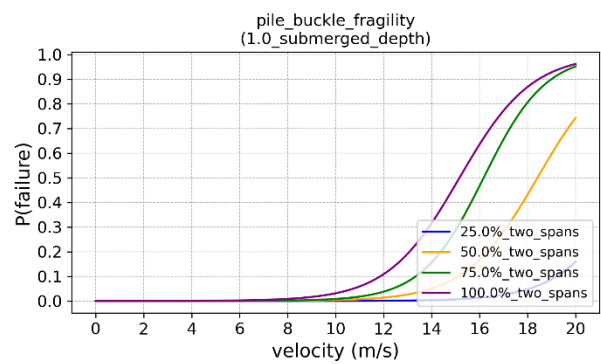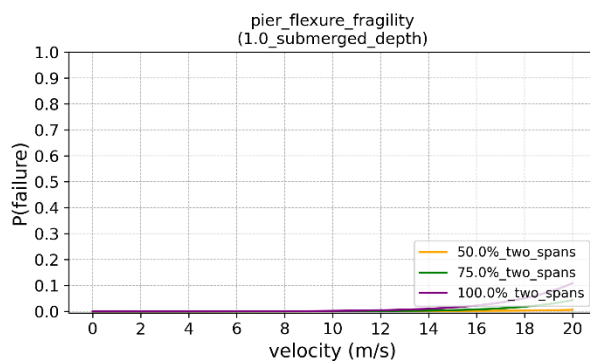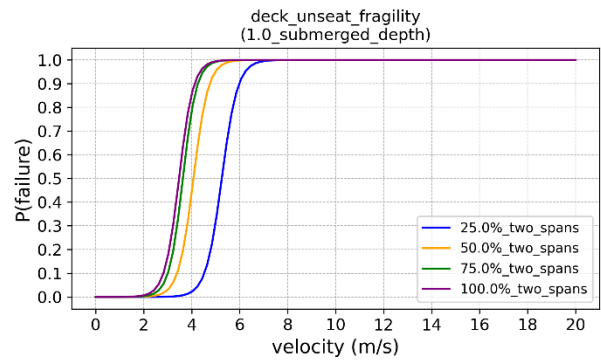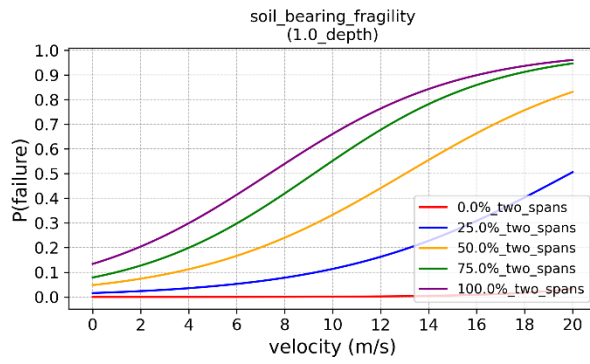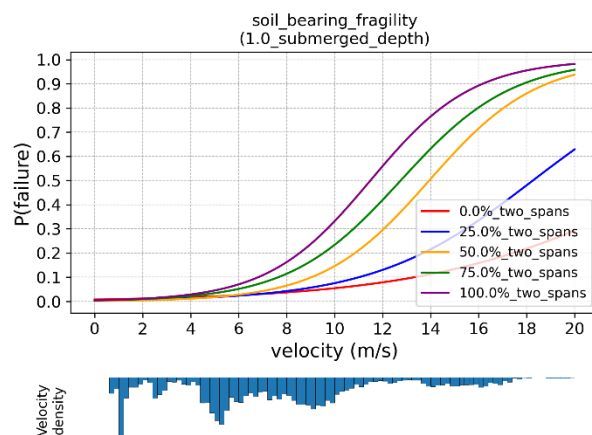
Figure 28: Cluster 5 (concrete t-girder) Fragility curves

Table 18: Cluster-5 P(failure) when depth = 75% of pier height

Debris (% span)	Deck unseating	Pile flexure	Pile buckle	Pile shear	scour	Soil bearing	Pier flexure
0%	0	0	0	0	0	0	0
25%	0	0.017	0	0	0.042	0.0551	0
50%	0	0.1199	0.0026	0	0.2047	0.2313	0
75%	0	0.2233	0.0193	0	0.3826	0.3525	0
100%	0	0.3059	0.0636	0	0.4944	0.471	0

Table 19: Cluster-5 P(failure) when just submergence of pier

Debris (% span)	Deck unseating	Pile flexure	Pile buckle	Pile shear	scour	Soil bearing	Pier flexure
0%	0	0	0	0	0.0017	0.0008	0
25%	0.1319	0.0569	0	0	0.0574	0.0688	0
50%	0.2357	0.156	0.0042	0	0.1844	0.1988	0
75%	0.3072	0.207	0.0335	0	0.3124	0.3299	0
100%	0.3491	0.2518	0.061	0	0.3917	0.4289	0

Table 20: Cluster-5 P(failure) for deck submergence

Debris (% span)	Deck unseating	Pile flexure	Pile buckle	Pile shear	scour	Soil bearing	Pier flexure
0%	0	0.0088	0	0	0.0449	0.0468	0
25%	0.6814	0.2342	0.0019	0	0.052	0.0717	0
50%	0.8014	0.3864	0.021	0	0.0837	0.1379	0.0003
75%	0.8207	0.4723	0.0527	0	0.0912	0.1849	0.0011
100%	0.8256	0.4916	0.0804	0	0.1279	0.2326	0.0035

The discussion for cluster 5 is similar to that of the cluster 1 discussion.

3.9 Cluster-6 (wooden truss) Fragility Curves

Due to the project time restrain and unavailability of data of the representative bridge, the fragility analysis could not be performed for this cluster.

There were only 7 wooden truss bridges in the cluster. So, generalization based on such a small sample could not be very accurate anyway. Although wooden truss bridge is not a common type of bridge that is built in the major roadways where significant traffic volume is expected, for future endeavor, however, it is recommended to complete this task with observed data to make the study results more comprehensive.

Look-up Tables

The following Look-up Tables (Table 22-26) are the final output of this project. In the result tables, maximum probability values among each kind of failure modes represent the most likely failure mode for a specified debris size and a water level, and hence, those values were selected to put in the look-up tables. The numeric code for mode of failure is explained in Table 21.

The parameters required to read the fragility tables are quite simple and easily accessible in the field even during extreme floods. The observer can report the bridge type and identify the cluster in which it belongs to. Then, failure probability of the bridge can be read from the table based on the water level and debris size. The water level can be reported as either 75% submerging the pier or fully submerging the pier or in extreme conditions, overflowing the deck submerging bridge railings. On the other hand, the debris size is expressed as percentage of average span of the bridge. It should be noted here that the water level below 75% was considered to be insignificant to cause bridge failures and was not analyzed in this project. Similarly, the maximum debris size was limited to the average of span lengths on two sides of the pier. The code in the square brackets adjacent to the probability values tells which component is likely to fail for the given flood and debris intensities.

For culverts, the failure probability has been expressed with respect to the return period of the flood.

Table 21: Failure codes

Code	Failure Component
[1]	Foundation
[2]	Deck
[3]	Pier

Table 22: Look-up table for cluster-1 (short span steel)

Debris size (% span)	Fragility (Probability of Failure)		
	pier 75%-submergence	Pier full-submergence	Deck full-submergence
0 %	0	0.0005 [1]	0.0044 [1]
25 %	0.1929 [1]	0.2722 [1]	0.6156 [2]
50 %	0.4341 [1]	0.4800 [1]	0.7446 [2]
75 %	0.5706 [1]	0.5557 [1]	0.7875 [2]
100 %	0.6647 [1]	0.6431 [1]	0.8103 [2]

Table 23: Look-up table for cluster-2 (medium-span steel)

Debris size (% span)	Fragility (Probability of Failure)		
	pier 75%-submergence	Pier full-submergence	Deck full-submergence
0 %	0.0001 [1]	0.0005 [1]	0.0161 [1]
25 %	0.2057 [1]	0.2276 [1]	0.4087 [2]
50 %	0.3654 [1]	0.3999 [1]	0.533 [2]
75 %	0.4981 [1]	0.5327 [1]	0.5692 [2]
100 %	0.5680 [1]	0.6276 [1]	0.6037 [2]

Table 24: Look-up table for cluster-3 (long-span steel)

Debris size (% span)	Fragility (Probability of Failure)		
	pier 75%-submergence	Pier full-submergence	Deck full-submergence
0 %	0	0	0.0001 [2]
25 %	0.0897 [1]	0.1339 [1]	0.1613 [1]
50 %	0.2905 [1]	0.3357 [1]	0.2520 [1]
75 %	0.4774 [1]	0.5364 [1]	0.2619 [1]
100 %	0.5646 [1]	0.6308 [1]	0.2386 [1]

Table 25: Look-up table for cluster-4 (culverts)

Cluster-4 (Culverts)	
Return Period (years)	**Probability of Failure**
2	0.020
5	0.048
10	0.088
20	0.698
50	0.896
100	0.946
200	0.950
500	0.976

Table 26: Look-up table for cluster-5 (concrete T-girders)

Cluster-5 (Concrete T-Girder)			
Debris size (% span)	**Fragility (Probability of Failure)**		
	pier 75%-submergence	**Pier full-submergence**	**Deck full-submergence**
0 %	0	0.0017 [1]	0.0468 [1]
25 %	0.0551 [1]	0.1319 [1]	0.6814 [2]
50 %	0.2313 [1]	0.2357 [2]	0.8014 [2]
75 %	0.3826 [1]	0.3299 [1]	0.8207 [2]
100 %	0.4944 [1]	0.4289 [1]	0.8256 [2]

Limitations

Being a first of a kind study in this direction of regional fragility assessment of bridge structures, there exists many limitations in it. Although most of the limitations have been already described in their respective contexts, some of the major limitations are listed here for a quick overview.

Statistical Limitations

- Only multi-span bridges were considered, focusing on pier foundation scour and entrapment of debris at piers and deck. Abutments scouring was not considered in the study.
- Due to unavailability of data, clustering parameters (material, type, average span length and total structure length) were mostly superstructure-based, although foundation type, debris

generation and entrapment probabilities, soil type, etc. are also considered to be important flood-related parameters.

Modelling Limitations

- If a MCS realization was a long span bridge, then debris size equaling one full span might not represent a realistic size of debris that could be carried out by the stream. (Diehl, 1997), for example, reported the maximum size of drift width and blocked spans to be 24 meters. Thus, fragility results of a cluster could be swayed to more extreme side (overestimation) if a greater number of long span bridges are present in a cluster.
- Due to unavailability of substructure data, only one type of foundation – pile foundation was used by using some scaling factors to proportionate with the reference bridges.
- Assumptions were made to estimate the soil type which affects the bearing capacity and depth of fixity. Only one kind of soil (cohesionless soil) was in the study.
- Only the static frictional resistance was considered between the girder and pier-cap, and hence, the connection strength at the bearing locations has been neglected. This makes this study more conservative. However, to accurately account the resistance of deck movement in the lateral direction, mechanisms of failure of various kinds of bridge bearings are suggested to be studied in the future.
- The pile cap was modelled as a rigid plate. Considering the flexibility of pile caps can affect the analysis results.

Regression model limitations

- Logistic regression simplifies the fitting of binary data with smooth 'S' shaped curve, when in reality, fragility curves may be not perfectly 'S' shaped.
- Forceful fitting of sigmoid curve, in some cases, resulted in some errors near zero velocity. However, the consequence of that is minimal as near zero velocity, the probability of failure as well as velocity distribution are not significant.

Others

- Due to unavailability of data, fragility analysis of wooden-truss cluster could not be performed.

Conclusions and Recommendations

In this project, bridges crossing hydraulic lines in the state of Vermont were chosen for fragility assessment. The project was completed in two phases. In the first phase, data of the bridges were collected, and clustering of the bridges was done based on key flood-related parameters. Using the K-prototype algorithm, six prominent clusters were obtained. In the second phase, fragility assessment of five of the clusters was done. The typical design parameters of each of the bridge types were accessed with the help of cluster-mean bridge. While finite element modeling was done to do the analysis of bridges, one of the six cluster- culvert was separately dealt with different failure mode than that of the bridges. The fragility output was presented in look-up tables, using which fragility of any of the bridge types can be instantly assessed based on easily reportable flood and debris intensity parameters at a bridge site. For culverts, output is based on return period of flood.

The procedure developed in this project to generate vulnerability lookup-tables is believed to serve bridge asset managers, local and state governments, and other related decision-makers to take immediate actions and strategies on the operations and maintenance of bridges during severe flood. Identifying the most vulnerable bridge or bridges in a region will help in mitigation of the possible economic and human life losses during flood.

References

AASHTO LRFD. (2012). *AASHTO LRFD bridge design specifications, customary U.S. units.* American Association of State Highway and Transportation Officials.

Ahamed, T., Duan, J. G., & Jo, H. (2021). Flood-fragility analysis of instream bridges–consideration of flow hydraulics, geotechnical uncertainties, and variable scour depth. *Structure and Infrastructure Engineering*, *17*(11), 1494–1507. https://doi.org/10.1080/15732479.2020.1815226

Almutairi, A., Lu, J., Wang, N., & Elgamal, A. (2016). *CA15-2582 Analysis of Multi-span Bridges Using OpenSees 13. TYPE OF REPORT AND PERIOD COVERED Final Report Unclassified ADA Notice*.

American Institute of Steel Construction (AISC). (2016). *Specification for Structural Steel Buildings*. ANSI/AISC 360-16.

Anderson, I., Hanley, J. P., Rizzo, D. M., Huston, D. R., & Dewoolkar, M. M. (2020). Evaluating Damage to Vermont Bridges by Hurricane Irene with Multivariate Bridge Inspection and Stream Hydrogeologic Data. *Journal of Bridge Engineering*, *25*(10). https://doi.org/10.1061/(asce)be.1943-5592.0001603

Anderson, I., Rizzo, D. M., Huston, D. R., & Dewoolkar, M. M. (2017). Analysis of bridge and stream conditions of over 300 Vermont bridges damaged in Tropical Storm Irene. *Structure and Infrastructure Engineering*, *13*(11), 1437–1450. https://doi.org/10.1080/15732479.2017.1285329

Anisha, A., Jacob, A., Davis, R., & Mangalathu, S. (2022). Fragility functions for highway RC bridge under various flood scenarios. *Engineering Structures*, *260*. https://doi.org/10.1016/j.engstruct.2022.114244

Arcement, G. J., & Schneider, V. R. (1989). *Guide for Selecting Manning's Roughness Coefficients for Natural Channels and Flood Plains*.

Argyroudis, S. A., & Mitoulis, S. A. (2021). Vulnerability of bridges to individual and multiple hazards- floods and earthquakes. *Reliability Engineering and System Safety*, *210*. https://doi.org/10.1016/j.ress.2021.107564

Arneson, L. A., Zevenbergen, L. W., Lagasse, P. F., & Clopper, P. E. (2012). *Evaluating Scour at Bridges, Fifth Edition*.

Arora, R. (2023). Reliability-based approach for fragility assessment of bridges under floods. *Structural Engineering and Mechanics*, *88*(4), 311–322. https://doi.org/10.12989/sem.2023.88.4.311

Aygün, B., Asce, S. M., Dueñas-Osorio, L., Asce, A. M., Padgett, J. E., Desroches, R., & Asce, M. (2010). *Efficient Longitudinal Seismic Fragility Assessment of a Multispan Continuous Steel Bridge on Liquefiable Soils*. https://doi.org/10.1061/ASCEBE.1943-5592.0000131

Bowles, J. E. (1997). *Foundation Analysis and Design*. McGraw–Hill Book Company.

Chaimahawan, P., Suparp, S., Joyklad, P., & Hussain, Q. (2021). Finite element analysis of reinforced concrete pile cap using ATENA. *Latin American Journal of Solids and Structures*, *18*(2), 1–17. https://doi.org/10.1590/1679-78256290

Clarke, B. G. (2018a). The engineering properties of glacial tills. *Geotechnical Research*, *5*(4), 262–277. https://doi.org/10.1680/jgere.18.00020

Clarke, B. G. (2018b). The engineering properties of glacial tills. *Geotechnical Research*, *5*(4), 262–277. https://doi.org/10.1680/jgere.18.00020

Diehl, T. H. (1997). *Potential Drift Accumulation at Bridges*.

El Hammouli, S., Hanna, A., Lin, L., & Khalifa, M. (2021). Role of Cap Thickness in Pile-Cap Foundation. *International Journal of Civil Infrastructure*. https://doi.org/10.11159/ijci.2021.013

FDOT. (2022). *Florida Department of Transportation Bridge Scour Manual FDOT Office Central Office*.

FHWA. (2014). *LRFD Seismic Analysis and Design of Bridges Reference Manual*.

FHWA HEC-09. (2005). *Debris Control Structures Evaluation and Countermeasures Third Edition*. http://www.fedworld.gov/ntis/

Haehnel, R. B., & Daly, S. F. (2004). Maximum Impact Force of Woody Debris on Floodplain Structures. *Journal of Hydraulic Engineering*, *130*(2), 112–120. https://doi.org/10.1061/(asce)0733-9429(2004)130:2(112)

Hognestad, E. (1951). (1951). *A study of combined bending and axial load in reinforced concrete members.*

Huang, Z. (1998). Extensions to the k-Means Algorithm for Clustering Large Data Sets with Categorical Values. In *Data Mining and Knowledge Discovery* (Vol. 12).

Hughes, W., Santos, L., Lu, Q., Malla, R., Ravishanker, N., & Zhang, W. (2023). Probabilistic risk assessment framework for predicting large woody debris accumulations and scour near bridges. *Structure and Infrastructure Engineering*. https://doi.org/10.1080/15732479.2023.2177875

Johnson, P. A., Clopper, P. E., Zevenbergen, L. W., & Lagasse, P. F. (2015). Quantifying Uncertainty and Reliability in Bridge Scour Estimations. *Journal of Hydraulic Engineering*, *141*(7). https://doi.org/10.1061/(asce)hy.1943-7900.0001017

Kim, H., Sim, S. H., Lee, J., Lee, Y. J., & Kim, J. M. (2017). Flood fragility analysis for bridges with multiple failure modes. *Advances in Mechanical Engineering*, *9*(3). https://doi.org/10.1177/1687814017696415

Kosič, M., Anžlin, A., & Bau', V. (2023). Flood vulnerability assessment: an effective tool to evaluate the lifecycle risk analysis of bridges. *Ce/Papers*, *6*(5), 817–823. https://doi.org/10.1002/cepa.2181

Kriegel, H. P., Kröger, P., Sander, J., & Zimek, A. (2011). Density-based clustering. *Wiley Interdisciplinary Reviews: Data Mining and Knowledge Discovery*, *1*(3), 231–240. https://doi.org/10.1002/widm.30

Lagasse, P. F. . (2010). *Effects of debris on bridge pier scour*. Transportation Research Board.

Lebbe, M., Lokuge, W., Setunge, S., Zhang, K., & Farook Kalendher, M. (2014). *Failure mechanisms of bridge infrastructure in an extreme flood event*.

Lee, S. M., Kim, J., & Lim Kang, S. (2007). Development of Fragility Curves for Bridges in Korea. In *165~174 Transportation Engineering* (Vol. 11, Issue 3).

Liang, X., Mosalam, K. M., & Günay, S. (2016). Direct Integration Algorithms for Efficient Nonlinear Seismic Response of Reinforced Concrete Highway Bridges. *Journal of Bridge Engineering*, *21*(7). https://doi.org/10.1061/(asce)be.1943-5592.0000895

Lin, C., Han, J., Bennett, C., & Parsons, R. L. (2014). Case History Analysis of Bridge Failures due to Scour. *Climatic Effects on Pavement and Geotechnical Infrastructure*, 204–216. https://doi.org/10.1061/9780784413326.021

MacQueen, J. (1967). Some methods for classification and analysis of multivariate observations. *Https://Doi.Org/*, *5.1*, 281–298. https://projecteuclid.org/ebooks/berkeley-symposium-on-mathematical-statistics-and-probability/Proceedings-of-the-Fifth-Berkeley-Symposium-on-Mathematical-Statistics-and/chapter/Some-methods-for-classification-and-analysis-of-multivariate-observations/bsmsp/1200512992

M.T. Davisson, & K.E. Robinson. (1965). Bending and Buckling of Partially Embedded Piles. *INTERNATIONAL SOCIETY FOR SOIL MECHANICS AND GEOTECHNICAL ENGINEERING*. https://www.issmge.org/publications/online-library

National Bridge Inventory | National Bridge Inventory | Geospatial at the Bureau of Transportation Statistics. (n.d.). Retrieved August 18, 2024, from https://data-usdot.opendata.arcgis.com/datasets/national-bridge-inventory/explore?filters=eyJTVEFURV9DT0RFXzAwMSI6WyIyMCJdfQ%3D%3D&showTable=true

Nelis J. de Vos. (n.d.). *kmodes categorical clustering library*. Retrieved August 20, 2024, from https://github.com/nicodv/kmodes

New York City, NY Laws. (n.d.). Retrieved August 18, 2024, from https://codelibrary.amlegal.com/codes/newyorkcity/latest/overview

Nielsen, F. (2016). *Undergraduate Topics in Computer Science Introduction to HPC with MPI for Data Science*. http://www.springer.com/series/7592

Panici, D., & de Almeida, G. A. M. (2018). Formation, Growth, and Failure of Debris Jams at Bridge Piers. *Water Resources Research*, *54*(9), 6226–6241. https://doi.org/10.1029/2017WR022177

Porter, K. (2021). *A Beginner's Guide to Earthquake Fragility Vulnerability and Risk*. https://www.sparisk.com/pubs/Porter-beginners-

Priestley, M. J. N. ., Seible, F. ., & Calvi, G. M. . (1996). *Seismic design and retrofit of bridges*. Wiley.

Pucci, A., Sousa, H. S., Giresini, L., Matos, J. C., & Castelli, F. (2023). Fragility of bridge decks exposed to hydraulic and driftwood actions. *Structure and Infrastructure Engineering*. https://doi.org/10.1080/15732479.2023.2272725

Rigby, E. H., Boyd, M. J., Roso, S., Silveri, P., & Davis, A. (2004). *Causes and Effects of Culvert Blockage During Large Storms*.

Rodwell, J., Williams, J. H., & Paulik, R. (2023). Empirical Fragility Assessment of Three-Waters and Railway Infrastructure Damaged by the 2015 Illapel Tsunami, Chile. *Journal of Marine Science and Engineering*, *11*(10). https://doi.org/10.3390/jmse11101991

Rousseeuw, P. J. (1987). Silhouettes: A graphical aid to the interpretation and validation of cluster analysis. *Journal of Computational and Applied Mathematics*, *20*(C), 53–65. https://doi.org/10.1016/0377-0427(87)90125-7

Schall, J. D., Thompson, P. L., Zerges, S. M., Kilgore, R. T., & Morris, J. L. (2012). *HYDRAULIC DESIGN OF HIGHWAY CULVERTS- Third Edition*.

Sellevold, J., Norem, H., Bruland, O., Rüther, N., & Pummer, E. (2024). Effects of Bottom-Up Blockage on Entrance Loss Coefficients and Head-Discharge Relationships for Pipe Culvert Inlets: Comparisons of Theoretical Methods and Experimental Results. *Journal of Irrigation and Drainage Engineering*, *150*(2). https://doi.org/10.1061/jidedh.ireng-10219

Seo, J., & Linzell, D. G. (2013). Nonlinear Seismic Response and Parametric Examination of Horizontally Curved Steel Bridges Using 3D Computational Models. *Journal of Bridge Engineering*, *18*(3), 220–231. https://doi.org/10.1061/(asce)be.1943-5592.0000345

Thomas Villars. (2021). Tunbridge- Vermont State Soil. In *Thomas Villars*. Soil Science Society of America.

Thorndike, R. L. (1953). Who belongs in the family? *Psychometrika*, *18*(4), 267–276. https://doi.org/10.1007/BF02289263/METRICS

USDA. (2015). *Soil Fact Sheet (Windsor County, Vermont)*.

Wardhana, K., Hadipriono, F. C., & Asce, F. (2003). Analysis of Recent Bridge Failures in the United States. *J. Perform. Constr. Facil.* https://doi.org/10.1061/ASCE0887-3828200317:3144

Wark, N., Smith, K., Kennedy, M., Widing, S., Antonio, J. S., & Wildey, R. (2015). *Hydraulics Manual, Vermont Agency of Transportation*.

Wellwood, N., Knight, S., Fenwick, J., & Oxon, D. P. (. (1989). A FLOOD LOADING METHODOLOGY FOR BRIDGES. *ARRB Conference*.

Zevenbergen, L., Engineering, R., Lagasse, P., Vice President, S., Clopper, P., & Water Resources Engineer, S. (2007). *Effects of Debris on Bridge Pier Scour*.

Zhao, Q., Xu, M., & Fränti, P. (2008). Knee point detection on bayesian information criterion. *Proceedings - International Conference on Tools with Artificial Intelligence, ICTAI*, *2*, 431–438. https://doi.org/10.1109/ICTAI.2008.154

Zhu, M., Elkhetali, I., & Scott, M. H. (2018). Validation of OpenSees for Tsunami Loading on Bridge Superstructures . *Journal of Bridge Engineering*, *23*(4). https://doi.org/10.1061/(asce)be.1943-5592.0001221

Transportation Infrastructure Durability Center
AT THE UNIVERSITY OF MAINE

35 Flagstaff Road
Orono, Maine 04469
tidc@maine.edu
207.581.4376

www.tidc-utc.org